Development of Battery-Supercapacitor Management Systems for Electric Vehicles

By

Mostafa Farrag

A Thesis Submitted in Partial Fulfilment of the Requirements for the Degree of Doctor of Philosophy

Department of Electronic and Electrical Engineering College of Engineering, Design and Physical Sciences

Brunel University London

First Supervisor: Dr Chun Sing Lai

Second Supervisor: Professor Mohamed Darwish

Acknowledgement

I would like to express my gratitude and appreciation to the EPSRC Doctoral Training Program for their generous funding and invaluable support in facilitating this research project.

I would also like to extend my profound gratitude to my supervisors, Dr Chun Sing Lai and Professor Mohamed Darwish for their invaluable advice, guidance, and unwavering support. Their strong conviction, enthusiastic endorsement, and constructive feedback have been exceptionally beneficial. I especially appreciate their understanding and patience, allowing me the freedom to explore and select my own areas of study.

Furthermore, I deeply appreciate the significant role my family has played in providing support, love, inspiration, and encouragement during my academic journey. I would especially like to thank my wife for her unwavering support and understanding throughout my journey.

Additionally, I am grateful to my friends and colleagues who have consistently provided encouragement during the duration of this project.

Abstract

The electric vehicle (EV) sector is rapidly advancing, representing a global shift toward sustainable, eco-friendly transportation. With an increasing focus on reducing carbon emissions and reliance on fossil fuels, EVs have become central to achieving environmental goals. However, widespread adoption is challenged by current limitations in energy storage, efficiency, and reliability. This thesis introduces an innovative hybrid energy storage system (HESS) tailored for EVs, integrating both batteries and supercapacitors to overcome these limitations. At the core of this HESS lies a battery management system (BMS) responsible for monitoring, optimising, and sustaining battery health and performance. The BMS is critical for ensuring safe operation, extending battery life, and maximising energy efficiency across a range of operational conditions.

This study tackles three principal difficulties in electric vehicle energy management: the efficient integration of HESS, operating stability, and improved efficiency under varying driving situations. The research examines various battery types, such as lead-acid, nickel-cadmium, nickel-metal-hydride, and lithium-ion, evaluating each for energy density, power output, lifespan, and charging efficiency. Lithium-ion batteries, commonly utilised in electric vehicles for their high energy density and consistent performance, are assessed for their compatibility with supercapacitors in hybrid energy storage systems. Supercapacitors, recognised for their quick charge-discharge capabilities and enhanced power density, augment lithium-ion batteries by alleviating stress during peak power demands. The resultant HESS design integrates the advantages of both components, providing a system that enhances efficiency while ensuring sustained performance and dependability in electric vehicles. A novel contribution of this research is the development of a fully active HESS topology, capable of dynamic energy allocation to reduce stress on the battery and SC.

Three common driving cycles were used in the simulations, including Artemis Rural, Artemis Motorway, and US06, to reflect varied driving situations. The simulations were performed using MATLAB/Simulink. In comparison with Proportional-Integral (PI) and Model Predictive Control (MPC) approaches, the results show that the Radial Basis Function (RBF) controller optimises energy flow and maintains system stability significantly. The RBF controller obtained a battery State of Charge (SOC) of 78.86% with the HESS in the Artemis Rural cycle, which is far higher than the 64.41% and 64.2% SOCs achieved by the MPC and PI controllers, respectively. In comparison to the MPC controller's 99.28% and the PI controller's 99.14% SOC, the RBF controller achieved a minimal SOC loss of 99.69% during the Artemis Motorway cycle. The RBF controller outperformed the MPC controller at 72.75% and the PI controller at 70.2% in the demanding US06 cycle, which is characterised by rapid acceleration and deceleration, by maintaining a SOC of 82.91%. Moreover, the RBF controller obtained

a substantial energy savings of 3.09 kWh in the US06 cycle when contrasted with the PI controller. The RBF controller is the most effective strategy for optimising HESS performance across a variety of operating conditions, as these results demonstrate.

The findings emphasise the HESS's ability to mitigate battery stress, optimise energy recovery, and ensure stable performance across varied driving conditions. The HESS minimises energy losses, enhances energy recovery efficiency, and extends battery lifespan by dynamically allocating energy between the battery and supercapacitor. These results establish benchmarks for the integration of HESS in EVs, contributing to sustainable transportation solutions.

Table of Contents

Acknowledgement 2
Abstract 3
Table of Contents 5
List of Figures 10
List of Tables 13
Abbreviations 14
Chapter 1 Introduction 17
1.1) Motivation 18
1.2) Background of EVs 20
1.3.1) HEV 20
1.3.1.1) Series Powertrain 21
1.3.1.2) Parallel Powertrain 21
1.3.1.3) Series/Parallel Powertrain 22
1.3.2) PHEV 22
1.3.3) Fully EV 23
1.3.3.1) Centralised Single Motor Driven Powertrain 24
1.3.3.2) Distributed Multi Motor Driven Powertrain 24
1.3.4) Charging Stations 26
1.3.4.1) Charging Infrastructure Regulations 26
1.3.4.1.1) Inductive Charging 27
1.3.4.1.2) Conductive Charging 28
1.3.4.1.3) Battery Swapping 29
1.3.5) EV Charging Modes 29
1.3.6) Type of Plugs 30
1.3) Challenges and Research Focus 31
1.4.1) Research Challenges 33
1.4.2) Objectives 33
1.4) Thesis Outline 34
1.5) Summary 35
Chapter 2 Literature Review 36
2.1) Background 36
2.2) Battery Technologies 36
2.2.1) Energy Density 39
2.2.2) Power Density 39

2.2.3) Current Rate 39
2.2.4) Life Cycle 39
2.3) Battery Types 40
2.3.1) Lead-Acid 40
2.3.2) Nickel-Cadmium 40
2.3.3) Nickel-Metal-Hydride 40
2.3.4) Lithium-ion Battery 40
2.3.4.1) Characteristics of Lithium-ion battery 41
2.3.5) Battery Charging Technique 43
2.3.6) Electric Vehicle Battery Modelling Techniques 46
2.3.7) Lithium-ion Battery Faults 47
2.3.7.1) Internal Battery Faults 48
2.3.7.2) External Battery Faults 48
2.4) Battery Management System 49
2.4.1) Key Functions of the Battery Management System 49
2.4.2.1) State of Charge 50
2.4.2.1.1) Book-Keeping Estimations 50
2.4.2.1.2) Direct Measurements 50
2.4.2.1.2.1) Open Circuit Voltage 50
2.4.2.1.2.2) Electromotive Force 51
2.4.2.1.2.3) Internal Resistance 51
2.4.2.1.2.4) Impedance Spectroscopy 51
2.4.2.1.3) Model Based Methods 51
2.4.2.2) State of Health 52
2.4.2.3) Thermal Management 53
2.4.2.4) Cell Balancing 54
2.4.2.4.1) Passive 54
2.4.2.4.2) Active 55
2.4.2) Structures of Battery Management System 55
2.4.3) Energy Management System 57
2.4.3.1) Hardware Level 58
2.4.3.1) Software Level 58
2.5) Regenerative Braking 61
2.5.1) Operation of Regenerative Braking 62
2.5.2) Control Strategy 64
2.5.3) Enhancement of Regenerative Braking System 64

2.5.3.1) Flywheel 65
2.5.3.1.1) Characteristic of Flywheel 66
2.5.3.2) Supercapacitors 66
2.6) Overview of Supercapacitors and Energy Storage 66
2.6.1) Electrostatic Double-Layer Capacitor 67
2.6.2) Pseudo Capacitor 68
2.6.4) Energy Storage 69
2.6.4.1) Passive 70
2.6.4.2) Semi-Active 70
2.6.4.2.1) Controlled SC 71
2.6.4.2.2) Controlled Battery 71
2.6.4.3) Fully Active 71
2.7) Traction Motor Selection 74
2.7.1) DC Brushless Motor 75
2.7.2) Induction Motor 75
2.7.3) Permanent Magnet Synchronous Motor 75
2.7.4) Switched Reluctance Motor 76
2.7.5) Study of Motor Drives Efficiency 76
2.8) Driving Cycles 78
2.8.1) Types of Driving Cycles 78
2.8.2) Developing Driving Cycle 80
2.9) Summary 80
Chapter 3 Control Strategies for Hybrid Energy Storage Systems in Electric Vehicles 81
3.1) Brief 81
3.2) Background 81
3.3) Designing and Modelling a Hybrid Energy Storage System 81
3.3.1) Structural Framework 82
3.3.2) Vehicle Model 82
3.3.3) Battery Model 83
3.3.4) Supercapacitor Model 85
3.4) Controller Design 86
3.4.1) Proportional-Integral Control 87
3.4.2) Model Predictive Control 88
3.4.3) Radial Basis Function Control 89
3.4.3.1) Leaning Strategies 91
3.4.3.2) Gaussian Activation Function 92

3.4.3.3) Parameter Adjustment Using Gradient Descent 92
3.4.3.4) Adaptive Leaning Rate 93
3.4.3.5) DC-DC Converter Optimisation 94
3.4.3.6) Adaptive Mechanisms and Efficiency 94
3.5) Comparative Analysis of Control Strategies 95
3.6) Summary 96
Chapter 4 Comparative Analysis of Hybrid Energy Storage Systems and Brushless DC Motor Speed Control Methods 98
4.1) Brief 98
4.2) Energy Storage Components and Discharge Characteristics 99
4.3) BLDC Motor Overview 100
4.3.1) Architecture 100
4.3.2) Mathematical Modelling of BLDC 103
4.4) Comparative Study 104
4.4.1) Simulation Setup 104
4.4.2) Results 106
4.4.3) Discussion 108
4.5) Summary 108
Chapter 5 Optimising Energy Efficiency in Electric Vehicles through Hybrid Energy Storage Systems and Advanced Control Strategies 109
5.1) Brief 109
5.2) Analysis and Performance Modelling of a Hybrid Energy Storage System 109
5.2.1) Vehicle Dynamics Model 110
5.2.2) Battery and Supercapacitor Models 110
5.3) Control Strategies for HESS 111
5.4) Simulations and Results 111
5.4.1) Chosen Driving Cycles 112
5.4.1.1) US06 113
5.4.1.2) SC03 115
5.4.1.3 Discussion 117
5.4.1.3.1 Battery Power Profile 117
5.4.1.3.2 Supercapacitor Power Profile 117
5.4.1.3.3 State of Charge 117
5.4.1.4 Conclusions 118
5.5) Summary 118

Chapter 6 Improving the Efficiency of Electric Vehicles: Advancements in Hybrid Energy Storage Systems 119
6.1) Brief 119
6.2) Contributions 119
6.3) Hybrid Energy Storage Systems and Control Models 119
6.4) Results and Discussion 120
6.4.1) Impact of HESSs on Battery Performance 122
6.4.1.1) Artemis Rural Cycle 123
6.4.1.2) Artemis Motorway Cycle 124
6.4.1.3) US06 Cycle 125
6.4.1.4) Energy Saved Calculation 126
6.4.1.4) Comment 126
6.4.2) Impact of HESSs on SC Performance 128
6.4.2.1) Artemis Rural Cycle 128
6.4.2.2) Artemis Motorway Cycle 129
6.4.2.3) US06 Cycle 131
6.4.3) Validation of Control Strategies 132
6.4.4) Overall System Efficiency and Performance 134
6.5) Summary 135
Chapter 7 Conclusions and Future Work 136
7.1) Conclusions 136
7.2) Future work 137
List of References 139
Appendices 150
Appendix A: Appendix A: MATLAB Simulation Code and Setup Details for Battery and Supercapacitor Discharge Characteristics 150
List of Publications 152
Journals 152
Conferences 152

List of Figures

Figure 1.1 - EV Sales Worldwide from 2016 to 2023 17
Figure 1.2 - Sales of New Cars from 2010 to 2023 18
Figure 1.3 - Savings in Cost per Kilometre for Various Vehicle Technologies 20
Figure 1.4 – Different Types of Vehicles 20
Figure 1.5 - Series Hybrid [9] 21
Figure 1.6 - Parallel Hybrid [9] 21
Figure 1.7 - Series/parallel hybrid [9] 22
Figure 1.8 - Series PHEV [11] 23
Figure 1.9 - Parallel PHEV [11] 23
Figure 1.10 - Single Motor Powertrain [12] 24
Figure 1.11 - Distributed Multi Motor Driven Powertrain: (**a**) Dual Motor Powertrain, (**b**) Triple Motor Powertrain, (**c**) Four Motor Powertrain [12] 26
Figure 1.12 - Methods for Charging EV Battery [15] 27
Figure 1.13 – Inductive Charging 28
Figure 1.14 - Key Influences on Electric Vehicle Adoption 32

Figure 2.1 - Operation of a Lithium-Ion Battery [24] 37
Figure 2.2 - Comparison of Various Battery Technologies [25] 38
Figure 2.3 - Operation of Lithium-ion Battery During Charging and Discharging [41] 41
Figure 2.4 - Charging and Discharging Characteristics of a Lithium-Ion Battery [42] 42
Figure 2.5 - Lithium-ion battery characteristics: (**a**) open-circuit voltage under various temperatures, (**b**) capacity of Lithium-ion batteries under various temperatures, (**c**) resistance of Lithium-ion batteries under various temperatures, (**d**) Persistence of battery capacity under warm and cold temperature conditions, (**e**) persistence of battery capacity under warm and cold temperature conditions [49]. 43
Figure 2.6 - Battery charging approaches [26] 44
Figure 2.7 - Lithium-ion Battery Modelling Approaches [53] 46
Figure 2.8 - Classification of Battery Defects [58] 48
Figure 2.9 - Block diagram of the BMS [12] 49
Figure 2.10 - Optimal Lithium-ion battery temperature range [12] 54
Figure 2.11 – Passive Balancing [12] 55
Figure 2.12 – Active Balancing [12] 55
Figure 2.13 - Layers of EMS in EVs [70] 58
Figure 2.14 - Strategies for High Level Supervisorial Control [23] 59
Figure 2.15 - Forward driving condition [75] 63
Figure 2.16 - Regenerative braking condition [75] 63
Figure 2.17 - Three-phase inverter [76] 64
Figure 2.18 - Flywheel Mechanism [78] 66
Figure 2.19 - Schematic representation of EDLC. (**a**) Charge state. (**b**) Discharge state [82] 68
Figure 2.20 - Schematic representation of pseudo-capacitor [83] 69
Figure 2.21 - Comparison of Energy Storage Devices [12] 70
Figure 2.22 - HESS configurations: (**a**) passive parallel, (**b**) controlled SC, (**c**) controlled battery, (**d**) fully active [12] 73
Figure 2.23 - Types of electrical motors [89] 74
Figure 2.24 - New European Driving Cycle [111] 79

Figure 2.25 - Federal Test Procedure Cycle [111] 79

Figure 3.1 – Vehicle Forces 83
Figure 3.2 - Battery Equivalent Circuit [116].. 85
Figure 3.3 - SC Equivalent Circuit [116] 86
Figure 3.4 - Construction of the Proposed System.. 87
Figure 3.5 – Simple RBF Structure [117] 90
Figure 3.6 – Detailed RBF Network 91
Figure 3.7 - Different Activation Functions: (**a**) Sigmoid, (**b**) Gaussian [117] 91
Figure 3.8 - RBF Controller Schematic with Gradient Descent Parameter Optimisation 93
Figure 3.9 - Exponential Function for Adaptive Learning Rate 94

Figure 4.1 - Discharge Characteristics of the Battery and the Supercapacitor 100
Figure 4.2 - Three-phase voltage Inverter for BLDC Motor Control [117] 101
Figure 4.3 - BLDC Motor with Six Step Commutation [117] 102
Figure 4.4 - Simulink BLDC Motor Model [117] 106
Figure 4.5 - Traditional PI Controller Speed Response 107
Figure 4.6 - RBF Controller Speed Response... 107

Figure 5.1 - Proposed Fully Active HESS Topology 110
Figure 5.2 - Flowchart of Operation of HESS... 112
Figure 5.3 - Selected driving cycles: (**a**) US06, (**b**) SC03... 113
Figure 5.4 - Power Demand of US06 Cycle 113
Figure 5.5 – Outcome Results of US06 Cycle: (**a**) Battery Profile using PI, (**b**) Battery Profile using RBF, (**c**) SC Profile using PI, (**d**) SC Profile using RBF, (**e**) Battery SOC using PI, (**f**) Battery SOC using RBF, (**g**) SC SOC using PI, (**h**) SC SOC using RBF 114
Figure 5.6 - Power Demand of US06 Cycle 115
Figure 5.7 - Outcome Results of SC03 Cycle: (**a**) Battery Profile using PI, (**b**) Battery Profile using RBF, (**c**) SC Profile using PI, (**d**) SC Profile using RBF, (**e**) Battery SOC using PI, (**f**) Battery SOC using RBF, (**g**) SC SOC using PI, (**h**) SC SOC using RBF 116

Figure 6.1 - Representation of Selected Driving Cycles: (**a**) Artemis Rural, (**b**) Artemis Motorway, (**c**) US06 122
Figure 6.2 - Battery SOC comparison over time for an HESS versus a standalone battery across various control strategies for the Artemis rural cycle. (**a**) SOC decay under the RBF, (**b**) SOC decay under the MPC, (**c**) SOC decay under the PI 124
Figure 6.3 - Battery SOC comparison over time for an HESS versus a standalone battery across various control strategies for the Artemis motorway cycle. (**a**) SOC decay under the RBF, (**b**) SOC decay under the MPC, (**c**) SOC decay under the PI 125
Figure 6.4 - Battery SOC comparison over time for an HESS versus a standalone battery across various control strategies for US06. (**a**) SOC decay under the RBF, (**b**) SOC decay under the MPC, (**c**) SOC decay under the PI 126

Figure 6.5 - Artemis Rural: (**a**) SOC of SC, (**b**) Charging/Discharging Profile of SC, (**c**) Charging/Discharging Profile of Battery 129
Figure 6.6 - Artemis Motorway: (a) SOC of SC, (b) Charging/Discharging Profile of SC, (c) Charging/Discharging Profile of Battery 131
Figure 6.7 - US06: (**a**) SOC of SC, (**b**) Charging/Discharging Profile of SC, (**c**) Charging/Discharging Profile of Battery 132
Figure 6.8 - Motor Profile of Selected Driving Cycles Motor (**a**) Artemis Rural, (**b**) Artemis Motorway, (**c**) US06........ 134

List of Tables

Table 1.1 - Pros and Cons of Inductive Charging [16] 28
Table 1.2 - Charging Modes [16], [19], [20], [21] 30
Table 1.3 - Standardisation of Power Plugs [10], [16], [22] 31

Table 2.1 - A Survey of Different Battery Technologies [12], [26], [27], [28], [29] 38
Table 2.2 - Battery Charging Algorithms [26] 45
Table 2.3 - Comparison of Different Battery Model Approaches [54], [55][56] 47
Table 2.4 - Outline of the various SOC approaches [27] 52
Table 2.5 - Overview of BMS topologies [69] 57
Table 2.6 - Comparison of Global Optimisation Algorithms [12] [70] 61
Table 2.7 - Pros and Cons of Regenerative Braking [72], [73] 62
Table 2.8 - Motor Drives Performance Evaluation [93], [96], [105], [106], [107][108] 77
Table 2.9 - Different Driving Cycle Categories [110] 79

Table 3.1 - Overview of control strategy performance in EVs [113] 96

Table 4.1 - Truth table for the Gate Pulse and Decoder [128] 103
Table 4.2 - Parameters Used in the Simulation [117] 105

Table 5.1 - Simulation Module-Specific Parameters 111
Table 5.2 - Attributes of each Driving Cycle 112

Table 6.1 - Specifications for EV, battery, and SC modules [133], [134] 121
Table 6. 2 - Characteristics of each Driving Cycle [135] 122
Table 6.3 - Comparison of Battery SOC for Artemis Rural 127
Table 6.4 - Comparison of Battery SOC for Artemis Motorway 127
Table 6.5 - Comparison of Battery SOC for US06 128

Abbreviations

AC	Alternating current
Ah	Ampere hour
AEKF	Adaptive extended Kalman filter
ANN	Artificial Neural Network
BEV	Battery electric vehicle
BLDC	Brushless direct current
BMS	Battery management system
CAN	Controller Area Network
CC	Coulomb Counting
CCS	Combined charging system
CHAdeMO	Charge de move
C_{rate}	Current rate
DC	Direct current
DP	Dynamic programming
EDLC	Electric double-layer capacitor
EKF	Extended Kalman filter
EMF	Electromotive Force
EMS	Energy Management System
ESS	Energy storage system
EV	Electromotive force
FTP 75	Federal test procedure
GPS	Global positioning system
HESS	Hybrid energy storage system
HEV	Hybrid electric vehicle

ICE	Internal combustion engine
IM	Induction motor
IR	Internal resistance
IS	Impedance spectroscopy
I-V-I	Constant current – constant voltage – constant current
KE	Kinetic energy
KF	Kalman filter
km/h	Kilo meter per hour
kWh	Kilo watt hour
LA	Lead acid
MOSFET	Metal oxide semiconductor field effect transistor
MPC	Model predictive control
NEDC	New European driving cycle
NICad	Nickel cadmium
NiMH	Nickel metal hydride
OCV	Open circuit voltage
P2D	Pseudo 2 dimensional
PHEV	Plug in hybrid electric vehicle
PMC	Power management control
PMSM	Permanent magnet synchronous motors
PNGV	Partnership for new generation of vehicle
PWM	Pulse width modulation
RBF	Radial Basis Function
RC	Resistor-capacitor
RPM	Revolutions per minute

SC	Supercapacitor
SOC	State of charge
SOH	State of health
SP	Single particle
SP3	Improved single particle model
SRM	Switch reluctance motor
UKF	Unscented Kalman filtering
VDFD	variable frequency drive
WTW	Whell to wheel

Chapter 1 Introduction

Recently, the world has noticed an unprecedented rise in the scale of the electric vehicle (EV) market, which may signal a growing interest in eco-friendly modes of transportation. The number of registered sales of EVs has surpassed 10 million sales by 2022, from 3.7 million in 2020 representing around 4% of total vehicles sold. This rate improved to 14% in 2022, an almighty leap towards mainstream adoption of EVs in the marketplace. That is why estimates show that EV sales will increase to fourteen million by the end of 2023, and will comprise 18% of all vehicle sales. Figure 1.1 shows the sharp rise in the sale of electric vehicles and their rising share in the market in the last decade, with the data being adopted from the International Energy Agency[1].

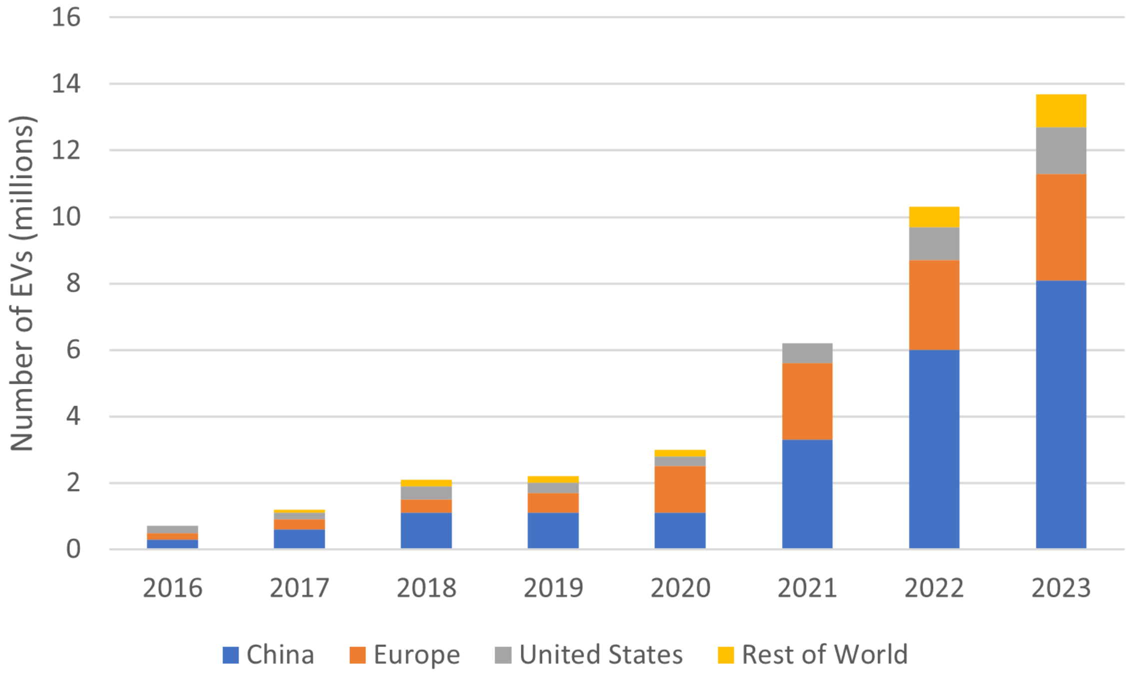

Figure 1.1 - EV Sales Worldwide from 2016 to 2023

The tremendous increase in EV adoption results from technological advancements, regulatory benefits, and growing environmental awareness. Global governments have implemented various measures to encourage the adoption of electric vehicles, including tax incentives, purchasing subsidies, and funding for charging infrastructure. Moreover, the fluctuation in the price of oil has motivated consumers to explore EVs [1].

Figure 1.2 presents insightful data concerning a significant aspect of the transforming automotive industry: the decline in sales of internal combustion engine (ICE) vehicles [2]. With the increase in sales of EVs, the market share of conventional ICE vehicles has consequently declined. This pattern highlights the changing consumer demand for more environmentally friendly transportation options and shows the influence of governmental actions that attempt to decrease carbon emissions and encourage greener options.

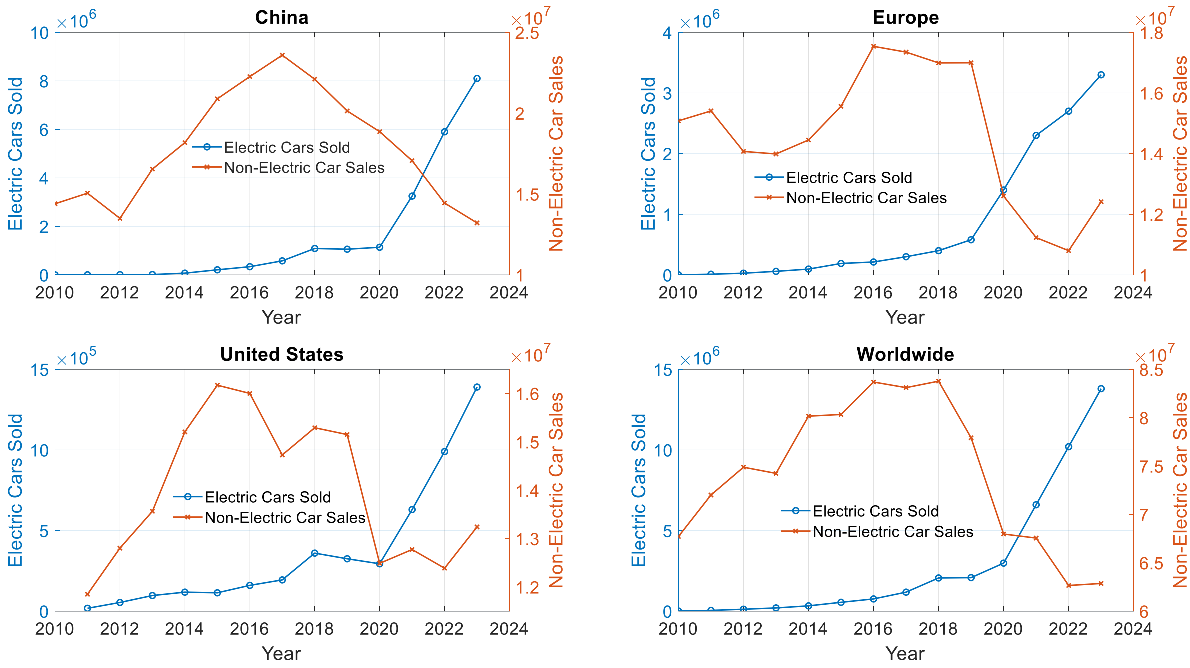

Figure 1.2 - Sales of New Cars from 2010 to 2023

Upon careful analysis of Figure 1.1 and Figure 1.2 together, a distinct scenario emerges, illustrating the advancement of the EV market and its profound influence on the wider automotive sector. Figure 1.1 presents a statistical analysis of the market expansion for EVs, whereas Figure 1.2 illustrates the associated drop in sales of ICE vehicles. The decrease in sales of ICE vehicles is a direct result of the rising popularity of EVs, which is driven by justifications such as breakthroughs in EV technology, legislative frameworks that provide incentives for cleaner vehicles, and increasing consumer awareness regarding environmental sustainability.

The significance of constant development along with encouraging legislation in maintaining the progress of EV uptake is highlighted by these interconnected components. As illustrated in the data, the outlook for the EV market is optimistic, with forecasts predicting consistent expansion and a growing proportion of EVs in the worldwide automotive market. By persistently tackling technological, regulatory, and environmental obstacles, the industry can continue its upward progress and make a substantial contribution to global sustainability objectives.

1.1) Motivation

EVs have come a long way from their mid-19th-century inception, when Scottish inventor Robert Anderson unveiled a prototype. The advancement of early EVs was greatly aided by the invention of rechargeable batteries in 1865 by Gaston Plante and subsequent refinements in 1881 by Camille Faure. At the close of the nineteenth century, these vehicles were more economically viable than gasoline-powered vehicles for use as taxis in New York City [3].

Throughout the 20th century, EVs experienced fluctuations in recognition. At the beginning, EVs occupied a favourable market position on account of their clear design and dependable nature, in contrast to the massive steam vehicles and less sophisticated petrol vehicles that dominated the era. Nevertheless, the introduction of the Ford Model T and the accessibility of inexpensive oil resulted in a transformation of public and commercial inclination towards gasoline-powered automobiles, ultimately leading to a reduction in the production and utilisation of EVs [3].

The oil crisis in the 1960s sparked a renewed interest in EVs, highlighting the importance of transportation options that are both environmentally benign and energy-efficient [1]. This established the foundation for the contemporary electric vehicle industry, distinguished by notable technological progress and a primary emphasis on diminishing carbon emissions and improving urban air quality [2]. Currently, the transition to EVs is motivated by the pressing necessity to decrease reliance on fossil fuels and tackle the environmental problems created by ICE. Due to the current crisis of severe air pollution and greenhouse gas emissions, EVs present a possible solution. They achieve this by eliminating emissions from the exhaust, thereby greatly reducing both urban air pollution and the negative implications of global climate change [2].

EVs have serious positive effects on the environment. Nearly 28% of the world's CO_2 emissions come from the transportation sector, with more than 70% of those emissions coming from vehicles on the road [4]. A big step towards lowering this carbon footprint would be to switch to EVs run by renewable energy. When renewable energy is used, the wheel-to-wheel (WTW) efficiency of EVs, which quantifies the overall energy conversion efficiency from the extraction of fuel to the delivery of power at the wheels, can achieve a maximum of 70%. The efficiency of petrol and diesel vehicles, which ranges from 11% to 37% [5].

The driving experience using EVs also turns out significantly better in other aspects. The lack of engine noise and vibrations boosts the overall comfort of the ride, resulting in a cleaner and better experience. Electric motors deliver immediate torque, providing robust and steady acceleration throughout the whole range of speeds [6]. This effectiveness not only enriches the enjoyment of driving but also improves the vehicle's responsiveness and reliability. Further, the EVs maintenance expenses and energy consumption prices are significantly reduced when compared to the maintenance and fuel expenses of conventional combustion vehicles. EVs have a considerably reduced energy cost per kilometre compared to regular vehicles, as demonstrated in Figure 1.3 [7].

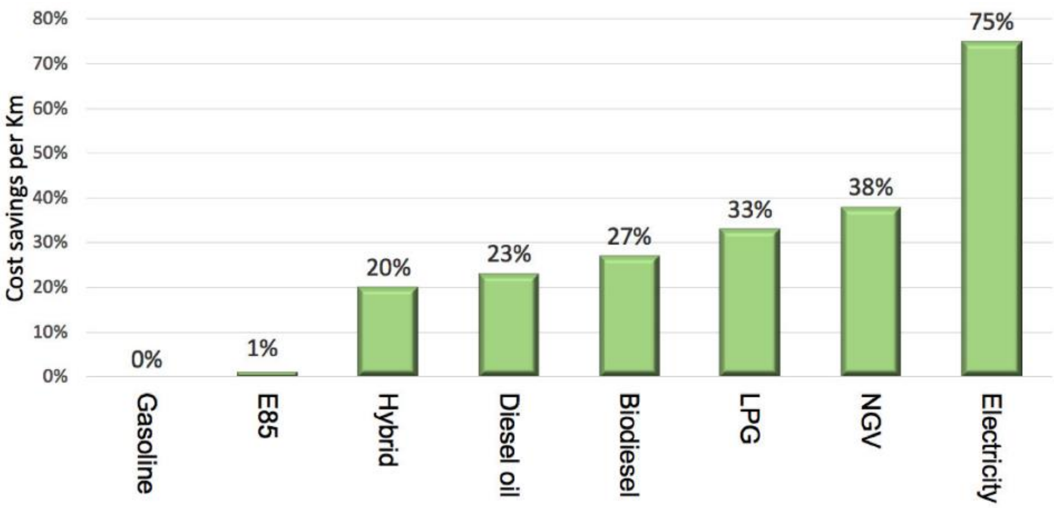

Figure 1.3 - Savings in Cost per Kilometre for Various Vehicle Technologies

1.2) Background of EVs

Since the start of EVs, many different kinds have been manufactured, including a wide array of technologies in their functioning. The reliability of the components of an advanced EV, mainly its energy supply during operation, determines the vehicle's classification, known as hybrid electric vehicle (HEV), plugin hybrid electric vehicle (PHEV), and fully EV, as illustrated in Figure 1.4. These many types have the same electric motor and battery as their primary commonality. Next subsection discusses various types of EV.

Figure 1.4 – Different Types of Vehicles

1.3.1) HEV

HEVs are electric-only vehicles. HEVs obtain their energy from the battery, whereas the HEV battery utilises a petrol engine as a reserve to provide electricity to run the electric motor. The following describes the objective of HEV:

- Fuel economy and vehicle efficiency are superior compared to ICE.
- Equipped with an electric motor.

Depending on the drivetrain, there is a variety of HEVs. EVs have a series of components known as a 'drivetrain' that transfers power from the motor to the wheels. This determines how the electric motor will function in conjunction with the traditional ICE. There are three different configurations used in HEVs are:

1.3.1.1) Series Powertrain

Complete conversion of the mechanical engine to electrical energy, as shown in Figure 1.5. There is no mechanical connection between the vehicle's engine or fuel cell and its wheels [8].

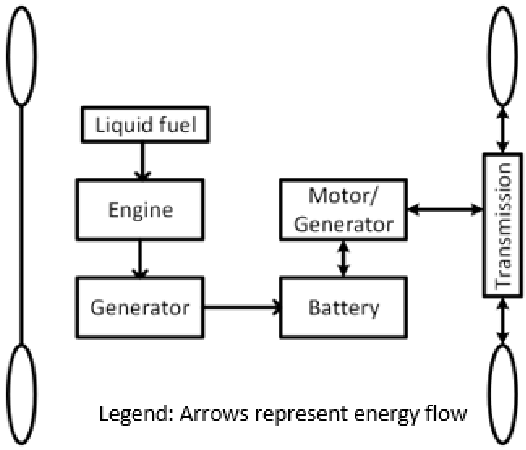

Figure 1.5 - Series Hybrid [9]

1.3.1.2) Parallel Powertrain

The drivetrain is connected to the engines as well as the electric motor/generator, as shown in Figure 1.6. The power sources can propel the vehicle independently or combined [8].

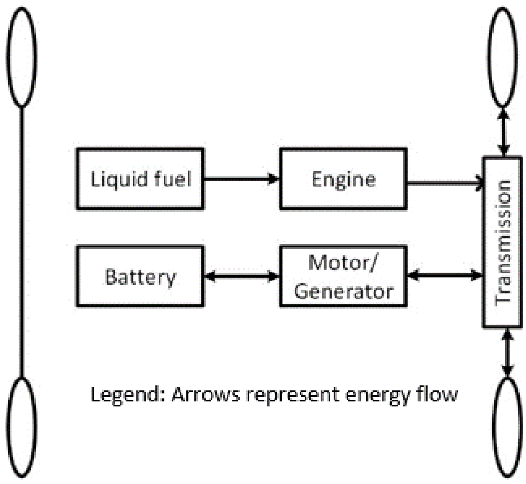

Figure 1.6 - Parallel Hybrid [9]

1.3.1.3) Series/Parallel Powertrain

The mechanical power of the engine can be partially turned into electrical and mechanical energy for driving purposes [8]. The hybrid layout consists of a series and a parallel arrangement, as shown in Figure 1.7.

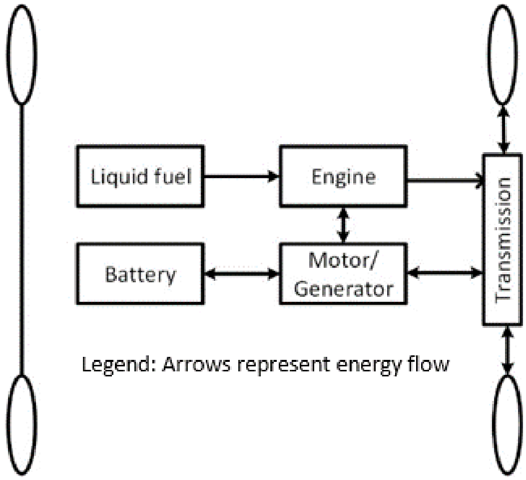

Figure 1.7 - Series/parallel hybrid [9]

1.3.2) PHEV

PHEVs combine fuel combustion with an electric motor to increase the vehicle's driving distance. A PHEV's battery can be recharged by connecting it to a conventional electrical plug. PHEVs may drive short distances with electric power and switch to fuel mode for longer trips. The vehicle's fuel consumption is optimised based on the distance driven by switching between the battery and petrol [10].

There are two configurations for PHEVs: series and hybrid. This concept is commonly known as a range-extended EV operating in series mode. The ICE functions as a generator, providing electricity to the battery through power electronics, thus extending the vehicle's range [10]. Figure 1.8 displays the configuration of the series PHEV.

During parallel mode of operation, the vehicle is propelled by both an ICE and an electric motor, and the driver can typically choose between the two power sources. A differential gear is utilised to mechanically link two power sources in the following configuration [10]. They comprise three key components: an ICE, a battery, and an electric motor, as depicted in Figure 1.9.

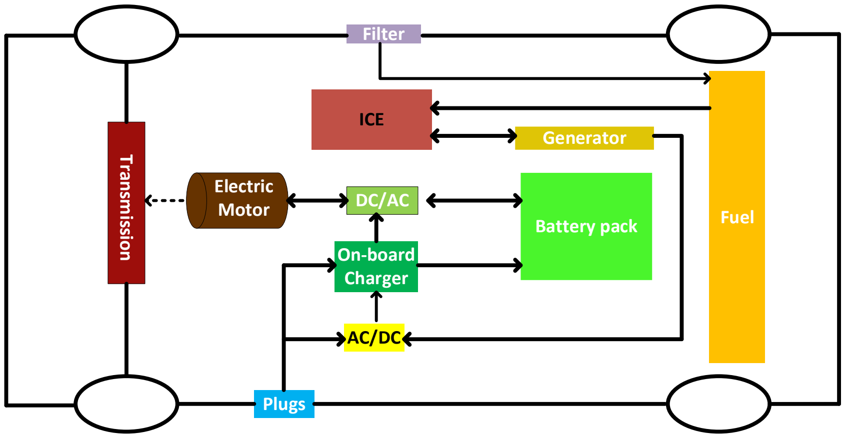

Figure 1.8 - Series PHEV [11]

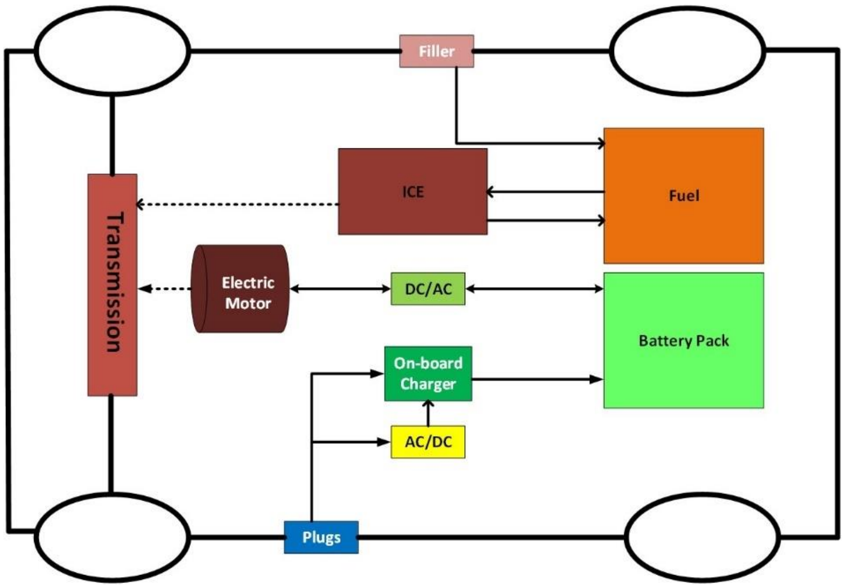

Figure 1.9 - Parallel PHEV [11]

1.3.3) Fully EV

The vehicle is solely powered by energy produced by a battery pack and does not rely on petrol. An electric vehicle's range is defined by the distance it can go before requiring a recharge. Today's battery electric vehicles are consistently improving their range. To recharge, they need to be connected to the electric power grid.

The EV powertrain is organised into many configurations to optimise power management, improve vehicle performance and durability, and minimise transmission energy loss. EV powertrains can be categorised into two types: centralised single motor-driven powertrains and distributed multi-motor driven powertrains, based on the number of motors utilised in the vehicle and their design. Some electric vehicles prioritise distributed multi-motor driven powertrains, which fall into three main categories: dual-motor, triple-motor, and four-motor powertrains [12] [13].

1.3.3.1) Centralised Single Motor Driven Powertrain

The centralised single motor speed-driven powertrain is a widespread configuration for modern EV, as depicted in Figure 1.10. The electric motor is set up in a front-wheel-drive arrangement in a single motor topology. Additionally, there is a differential that enables the wheels to revolve at different rates. The motor transmits electrical energy from the battery into mechanical energy, enabling the vehicle to move. During the regenerative procedure, it functions as a generator, transferring energy to the energy source [12] [13].

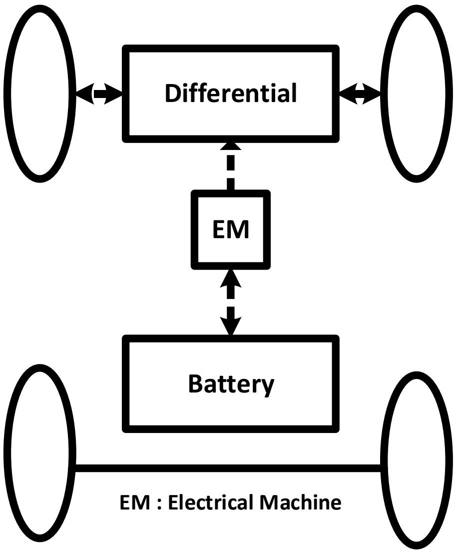

Figure 1.10 - Single Motor Powertrain [12]

1.3.3.2) Distributed Multi Motor Driven Powertrain

In a dual-motor layout, two motors are positioned in separate locations within the vehicle, as shown in Figure 1.11a. This setup inherently delivers increased horsepower due to the merged torque of two motors, resulting in a substantial boost in acceleration. A dual-motor system provides improved efficiency and speed compared to a single motor in an electric vehicle, especially at higher elevations[12].

The system includes two motors, one on each axle, attached to planetary gears, transferring torque via a fixed gear shaft. One or two different battery packs can power the front and back motors. A two-motor, two-axle system allows for flexible power and torque distribution, along with the ability to utilise various gear ratios in the gearboxes. Dual traction drives increase overall tractive effort at all speeds as opposed to a single drive with the same power ratings [14]. Utilising several traction motors enhances vehicle torque vectoring, leading to improved traction, stability control, and overall reliability. The dual-motor technology offers advantages such as increased speeds, rapid deceleration, and the option to utilise one motor for propulsion while the other recharges, thus increasing the travel distance without the need for regular recharging. Dual-motor systems are pricier and more intricate to put together, and they do not have standard transmissions.

A triple-motor powertrain system consists of one motor on the front axle and two motors on the rear axle, resulting in an all-wheel-drive vehicle, as shown in Figure 1.11b. The rear motors power each wheel for improved efficiency during regular driving, while the front motor engages to boost performance. Every electric motor is linked to the corresponding wheel on the rear axle using a single-speed gearbox. An electric torque vectoring mechanism eliminates the necessity of a mechanical differential, significantly improving the performance, handling, stability, and traction of the all-wheel-drive system [12].

Four-motor powertrain systems, seen in Figure 1.11c, are categorised as exceptional managing all-wheel-drive systems. Every wheel is equipped with an own motor, enabling accurate application of torque. Electronic torque vectoring in an electric vehicle with four motors enhances speed and responsiveness by electronically controlling power distribution to each motor, as opposed to using mechanical methods [12].

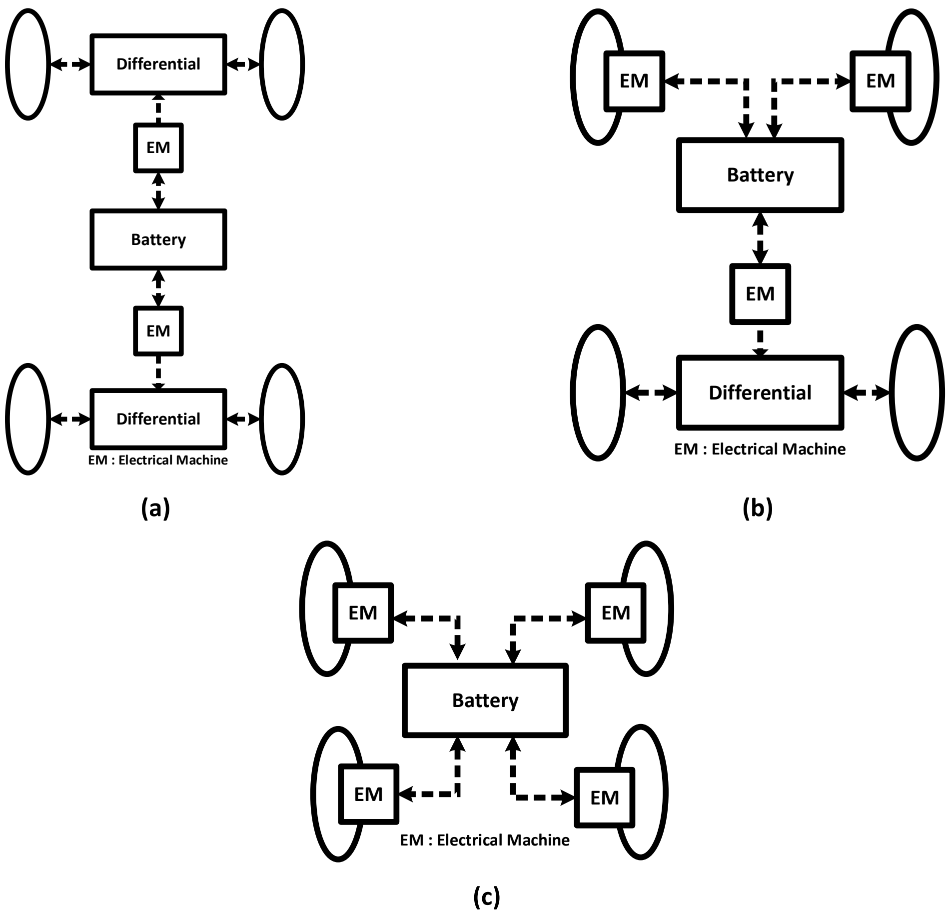

Figure 1.11 - Distributed Multi Motor Driven Powertrain: (**a**) Dual Motor Powertrain, (**b**) Triple Motor Powertrain, (**c**) Four Motor Powertrain [12]

1.3.4) Charging Stations

A charging station is a device that connects an EV to a power source to recharge its battery. Installing charging facilities is crucial for encouraging the widespread use of EVs, both for personal transportation and in work environments. Several municipal facilities privately construct charging infrastructure for their personal use, while local governments promote the adoption of EVs by establishing charging stations for the public and offering subsidised EV parking. Residents usually install private charging stations in their driveways or garages, they are connected to the primary power source. Furthermore, there exist multiple standards for charging adapters.

1.3.4.1) Charging Infrastructure Regulations

There are different methods available for charging EVs, including conductive charging, inductive charging, and battery swapping. Figure 1.12 demonstrates several charging methods.

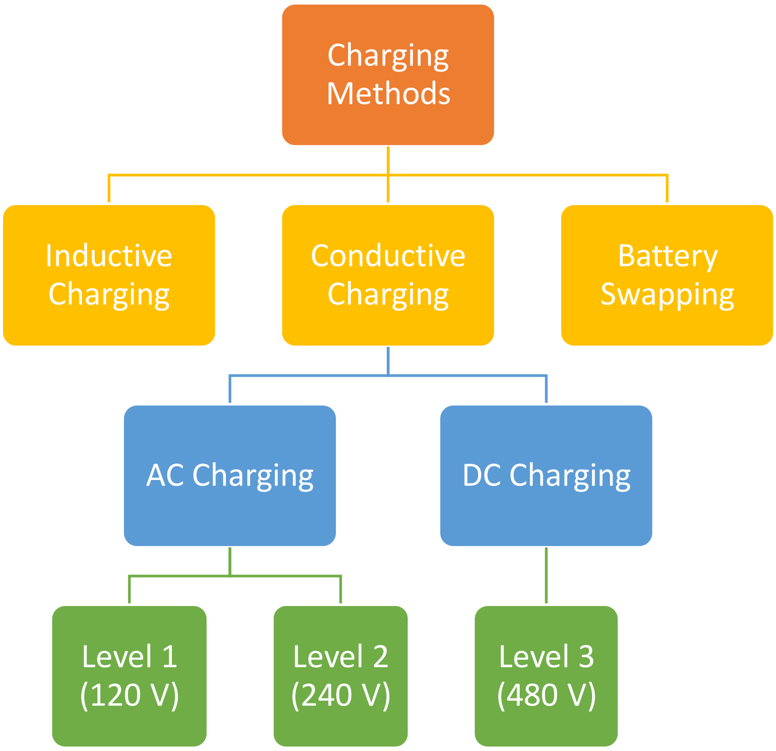

Figure 1.12 - Methods for Charging EV Battery [15]

1.3.4.1.1) Inductive Charging

Inductive charging utilises an electromagnetic field to transmit electrical energy from a charging unit to a battery without the need for an actual connection, as shown in Figure 1.13. This method utilises a transmitter circuit to generate an alternating current (AC) that flows through a coil, thus forming a magnetic field. The presence of this field causes an electric current to be generated in a secondary coil that is located nearby [10]. Subsequently, the vehicle transforms the induced AC into direct current (DC) to recharge the battery. These systems, particularly advantageous on bus routes, reduce the requirement for conventional charging stations by integrating charging capabilities directly into the road surface. Presently, induction charging systems have restrictions on the amount of power they can handle, typically ranging from 3.3 kW to 20 kW in more modern configurations. Consequently, this leads to extended charging durations [10][16]. However, ongoing advancements are being made in this technology. It is expected that rapid induction charging will become possible in the next decade as technology improves and the number of EVs on the road increases, making it more appealing to deploy this type of infrastructure. Table 1.1 illustrates the pros and cons of the inductive charging method.

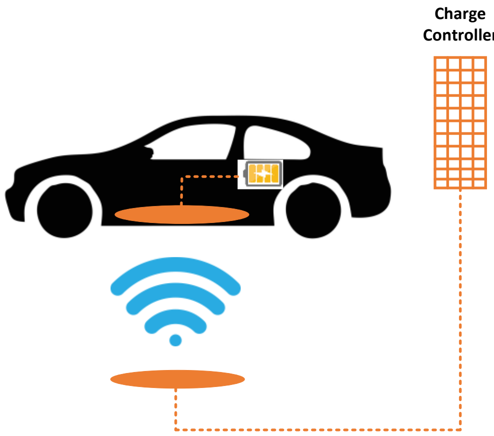

Figure 2.13 – Inductive Charging

Table 1.1 - Pros and Cons of Inductive Charging [16]

Pros	Cons
Reliable	Slow charging
Protected Connections	Expensive
Low infection risk	Inconvenience
Increased convenience and aesthetic quality	
Cables not required	

1.3.4.1.2) Conductive Charging

This charging method encompasses both AC and DC options. AC charging is categorised into two levels: level 1 and level 2. On the other hand, DC charging encompasses level 3 [15]. Level 1 chargers utilise standard 120-volt AC connectors usually found in residential outlets and do not require extra charging equipment [17]. The process of recharging a battery normally requires a time frame of 8 to 12 hours, and it is commonly carried out at home during the night when electricity costs are cheaper [16], [17]. Level 2 chargers utilise a 240-volt AC plug and necessitate deployment either in residential settings or public areas. These chargers have a charging time of 4 to 6 hours for a battery and are commonly found in public parking locations [17]. Level 3 charging, also known as DC rapid charging, uses a 480 V DC connection and can fully charge the battery of an EV in around 20-30 minutes. This makes it well-suited for commercial and public locations [17].

1.3.4.1.3) Battery Swapping

Battery swapping is a process in which the battery of an EV is taken out and charged separately, meanwhile, a fully charged battery is put into the vehicle at the same time. This strategy provides numerous benefits for both vehicle owners and the electrical infrastructure. The main benefit for automobile owners is the significant decrease in charging time to around five minutes, which may relieve concerns about the distance a car can go on a single charge and reduce the requirement for high battery capacities [10] [18].

From a social standpoint, this approach is attractive as it facilitates battery charging during periods of low electrical demand, thereby mitigating power grid strain, and preventing voltage issues. Moreover, these batteries have the potential to reduce the maximum amount of power needed at any given time by returning energy to the electrical grid. This not only improves the stability of the system but also brings advantages to the community and promotes the integration of renewable energy sources [10].

Nevertheless, the approach does present certain difficulties. The primary challenge lies in achieving battery standardisation, since manufacturers may be hesitant to reach a consensus on a universally accepted battery model. This reluctance could potentially impede the progress of vehicle design and development. Due to the weight of the batteries, which varies between 100 kg and 500 kg, automated handling is required. Moreover, the substantial expenses associated with establishing battery switching stations can deter potential investors. [10] [18].

1.3.5) EV Charging Modes

The charging modes provide extensive guidance regarding how to securely attach an EV to a charging station. These are categorised into four distinct categories, as seen in Table 1.2.

Table 1.2 - Charging Modes [16], [19], [20], [21]

Mode	Allowed current per phase	Charging time	Power supply	Description	Connection
1	16 A	4-8 h	Single-phase	Residential socket outlet	
2	32 A	2-4 h	Single-phase or three-phase	Residential plug with cable protection	
3	63 A	1-2h	Three-phase	The controlled, protected EV plug outlet	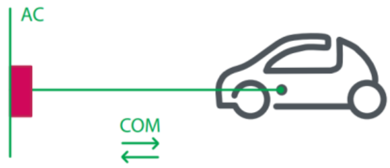
4	100 -125 A (DC)	5-30 min		DC charging	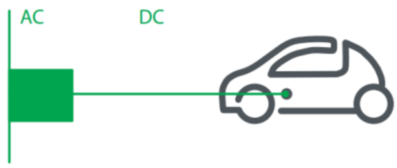

1.3.6) Type of Plugs

Nowadays, EVs utilise various charging connectors, which are carefully described in Table 1.3. The wide range of charging technology options available reflects the changing standards and compatibility needs in the EV sector. While plugs may appear similar in design, their charging capacity is determined by the power system they are connected to; higher-power plugs like 120 kW utilise advanced DC charging systems with greater current and voltage, whereas 43 kW plugs typically rely on AC charging, constrained by onboard charger limitations.

Table 1.3 - Standardisation of Power Plugs [10], [16], [22]

Type of Plugs	Description	Symbol
Type 1	Permits charging of up to 7.4 kW using a single phase of AC current. Mainly used in America.	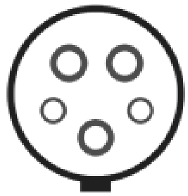
Type 2	Allows for AC triple-phase charging of up to 43 kW. European standard.	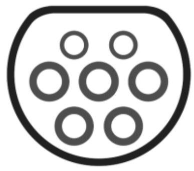
Tesla supercharger	Tesla has developed its own type 2 connection, which is capable of producing 120 kW in both alternating current and continuous current to fit within the European market.	
Combined charging system (CCS)	Two extra power connections make type 2 compatible with AC and DC charging. CCS specifies 80 kW to 350 kW charging power.	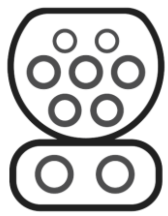
Charge de move (CHAdeMO)	The connector consists of two big pins for DC power and additional pins for CAN-BUS connectivity. CHAdeMO fast chargers currently offer a maximum power output of 50 kW.	

1.3) Challenges and Research Focus

Despite EVs delivering tremendous benefits, their general acceptance has been hampered by various obstacles. The key obstacle that inhibits widespread adoption is the significant initial expenses, mainly due to the cost-prohibitive battery technology. Furthermore, it is imperative to tackle the concerns regarding limited driving distance and extended charging durations to further improve the competitiveness of EVs in comparison to conventional ICE vehicles. Nevertheless, continuous progress in battery technology, such as energy density enhancements and cost decreases, is slowly resolving these problems. Government actions and incentives are crucial in supporting the shift towards EVs [23]. Significant steps for addressing economic and practical constraints include incentives such as tax cuts and purchase subsidies [23]. These solutions not only facilitate the initial adoption of EVs but also enhance the long-term viability of the EV ecosystem.

To surpass vehicles powered by ICE, several challenges must be addressed. The challenges can be classified into practical, economic, social, and environmental factors, as illustrated in Figure 1.14. Practically, the issues that need to be addressed include long charging periods, limited availability of public fast chargers, heavy battery weight, moderate mileage and autonomy, and underdeveloped energy storage and management systems [23]. From an economic standpoint, the major concerns are the expensive cost, the rise in electricity use leading to higher energy expenses, and the lack of profitability in investments [23]. Consumers experience social fear related to a variety of factors, including safety concerns and a reluctance to embrace change, even when rules are in place to encourage it [23]. In terms of environmental impact, the electricity source must be derived from renewable sources. Additionally, the recycling of toxic battery packs is necessary, and the construction process requires the use of rare materials [23].

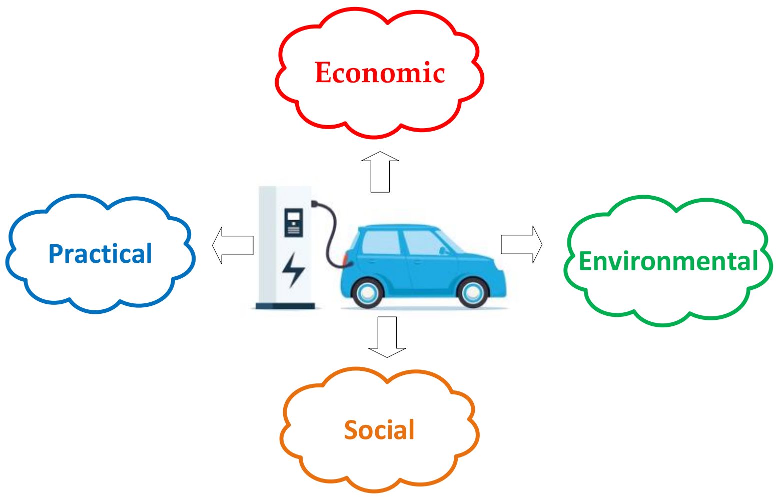

Figure 1.14 - Key Influences on Electric Vehicle Adoption

The goal of this study is to optimise hybrid energy storage systems (HESS) for EVs by combining batteries and supercapacitors (SC) to improve both efficiency and reliability. The study focuses on many research issues such as efficiency and integration barriers, real-time operation limitations, and the stability and resilience of energy management systems (EMS). This initiative aims to address current obstacles and promote the wider use of EVs through the development of complex control strategies and assessing their effectiveness in different driving situations.

Ultimately, the rapid increase in EV sales and the ongoing momentum emphasise the essential contribution of EVs in promoting sustainable mobility. This thesis contributes to the goal by tackling significant technical obstacles and progressing the advancement of efficient and dependable energy management systems for EVs.

1.4.1) Research Challenges

This study investigates six research concerns that are associated with the HESS.

1) Efficiency and Integration Challenges: Examine the obstacles related to effectiveness and the intricacies of merging battery and SC systems in EVs.
2) Boundaries of Control Strategies: Investigate the constraints of existing control strategies (rule-based and optimisation-based) in regulating the power transfer between batteries and SCs.
3) Real-time Operation Constraints: Discuss the difficulties associated with managing HESS in EVs in real-time, considering different driving scenarios.
4) Systems Stability and Robustness: Analyse concerns associated with the energy management system's stabilisation and durability despite environmental fluctuations and dynamics load.
5) Control Algorithm Optimisation: Examine the efficacy of several control algorithms, including proportional–integral controller (PI), model predictive controller (MPC), and radial basis function (RBF), in effectively regulating power flows inside HESS.
6) Evaluating the Influence of Power Management on System Performance: Assess the impact of complex power management systems on the performance characteristics of EVs, such as acceleration responsiveness and energy recovery efficiency.

1.4.2) Objectives

This study utilises five performance metrics of HESS to evaluate the effectiveness of the solutions to the research problems identified:

1) Develop HESS: Evaluates the limitations of traditional energy storage systems and focuses on the design and development of an optimised HESS that combines batteries and supercapacitors. Improvements in energy storage capacity, system reliability, and operational efficiency are highlighted in **Chapter 3**, which discusses the structural framework and advantages of the proposed system.
2) Enhance Control strategies: Advanced control strategies, including Proportional-Integral (PI), Model Predictive Control (MPC), and Radial Basis Function (RBF) controllers, are developed and compared to traditional rule-based methods. The objective focuses on reducing energy losses and enhancing power management, which is detailed in **Chapters 3, 4, 5 & 6** , where the strategies are evaluated through comparative simulations.

3) Asses System Adaptability: The adaptability of the HESS is assessed under diverse driving conditions, including urban, rural, and highway scenarios, using standard driving cycles such as Artemis Rural, Artemis Motorway, and US06. The system's ability to handle dynamic load demands is discussed in **Chapter 5 & 6**, where its performance under real-world simulations is examined.
4) Asses Operational Efficiency: Implement control strategies to improve the HESS's responsiveness to environmental and load variations, ensuring optimal energy distribution and performance under varying conditions. **Chapter 6** presents validation of the system's operational capabilities through simulations and performance modelling.
5) Evaluate the Performance of Control Strategy: The performance of the developed control strategies is assessed through simulations and analysis to ensure their reliability and effectiveness in energy management for EVs. Their impact on energy recovery, state-of-charge stability, and battery lifespan is benchmarked against conventional systems. **Chapters 5 & 6** present a comprehensive evaluation, supported by simulation results, to validate the suitability of these strategies for hybrid energy storage systems.

1.4) Thesis Outline

This thesis is broken down into seven different chapters, each of which presents relevance to one of the purposes of the dissertation.

Chapter 1: Provides relevant background information concerning the implementation of EVs. Following that, an in-depth explanation of the research motivation, goals, and objectives, along with the structure of the dissertation, will be presented.

Chapter 2: This chapter provides a comprehensive review of existing literature on battery technologies, BMS, and HESS. A thorough examination of the current body of literature on battery technologies, BMS, and HESS is presented in this chapter. This section delves into the fundamentals of a variety of battery types, including their specific features and barriers. In addition, the chapter investigates the most recent advancements in supercapacitor technologies and their integration with batteries to improve the performance of EVs.

Chapter 3: This chapter delves into the design and modelling of HESS. It introduces a variety of control strategies, including RBF control, MPC, and PI control, to facilitate the management of power transfer between SCs and batteries. The chapter provides a comparative analysis of these control strategies, which is based on the results of the simulations.

Chapter 4: This chapter provides an in-depth overview of several energy storage components and their discharge characteristics. It offers a comprehensive examination of the mathematical modelling and architecture of brushless direct current motors. The chapter assesses the performance of EVs by examining the implications of various brushless direct current motors motor speed control techniques through simulations.

Chapter 5: The primary objective of this chapter is to enhance the energy efficacy of EVs by incorporating advanced control strategies and HESS. It provides a comprehensive performance modelling and analysis of HESS under a variety of driving conditions. The chapter contains simulation results and examines the influence of selected driving cycles on system efficiency.

Chapter 6: This chapter emphasises the research's contributions to the advancement of HESS technology. It presents the results of experimental validations and examines the influence of HESS on the performance of supercapacitors and batteries. The chapter also evaluates the overall system efficacy and validates the effectiveness of the control strategies that have been developed.

Chapter 7: The primary findings and contributions of the research are summarised in this chapter. It presents the findings of the investigation and outlines potential areas for future research to enhance hybrid energy storage systems and control strategies for EVs.

1.5) Summary

Chapter 1 delivers a summary of the expansion and importance of the EV sector, underlining its increasing market dominance as a result of technology progress, legislative incentives, and heightened environmental consciousness. The chapter provides a comprehensive account of the decrease in sales of ICE vehicles in preference to EVs. This shift is primarily influenced by factors such as variations in oil prices and governmental laws that aim to decrease carbon emissions. Historical context by charting the development of EVs from their first introduction in the mid-19th century to different technological advancements and changes in the market has been covered. The chapter highlights the ecological advantages of EVs, such as their ability to mitigate urban air pollution and greenhouse gas emissions. It also elucidates the technical characteristics of various types of EVs, covering HEVs, PHEVs, and fully EVs. Additionally, explores several EV charging techniques and the obstacles that impede the general adoption of EVs, including expensive upfront expenses, restricted driving distances, and lengthy charging durations. The chapter finishes by highlighting the research emphasis on improving HESS for EVs by implementing advanced control techniques and real-time operation to boost efficiency and reliability.

Chapter 2 Literature Review

2.1) Background

The literature study begins by providing an overview of the vital purpose that batteries serve in EVs, acting as the major component responsible for converting chemical energy into electrical energy in order to power the vehicle. This section explores the fundamental elements of battery technology, encompassing the types, properties, and operational principles of several battery chemistries, such as lead-acid, nickel-cadmium, nickel-metal-hydride, and lithium-ion batteries. A comprehensive examination of the energy density, power density, charge and discharge rates, and lifecycle of these batteries will be conducted, emphasising their importance in the performance and efficacy of EVs.

Moreover, the review investigates the technological advancements and challenges associated with battery management systems, which are essential for the safe, efficient, and reliable operation of batteries in EVs. The BMS functionalities, including thermal management, state of health monitoring, state of charge estimation, and cell balancing, are thoroughly examined. The optimisation of battery performance and longevity is also addressed through the integration of real-time data analytics and advanced control algorithms.

The objective of this chapter is to establish a comprehensive understanding of the current state of battery technology and management systems in EVs, thereby laying the groundwork for ongoing discussions on HESS. HESS are systems that integrate batteries and SCs to improve the overall efficiency and reliability of EVs.

2.2) Battery Technologies

The battery is an essential element in EV, transforming chemical energy into electrical energy to propel the EV. Figure 3.1 depicts the internal components of a battery as it performs the procedure of converting energy. The battery comprises three primary components, each performing a crucial function in facilitating the battery's operation throughout the redox reactions:

- Anode (negative electrode): Releases electrons and undergoes oxidation in the process of the redox reaction. Typically, it is composed of materials such as graphite or lithium metal, which can release electrons.
- Cathode (positive electrode): Receives electrons and undergoes a reduction in the redox reaction. The cathode materials, such as lithium cobalt oxide or lithium iron phosphate, are selected based on their high electron acceptance capacity.

- Electrolyte: Substance that facilitates the movement of ions between the cathode and anode in a battery. Usually, it is a liquid ionic solution or a polymer gel that enables the movement of charged particles while blocking the direct flow of electrons, ensuring the battery's ability to produce an electric current.
- Separator: Resides between the anode and cathode. Its primary function is to avoid direct contact between the electrodes, while still enabling the passage of ions.

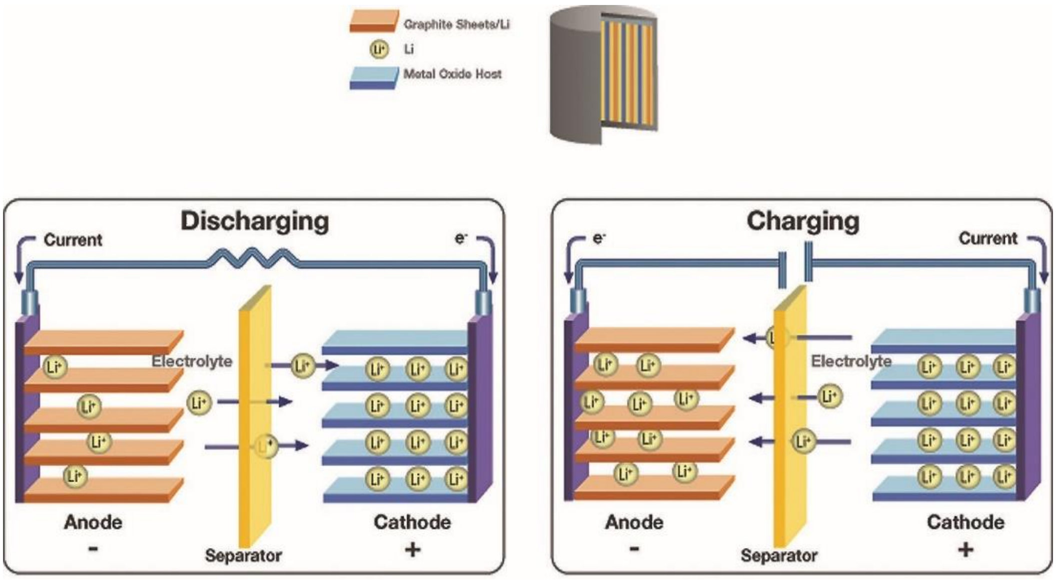

Figure 2.1 - Operation of a Lithium-Ion Battery [24]

To summarise the operation lithium-ion battery that during the discharging period, lithium-ions flow from the anode to the cathode through the electrolyte, while electrons flow through the external circuit, providing power to the device (e.g., EV). This flow of electrons is shown as the current above the battery. During the charging period, the migration of electrons in the opposite direction is driven by an external power source. Lithium-ions undergo a process of recharging by moving from the cathode to the anode, thereby restoring the battery's energy for subsequent utilisation.

EVs require batteries with both high energy density and high-power output to achieve efficient acceleration. Minimising the weight and volume of these batteries is of utmost importance since they have a substantial impact on both the cost and the total mass of an EV [10]. Figure 2.2 presents an overview of different battery technologies, highlighting their distinct attributes.

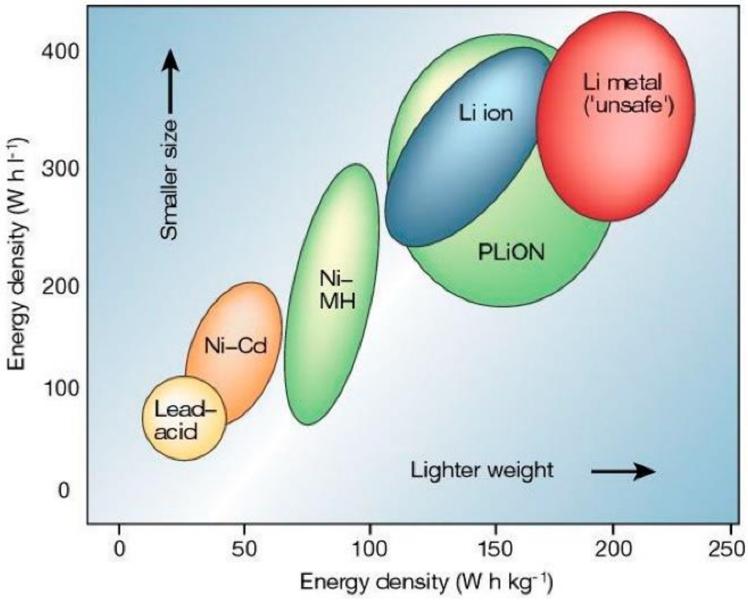

Figure 2.2 - Comparison of Various Battery Technologies [25]

A diverse range of battery types, such as Lead Acid (LA), Nickel-Cadmium (NiCad), Nickel Metal Hydride (NiMH), and lithium-based batteries (Lithium-Ion and Lithium-Polymer), are commercially available. To conduct a comprehensive comparison of these technologies, it is crucial to take into consideration seven vital elements. Table 2.1 presents the attributes of every battery technology [26], [27]. The next subsection will discuss several of these attributes.

Table 2.1 - A Survey of Different Battery Technologies [12], [26], [27], [28], [29]

	LA	**NiCad**	**NiMH**	**Lithium**
Energy Density (Wh/Kg)	40 - 60	35 – 54	70 – 100	110 - 160
Power Density (W/L)	100 -400	80 -600	250- 1000	1500 - 10000
Life Cycle	1500	500	200 – 300	500 - 1000
Cell Voltage (V)	1.2	1.2	2	3.6
Charging Rate	> 2 C	0.5-1 C	0.2 C	2 C
Temperature (^{O}C)	-40 to + 60	-20 to +60	-20 to +60	-20 to +60
Efficiency (%)	70	80	75	80

2.2.1) Energy Density

The battery pack is the primary attribute of EVs particularly when it comes to storing energy. The energy storage capacity, measured in kilowatt-hour (kWh), has a considerable impact on both the electric range of an EV and the total weight of its battery. Energy density, expressed as watt-hours per kilogram (Wh/kg), represents the relationship between a battery's energy capacity and its overall mass. The expression for energy density can be found in Equation 2.1 [30].

$$Energy\ Density = \frac{Rated\ Wh\ Capacity}{Battery\ Mass} \tag{2.1}$$

2.2.2) Power Density

Battery power density refers to the maximum amount of power that can be obtained per unit of mass or volume. Lithium-ion batteries are considered highly desirable due to their comparatively high power density, high energy density, and low self-discharge. This makes them one of the top choices in the market [31], [32], [33]. Lithium-ion batteries have been widely used in current EV applications owing to their excellent performance. The expression for power density can be represented by Equation 2.2 [30].

$$Power\ Density = \frac{Rated\ Peak\ Power}{Battery\ Mass} \tag{2.2}$$

2.2.3) Current Rate

The current rate (C_{rate}) is utilised to standardise the measurement of battery current with respect to its capacity. C_{rate} quantifies the rate at which a battery charges or discharges relative to its full capacity. The capacity refers to the total Ampere-hours (Ah) that the battery can provide when it is discharged from its nominal voltage at full capacity to the minimum allowed voltage. At a temperature of 1 degree Celsius, the battery will lose its charge within a time span of 1 hour [31]. Equation 2.3 represents the expression for the C_{rate}.

$$C_{rate} = \frac{Current\ (A)}{Capacity\ (Ah)} \tag{2.3}$$

Furthermore, the battery cell's capacity can be denoted by Equation 2.4.

$$Capacity\ (Ah) = Current\ (A) * Time\ (hrs) \tag{2.4}$$

2.2.4) Life Cycle

Battery cycle life defines the total number of charge and discharge cycles that a battery can undergo until its nominal capacity decreases below a certain threshold of its rated value. Various charge and discharge conditions have distinct impacts on cycle life, including factors such as C_{rate} and depth of discharge. Therefore, a high depth of discharge is frequently linked to a reduced battery lifespan [34].

2.3) Battery Types

Battery technologies are essential for the advancement and functionality of EVs, providing several benefits and obstacles that affect their effectiveness, expense, and security.

2.3.1) Lead-Acid

The initial batteries employed were lead-acid batteries. Due to their affordable cost, they have continued to be a favoured option for numerous new EV advancements. Some drawbacks of this technology are its low power and energy density, limited longevity, and toxic nature [10], [35].

2.3.2) Nickel-Cadmium

The memory effect of this battery type renders it unsuitable for EVs as it diminishes capacity over time and restricts its lifespan. Furthermore, cadmium is a hazardous metal that requires proper handling. Following the guidelines set by the European End-of-Life Directive (2000/53/EC) [35], [36], [37], [38], [39], the utilisation of heavy metals, specifically nickel cadmium, has been limited in all vehicles that are being sold since July 2003.

2.3.3) Nickel-Metal-Hydride

The specific energy ranges from around 70 to 100 Wh/kg, whereas the specific power is exceptional. It possesses a lengthy life cycle, a wide temperature range, and strong resistance. These batteries are commonly used in HEVs and PHEVs. Nevertheless, the presence of significant self-discharge and memory effect hinders their ability to achieve a full charge of 100% [25].

2.3.4) Lithium-ion Battery

Lithium-ion batteries comprise a copper foil that serves as the current collector for the anode, a porous anode typically composed of graphite, a separator to prevent contact between the anode and cathode, and a porous cathode made of a transition metal oxide with aluminium foil acting as the cathode current collector. Within every permeable phase, a liquid electrolyte is included to facilitate the migration of lithium ions [40]. Figure 2.3 displays the process of charging the battery. Lithium is present in the gaps of carbon graphite layers when the battery is fully charged. Lithium transforms into lithium ions during the discharge process and releases one electron [40].

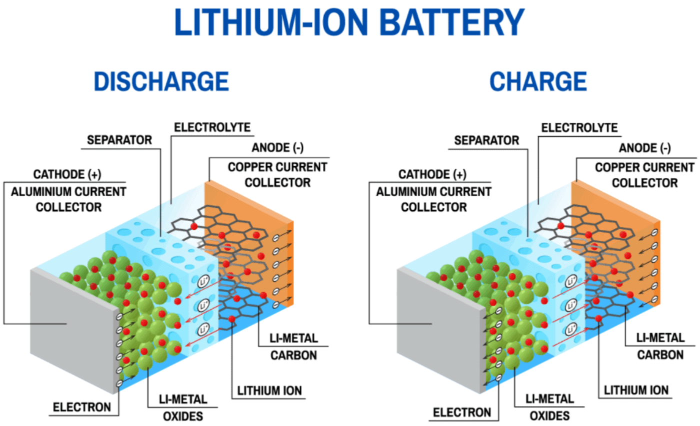

Figure 2.3 - Operation of Lithium-ion Battery During Charging and Discharging [41]

2.3.4.1) Characteristics of Lithium-ion battery

The charge and discharge cycles of lithium-ion batteries are characterised by unique features, as depicted in Figure 2.4. During the pre-charge mode, the battery voltage is initially low. Charging starts with a reduced current, referred to as the pre-charge current, in order to raise the voltage to a safer level. As the voltage increases, the charging capacity also increases while the current remains constant. This is achieved by utilising a constant current source, which establishes the constant current regulation mode [42]. This stage guarantees efficient charging without the risk of excessive heat generation. Once the battery voltage reaches the specified regulation voltage, the charger switches to the constant voltage regulation mode. In this mode, the voltage is maintained at a constant level, and the current gradually falls as it approaches the critical threshold. This stage serves to avoid overcharging and alleviate strain on the battery cells. The charging process ends when the current reaches a predetermined threshold, signalling that the battery is completely charged without any risk of overcharging [42]. This is crucial for preserving the health and lifespan of the battery. Once the battery reaches a specific degree of discharge, it switches to the recharge mode, which allows the battery to be replenished by starting the cycle again. During the discharge process, the battery sustains a consistent voltage and current. The voltage progressively decreases while there is a slight increase in current to the load over time [42]. This continues until a specific voltage cut-off point is reached to avoid complete depletion and potential harm to the battery. These characteristics guarantee the efficiency and safety of lithium-ion batteries, striking a compromise between the pace of charging and the lifespan of the battery.

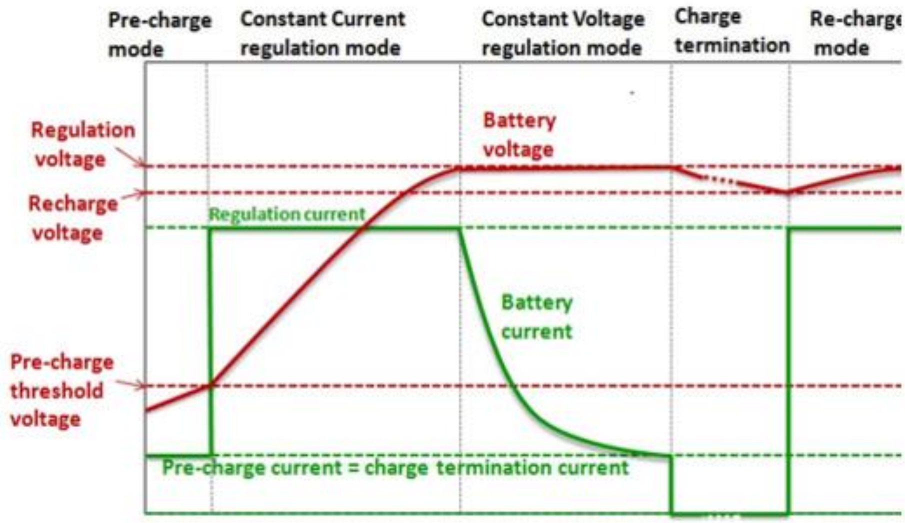

Figure 2.4 - Charging and Discharging Characteristics of a Lithium-Ion Battery [42]

Battery electrical performance is dependent on the following [43], [44], [45], [46]:

1. Ambient temperature
2. State of health
3. Operating voltage platform
4. Internal resistance

Figure 2.5 depicts the diverse effects of temperature and cycling on battery performance. Figure 2.5a depicts the influence of ambient temperature on the battery's operating voltage at three distinct temperatures: -10°C, 10°C, and 50°C. At -10°C, the operating voltage markedly diminishes for the similar state of charge (SOC) in comparison to 10°C and 50°C. [47] [48]. Figure 2.5b illustrates the rapid fall in battery capacity around 0°C, while Figure 2.5c displays a significant increase in internal resistance at lower temperatures. Both findings indicate poorer efficiency in cold conditions [49]. Battery capacity persistence at standard (25°C) and moderate (45°C) temperatures is illustrated in Figure 2.5d. The capacity diminishes more rapidly at 45°C as a result of the accelerated material degradation and side reactions that are induced by thermal stress. Conversely, the battery operates within its optimal range at 25°C, ensuring that its capacity is maintained for extended cycles. This underscores the necessity of effective thermal management and the critical impact of elevated temperatures on battery lifespan. Finally, Figure 2.5e illustrates the effect of ageing on battery performance. As the number of cycles increases, the internal resistance of the battery rises, causing a progressive decrease in terminal voltage [50]. This phenomenon highlights the long-term deterioration of battery performance while the current remains constant [51].

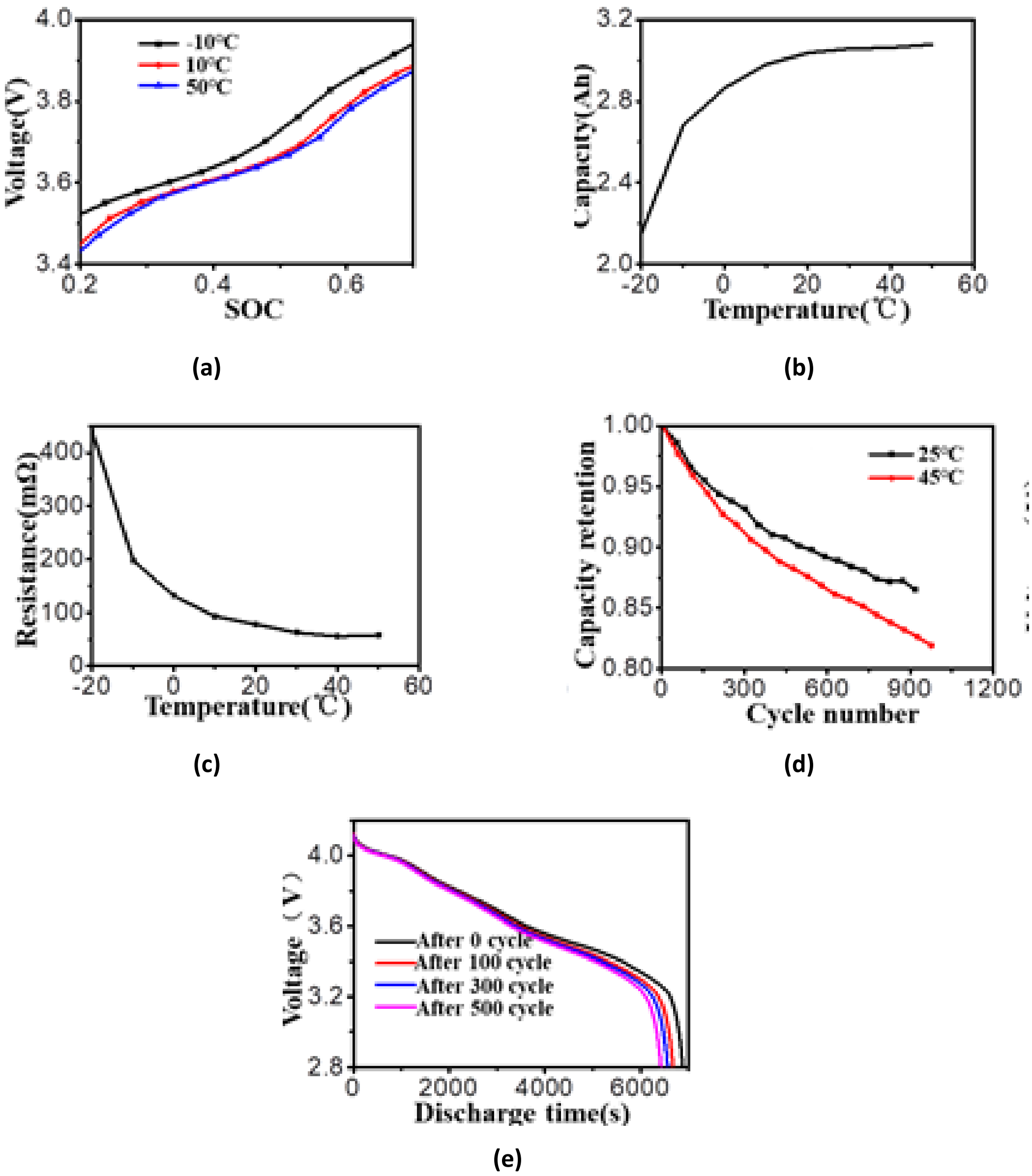

Figure 2.5 - Lithium-ion battery characteristics: (**a**) open-circuit voltage under various temperatures, (**b**) capacity of Lithium-ion batteries under various temperatures, (**c**) resistance of Lithium-ion batteries under various temperatures, (**d**) Persistence of battery capacity under warm and cold temperature conditions, (**e**) persistence of battery capacity under warm and cold temperature conditions [49].

2.3.5) Battery Charging Technique

Charging algorithms and battery charging rates are two important constraints for the battery. Charging algorithms are designed to fulfil the following requirements:

- Improve charging efficiency
- Reduce the charging time
- Enhancing the battery life

Figure 2.6 and Table 2.2 display various methods and algorithms used for battery charging. Slow charging and quick charging are the two predominant rates at which batteries are commonly charged. The arrows in Figure 2.6 indicate the possible transitions or relationships between various battery charging approaches. They suggest that these charging methods can be adapted or combined based on specific needs, allowing for flexible charging strategies within a battery management system. The different charge rates are mostly governed by the level of demand [26]. Undoubtedly, slow charging is the most practical approach to charging an EV since the charging circuit instantly cuts off after the process of charging has concluded [26]. The charging time ranges from 10 to 16 hours at a rate of 0.1 C [26]. The fast charging rate usually ranges from 0.3 C to 1 C, which can result in excessive heat when the battery is fully charged. It is advisable to set a temperature limit [26].

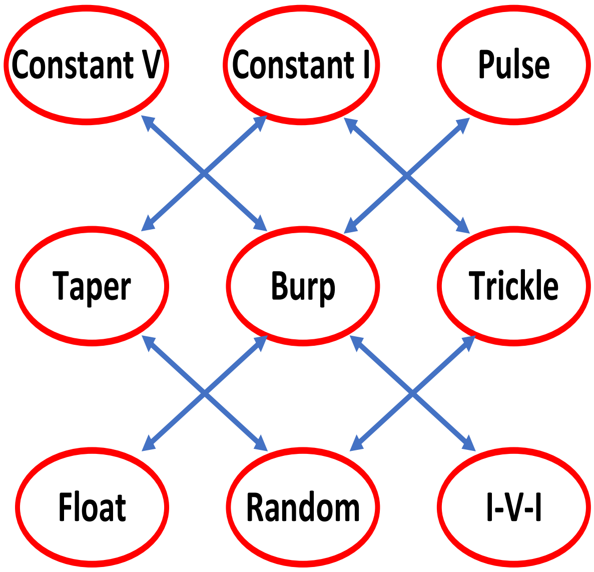

Figure 2.6 - Battery charging approaches [26]

Table 2.2 - Battery Charging Algorithms [26]

Technique	Principle
Constant voltage	Charging the battery with a consistent voltage. While the battery is being charged, the current progressively decreases.
Constant current	Consistent flow of electric current by adjusting the voltage at the terminal.
Pulsed charge	Battery is supplied with current pulses. The duty cycle of these pulses can be modified to regulate the rate at which charging occurs. Each pulse has a duration of approximately one second and is then followed by 30 milliseconds of recuperation to stabilise the chemical reaction of the battery.
Taper charge	Employs an uncontrolled steady voltage that gradually reduces the charging current as the battery voltage rises.
Burp	After every charging pulse, there should be a brief discharge pulse to help enhance charge acceptance and lessen polarisation effects.
Trickle charge	Delivers a minimal and uninterrupted electrical current to mitigate the natural loss of charge, usually when in a state of inactivity.
Float charge	Utilised during crucial power demands, the battery and load are interconnected in parallel, functioning as an alternative system. It keeps the battery fully charged without causing overcharging.
Random charging	Random bursts of charging
I-V-I charging	The battery is initially charged using a constant rate of electric current ('I') until the voltage exceeds a predetermined threshold. Afterwards, the charger transitions to a phase called constant voltage ('V'), during which the current gradually declines until it drops below a certain threshold. Ultimately, the charger switches back to the constant current mode ('I') and remains in this mode until the voltage reaches a pre-established threshold, at which point the charger is deactivated.

2.3.6) Electric Vehicle Battery Modelling Techniques

The initial step in online model-based estimation is the creation of a battery model. The objective of the battery model is to replicate the battery's functionality inside a simulated environment. When examining the behaviour of battery cells, there are three primary criteria that must be considered [52]:

- Model complexity
- Model accuracy
- Simulation runtime

Figure 2.7 displays five distinct battery models: empirical, electrochemical, electrical equivalent circuit, electrochemical impedance, and data-driven models. The electrochemical model and the equivalent circuit model are widely employed by researchers to understand the behaviour of battery cells [24] [53]. Table 2.3 presents an overview of various battery modelling methodologies and summarises the strengths of each model. Electrochemical models excel in precision and prediction for design. Impedance models balance precision and adaptability. Equivalent circuit models suit real-time control. Empirical models focus on real-time use. Lastly data-driven models are ideal for offline analysis.

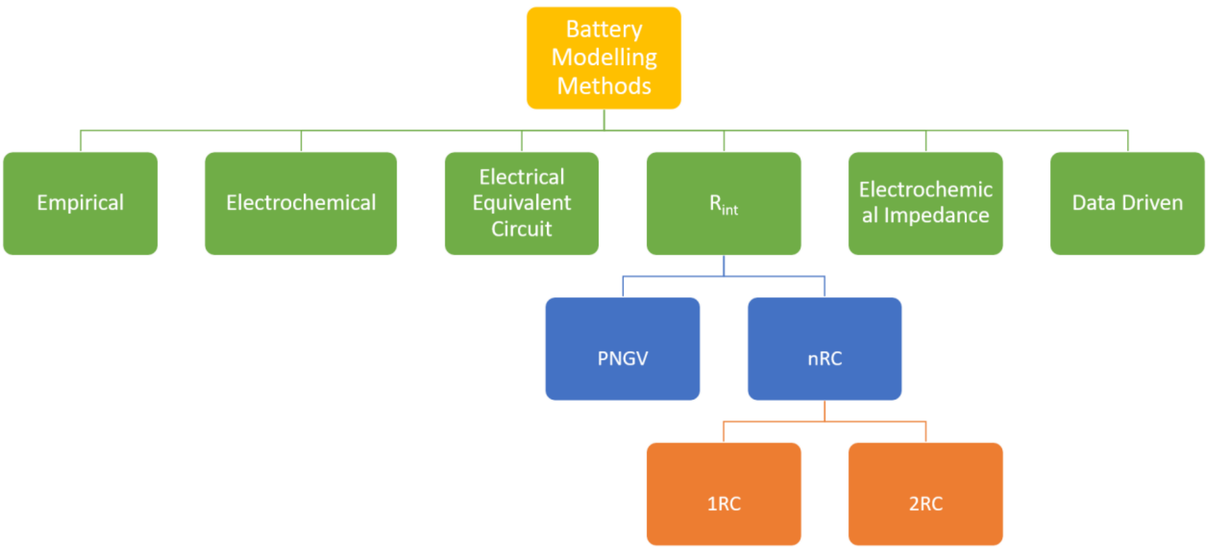

Figure 2.7 - Lithium-ion Battery Modelling Approaches [53]

Table 2.3 - Comparison of Different Battery Model Approaches [54], [55][56]

Model approach	Adaptation	Precision	Real-time	Prediction	Complexity	Applications
Electrochemical	VL	VH	M	M	VH	Battery design
Electrochemical impedance	L	H	M	M	M	
Equivalent circuit	VL	M	H	M	L	Real-time control & SOC estimation
Empirical	VL	L	M	H	M	Constant operation solely
Data-driven	L	M	H	M	M	Offline investigation

VL: Very Low, L: Low, M: Medium, H: High, VH: Very High

2.3.7) Lithium-ion Battery Faults

Lithium-ion battery issues are categorised as either internal or exterior. Refs [57] & [58] provided a comprehensive analysis of failure processes and modes for rechargeable Lithium-based batteries. This section gives a preliminary overview on the causes and processes of faults. Studying such processes is critical in furthering efforts to create fault diagnosis models, which are useful in preventing security risks for Lithium-ion battery applications. Figure 2.8 outlines a clear view of different possible dilemmas that may be faced in Lithium-ion batteries.

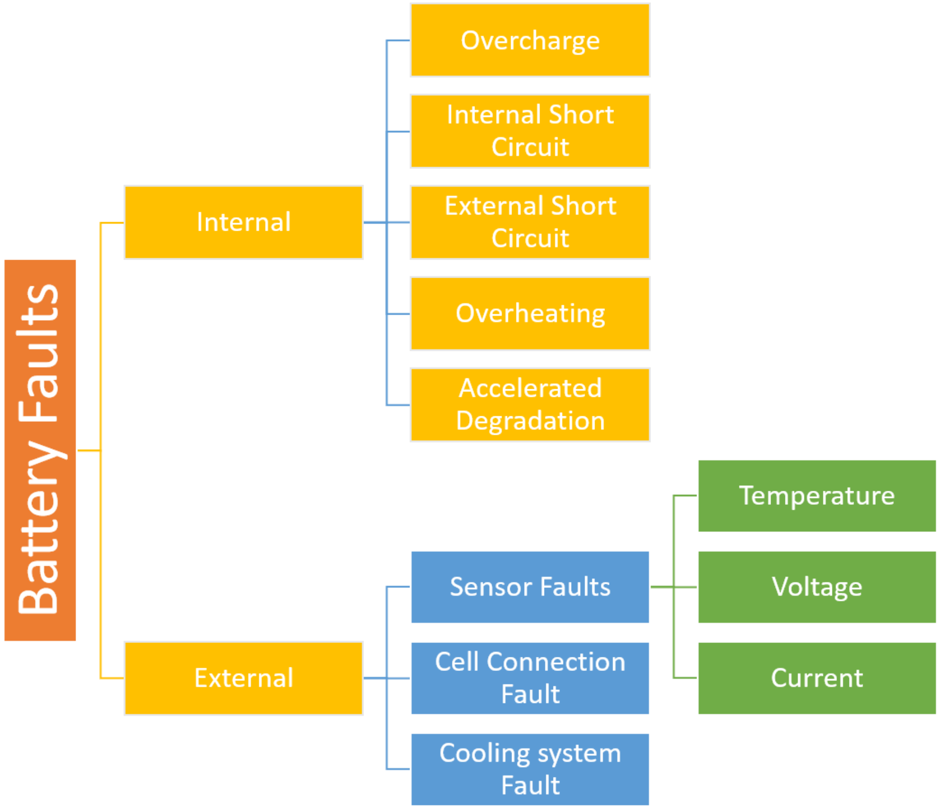

Figure 2.8 - Classification of Battery Defects [58]

2.3.7.1) Internal Battery Faults

Diagnosing internal battery issues is a challenging procedure due to the complex and partially understood mechanism of the Lithium-ion cell [57]. Internal battery issues include issues of overcharging, over discharging, shorting either internally or externally, generation of heat, rapid rising of temperature and quick depletion. Some of these include capacity deterioration, charge transfer rate reduction, loss of energy density, and cycle life reduction, but the most dangerous ones are thermal runaway and rapid deterioration. Both of these can have severe effects on the functionality and safety of Lithium-ion batteries as well as pose a direct threat to the users [59].

2.3.7.2) External Battery Faults

Generally, an external short circuit develops when the tabs are linked via a channel with low resistance [57]. Another reason is electrolyte leakage owing to cell expansion, as a result of side reaction gas production during overcharge [60]. It may also be caused by absorption in water and collision deformation. Specifically, an external short circuit occurs when an external heat-conducting substance makes simultaneous interaction with the positive and negative terminals, resulting in an electrical connection between the electrodes [61].

2.4) Battery Management System

Monitoring charge rates throughout the entire pack to a safe threshold, thereby ensuring optimal performance and extended battery life, necessitates the implementation of a complex electronic control system known as the battery management system (BMS) [26], [27]. Different types of cells are available, each possessing unique qualities. Composing mechanical support structures, thermal interfaces, and essential attachments, modules are generated through the interconnection of numerous cells.

2.4.1) Key Functions of the Battery Management System

The vital role of a Battery Management System (BMS) in tracking and controlling battery state is shown in Figure 2.9. Based on the voltage and current readings from the battery, this system can estimate the SOC and state of health (SOH). To enable batteries to run smoothly and for as long as possible, it also manages their temperature and charges them evenly. Representation of "therm 2" and "V_2" represents specific thermistor and voltage measurement points, respectively. Furthermore, the BMS utilises the controller area network (CAN) protocol to guarantee the reliable interchange of data between components, thereby facilitating the efficient communication necessary for monitoring and control. Batteries rely on the BMS's precision in monitoring these parameters to keep them safe, efficient, and reliable in a range of uses [12], [26], [27].

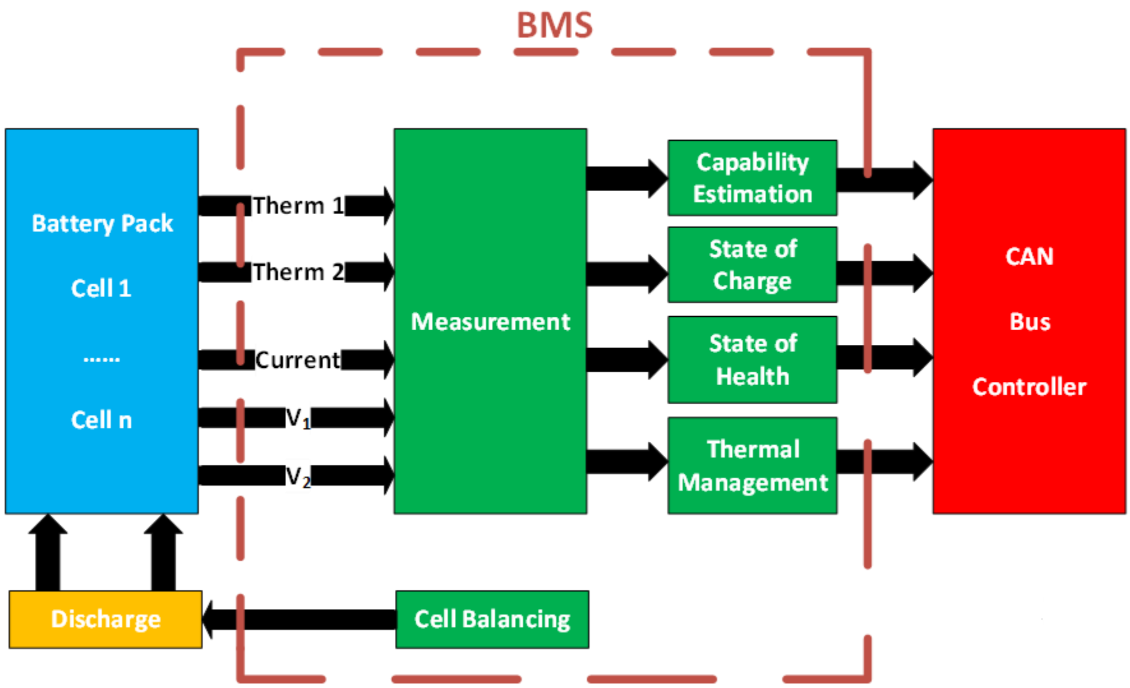

Figure 2.9 - Block diagram of the BMS [12]

2.4.2.1) State of Charge

The determination of the SOC is a crucial operation of the BMS, since it establishes the current amount of charge present in the battery. SOC is the quantitative measure of the current charge level of a battery, expressed as a ratio between the actual charge and the maximum charge capacity. The calculation is performed by comparing the remaining charge ($Q_{remainng}$) to the maximum charge capacity (Q_{max}), as indicated in Equation 2.5. The calculation of the SOC is essential for evaluating battery performance and guaranteeing effective energy management.

$$SoC = \frac{Q_{remaining}\ (t)}{Q_{max}\ (t)} * 100\ \% \tag{2.5}$$

Various techniques are commonly utilised for measuring the SOC in batteries [12]:

- Book-keeping estimations – Determined using charging/discharging current
- Direct measurements - Determined using physical properties.
- Model based – Determined using by designing adaptive filters and observers.

2.4.2.1.1) Book-Keeping Estimations

Coulomb Counting (CC) is a widely used method for approximating a battery's SOC. This approach computes the amount of charge transported into or out of the battery by adding up the charge flow over time [62]. Nevertheless, CC is subject to a significant constraint: the precision of SOC estimation is greatly influenced by the original SOC value. Given the initial SOC, this method can offer precise estimations, albeit limited to a brief duration [63]. Over time, mistakes in measurements, ambient conditions, and battery ageing contribute to the accumulation of errors, resulting in substantial variations from the real SOC. In addition, the strategy does not consider the battery's efficiency losses or self-discharge, which further affects its reliability over long periods. Although CC can be beneficial in specific situations, it necessitates regular recalibration and is frequently combined with other techniques to enhance the accuracy of SOC estimation.

2.4.2.1.2) Direct Measurements

Four main direct measuring methodologies typically employed for assessing the SOC are Open Circuit Voltage (OCV), Electromotive Force (EMF), Internal Resistance (IR) and Impedance Spectroscopy (IS). Every approach possesses unique attributes and applications.

2.4.2.1.2.1) Open Circuit Voltage

This approach involves assessing the battery's voltage under no load conditions. By utilising the battery's established discharge curve, the voltage measurements can be transformed into a

SOC value. The correlation between voltage and SOC is substantially researched and acts as the foundation for this estimating method [62].

2.4.2.1.2.2) Electromotive Force

This method estimates the projected EMF voltage at the state of full battery charge. To offset impedance distortion, terminal voltage, current, impedance, and C_{rate} are considered [64]. Nevertheless, temperature, time, and ageing effects on the battery are not considered in this method.

2.4.2.1.2.3) Internal Resistance

This technique ascertains the SOC by evaluating the battery's internal resistance, which is determined by the current during the charging or di process. Although this technique provides significant metrics, it is frequently not regarded as adequate for reliable SOC estimates due to multiple contributing factors.

2.4.2.1.2.4) Impedance Spectroscopy

This approach employs the injection of currents at several discrete frequency levels into the battery to determine its internal impedance. This approach enables a comprehensive examination of the battery's impedance profile, which can be utilised for real-time SOC assessment.

2.4.2.1.3) Model Based Methods

The constraints of real-time data present issues for both direct measurement and bookkeeping estimating methods. To overcome such constraints, model-based methods for estimating the SOC are adopted. Notable among these techniques are Kalman Filtering (KF), the Extended Kalman Filter (EKF), the Adaptive Extended Kalman Filter (AEKF), and the Unscented Kalman Filter (UKF). In study [62], [65], to determine the internal conditions of dynamic systems, these techniques employ algorithms. EKF and AEKF are appropriate for nonlinear systems, whereas KF is effective for linear systems. Specifically, the UKF employs a nonlinear unscented transformation method [27]. Table 2.6 provides a thorough analysis of different SOC estimation techniques, focusing on their strengths, weaknesses, and adaptability for EV.

Table 2.4 - Outline of the various SOC approaches [27]

Method	Pros	Cons	Applicable EV
CC	Less complex and very basic	Its accuracy shifts depending on factors such as its age, level of self-discharging, and temperature, all of which are unknown at the outset.	Yes
OCV	Simple and straightforward to execute with high precision	Not compatible with EV	No
EMF	Less expensive and straightforward	Following the current upheaval, it takes a large amount of time.	No
IR	Simple and straightforward.	Low precision, difficult work to measure a low resistance value	No
IS	SOC precision is reasonable	It's ideal for charging/discharging currents that are the same.	No
KF	External perturbations affect the system in real-time, and the system determines the state with great accuracy.	Does not estimate the state of a nonlinear system directly.	Yes
EKF	System State accurately simulates amid noisy and erroneous initial conditions.	Not robust	Yes
UKF	Appropriate precision, less cost	Temperature, ageing, and hysteresis of the Lithium-ion battery have an impact on the model's accuracy.	Yes

2.4.2.2) State of Health

The SOH of a battery is an important metric to use when deciding whether to replace the battery [12]. According to Equation 2.6 it is shown as the ratio of the original full charge capacity to the current full charge capacity [62].

$$SOH = \frac{Q_{Present}}{Q_{Fresh}} * 100\ \% \qquad (2.6)$$

Where

$Q_{Present}$: Charge capacity

Q_{Fresh}: Full charge capacity

SOH is essential for the proper functioning of BMS as it guarantees the safe and reliable performance of Lithium-ion batteries by forecasting their remaining lifespan and assessing possible failure scenarios [12]. Temperature and the rate of discharge/charge current are the primary parameters that affect battery aging. Despite careful study [62], [66], [67], there are currently no accurate mathematical models available for evaluating the SOH of Lithium-ion batteries. This is mostly due to the highly complex and often poorly understood internal dynamics.

Several studies indicate that observing voltage [62], [66], [67], whether by online devices or manual testing, offers partial findings but fails to present a comprehensive assessment of the battery's condition. Voltage measurements indicate the level of charge in the battery rather than its overall condition. An alternative and more efficient approach to evaluate the condition of a battery is by measuring its impedance. Impedance testing enhances the comprehension of the battery's internal resistance, so providing a more comprehensive assessment of its overall condition. Impedance readings, when monitored over a period of time, can be important indicators that often detect possible faults at an earlier stage compared to voltage testing alone. Generally, the internal resistance or impedance of a battery tends to rise as time passes, indicating a decline in the cell's condition [66], [67].

2.4.2.3) Thermal Management

Lithium-ion batteries require a specified temperature range to function at their best and avoid any adverse effects as shown in Figure 2.10. Using these batteries outside their specified temperature range can result in a decline in performance and permanent damage to the cells. In extreme instances, it can lead to thermal runaway, a condition in which the battery experiences excessive overheating, potentially resulting in an explosion. BMS is utilised to regulate the temperature. These technologies regulate the temperature of the battery pack by either increasing or decreasing it as required. The battery pack contains temperature sensors that continuously monitor the temperatures of the cells. The information collected is processed by the BMS to effectively circulate coolant and ensure that the cells remain within the optimal temperature range [68]. Typical coolants employed in these systems consist of air, water/glycol mixtures, dielectric oil, and refrigerants [26].

By implementing effective temperature control, BMS not only improve the durability of lithium-ion batteries but also improves their stability and reliability in a wide range of applications. By incorporating sophisticated cooling methods and continuous monitoring, the potential hazards posed by excessive temperatures in lithium-ion battery systems are reduced, resulting in enhanced efficiency and safety [12].

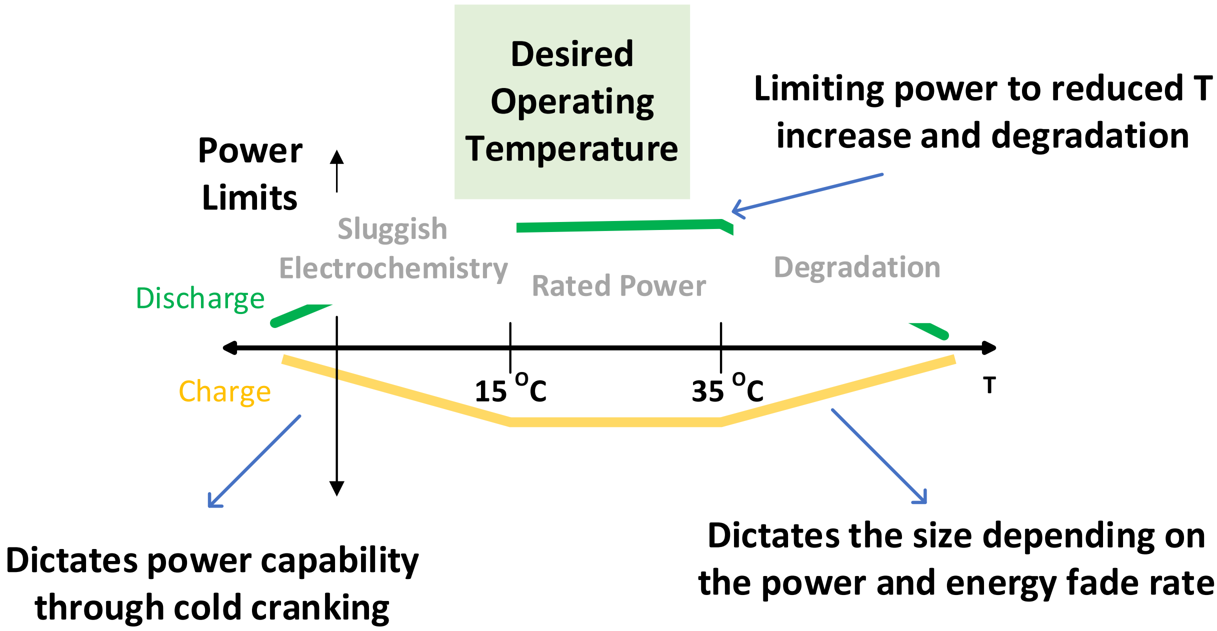

Figure 2.10 - Optimal Lithium-ion battery temperature range [12]

2.4.2.4) Cell Balancing

Cell Balancing is an essential control approach used in the BMS. Cell balancing refers to the procedure of levelling the voltages across individual cells. Every individual cell within the battery pack possesses a distinct level of charge, which undergoes alteration as the number of charge-discharge cycles increases [26]. Battery cell balancing is crucial for guaranteeing the accurate charging and discharging of each individual cell within a battery pack [12]. Inadequate charging and draining can cause thermal runaway, which may lead to disastrous malfunctions. There are two main methods for cell balancing:

2.4.2.4.1) Passive

Passive balancing helps dissipate the surplus voltage of a cell that exhibits a higher voltage than other cells, thus achieving voltage uniformity across all cells. The surplus voltage or charge is discharged by a resistor, known as $R_{Discharge}$, as depicted in Figure 2.11. Nevertheless, this approach to cell balancing is usually avoided since, as the battery is discharged, the battery module's overall performance is limited by the least powerful cell in the series [12]. Consequently, the overall capacity and efficiency of the battery pack are diminished, thereby reducing its effectiveness for applications that demand consistent power output [26].

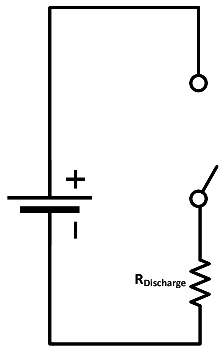

Figure 2.11 – Passive Balancing [12]

2.4.2.4.2) Active

Active balancing is a superior technique for preserving cell energy balance in contrast with passive balancing, resulting in higher energy efficiency. This method entails the redistribution of energy among the cells rather than its dissipation and wastage, as depicted in Figure 2.12 [12]. Power electronic devices improve energy transmission by redistributing energy from stronger cells to weaker ones, resulting in optimised energy utilisation and increased module capacity [26].

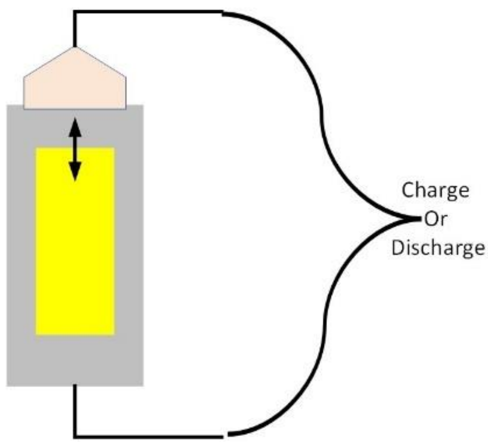

Figure 2.12 – Active Balancing [12]

2.4.2) Structures of Battery Management System

BMS are available in three primary configurations: centralised, modular, and distributed. Table 2.5 presents a comprehensive analysis of the benefits and drawbacks of each BMS configuration.

In a centralised BMS topology, each cell directly connects to a singular master control unit. This unit oversees, safeguards, and maintains balance among all the cells in the system. The centralised procedure streamlines the whole system architecture and diminishes its complexity of connections

[12]. Nevertheless, it should be noted that a malfunction in the master control unit can potentially affect the entire system [69].

The modular BMS topology employs several subordinate BMS controllers to manage data from the cells and transmit it to the primary controller. This setup improves the ability to handle increased workloads and adapt to changing requirements, making it easier to maintain and implement updates. Additionally, it enhances fault tolerance by ensuring that the failure of a single slave controller does not jeopardise the integrity of the entire system [12]. Nevertheless, the modular technique can get more intricate and expensive as a result of the enhanced quantity of components and connections [69].

Each cell in the distributed BMS topology is equipped with modest voltage and discharge monitor circuits. These circuits establish direct communication with the master controller. This topology provides the utmost amount of scalability and redundancy, as each cell functions autonomously. The use of distributed BMS is especially beneficial in situations when it is crucial to monitor and regulate individual cells within big battery packs [12]. Nevertheless, the implementation of this system can be intricate and necessitates the use of advanced communication protocols to effectively handle the substantial volume of data produced [69].

To achieve optimal efficiency, reliability, and safety, it is important to select the most suitable BMS topology by considering the unique requirements and limitations of the application [12].

Table 2.5 - Overview of BMS topologies [69]

Topology	Pros	Cons	Connection
Centralised	Less hardware & single assembly	The controller is the only source of cell balance, excessive heat can be generated.	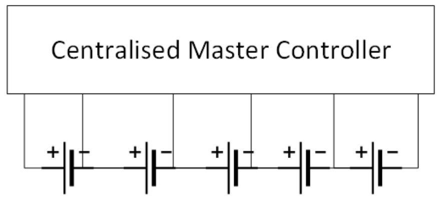
Modular	Wire's to cells are easier to manage & simple extension to larger battery packs	Communication is quite difficult & cost is slightly higher compared to centralised	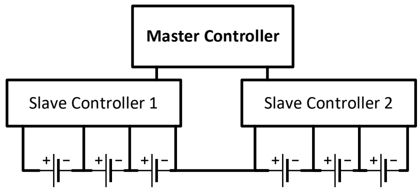
Distributed	Simple & reliable	The difficulty of mounting every cell	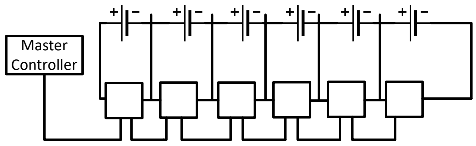

2.4.3) Energy Management System

EMS systems are crucial in EVs to ensure effective energy utilisation and maintain optimal performance. These systems consist of multiple layers, including both hardware-based controls at a low level and software-based supervision at a high level. The EMS structure consists of two main control layers: the low-level component layer and the low-level control layer. These levels work together to ensure efficient EMS [12], as depicted in Figure 2.13.

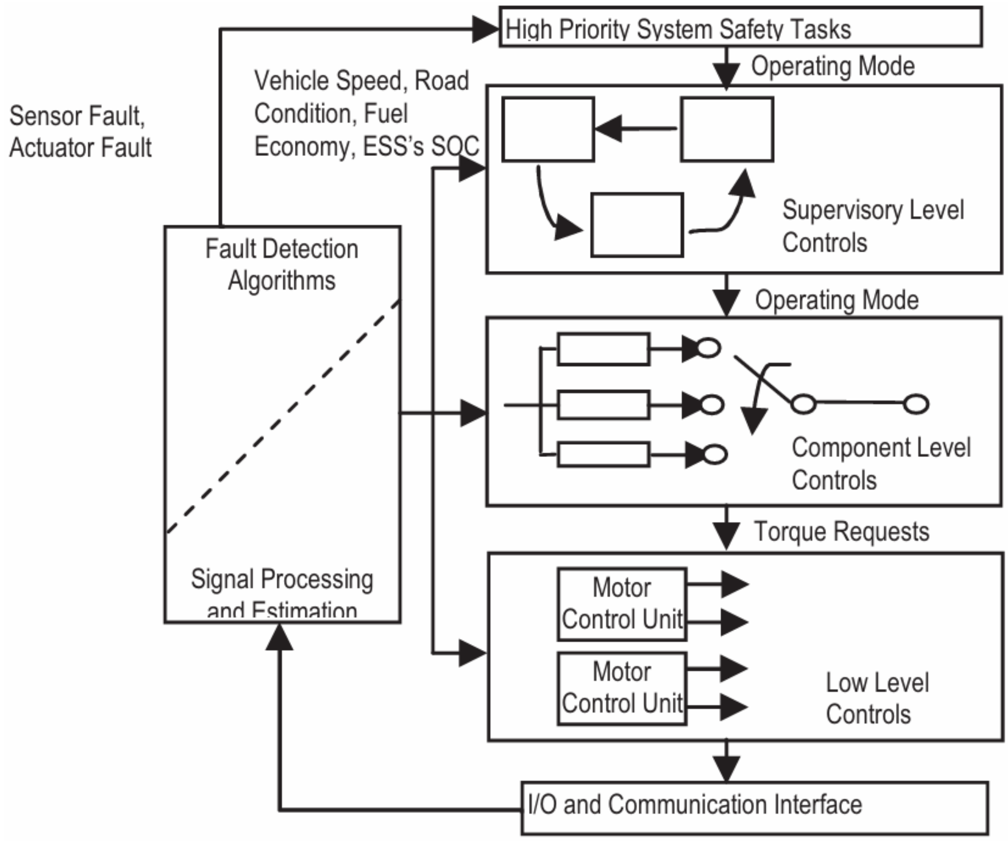

Figure 2.13 - Layers of EMS in EVs [70]

2.4.3.1) Hardware Level

The primary objective of the low-level control layer in EVs is hardware-based management. This layer consists of electric motors, batteries, and power converters. The execution of real-time tasks that necessitate rapid responses and accurate operations falls under the scope of this layer. Such tasks encompass motor control, battery charging and discharging, and maintaining efficiency in power conversion [12]. The hardware control layer is vital in enabling precise and timely actions, guaranteeing EV components' secure and effective functioning [71].

The vehicle powertrain is a crucial component of the hardware control layer, since it substantially impacts the design and performance of the EMS. The EV powertrain can be arranged in many configurations to produce the most efficient power management results, improve vehicle performance and durability, and reduce energy transfer losses [71]. Typically, these designs fall into categories according to the quantity and placement of the motors in the vehicle, as discussed in Chapter 1.

2.4.3.1) Software Level

The high-level supervisory control technique is an important control strategy in the field of optimising the operation of EVs. This technique greatly improves the general performance of the vehicle by utilising both accurate information and advanced predictive analysis. The primary responsibility of the high-level supervisory controller is to synchronise the operations of individual components based on event-based or time-based conditions. This is crucial for effectively managing the ever-changing nature of EV systems, which are defined by continually varying data inputs. As a result, advanced control algorithms are used to improve the functioning of basic components.

The design of high-level supervisory control can be divided into two main classes: rule-based (RB) control and optimisation techniques, as demonstrated in Figure 2.14. Rule-based control is based on human knowledge, heuristic, intuition, and even mathematical models and driving cycles [12]. There are two main types of rule-based methods that are deterministic and fuzzy. Deterministic rule-based like thermostat (on/off) control, power follower strategies, and state machine-based strategies. Fuzzy rule-based method that add some flexibility and resilience to deal with uncertainty.

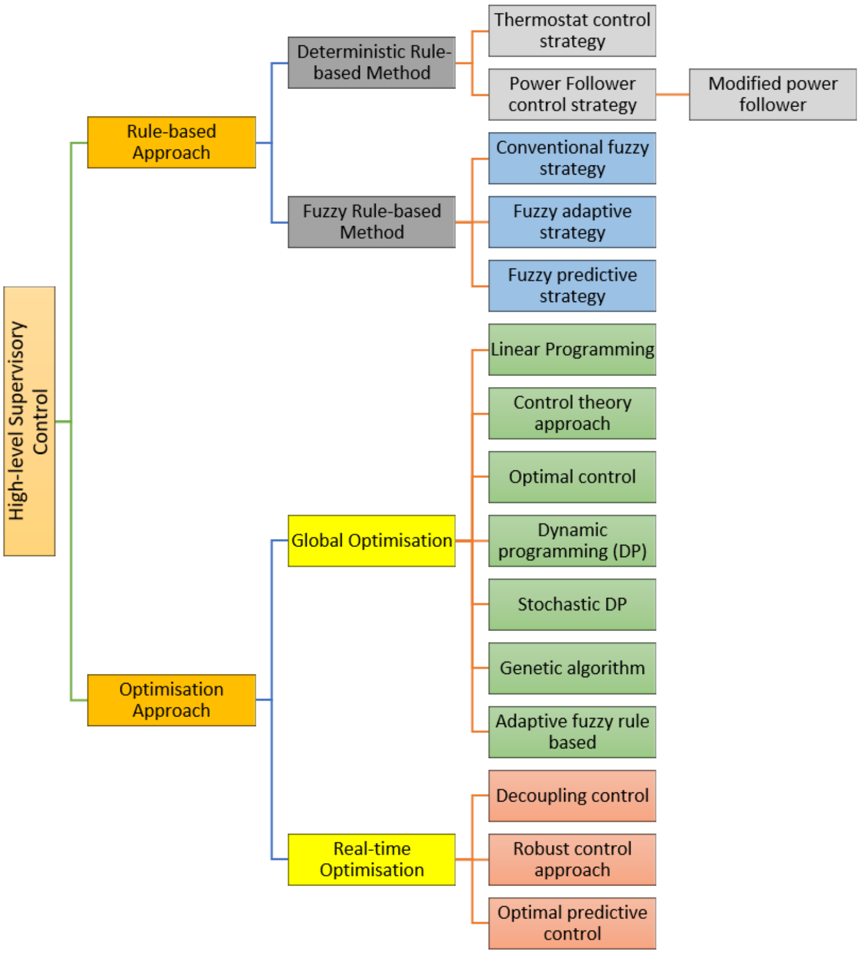

Figure 2.14 - Strategies for High Level Supervisorial Control [23]

On the other hand, optimisation strategies are engineered to methodically reduce the value of cost functions by employing numerical or analytical techniques. These methodologies can be additionally categorised as real-time optimisation (RTO) techniques and global optimisation. Genetic algorithms, linear programming, optimal control, stochastic dynamic programming (DP), and DP are all examples of global optimisation strategies. To attain optimal performance, these methodologies are considered as a wide range of variables and limitations. For example, DP is extensively acknowledged for its capacity to resolve sequential decision-making issues; however, its practical implementation in real-time situations may be constrained by its substantial computational requirements.

Table 2.6 presents an evaluation of different global optimisation algorithms for high-level supervisory control [12] [70]. The analysis considers factors such as computation intensity, robustness, real-time capability, availability of analytical solutions, and compile structure, to highlight the trade-offs involved in selecting the most suitable algorithm.

The incorporation of complex algorithms is involved in the integration of high-level supervisory control into the EMS of EVs. Offline EMS algorithms are specifically created for predefined scenarios and employ stochastic optimum control techniques to effectively navigate intricate dynamic systems. These algorithms' function based on the assumption of making decisions in a specific order while dealing with uncertainty, to optimise the long-term objectives of the system. DP is a fundamental approach used to solve these problems, although its use is limited by computing capability [71].

Online EMS algorithms, such as MPC, offer a prompt answer by addressing the optimisation issues within limited timeframes utilising predictive models. MPC is highly efficient in managing the limitations and complex characteristics of extensive systems, guaranteeing that the vehicle functions according to the specified specifications [71].

In addition, EMS that are upgraded with Global Positioning System (GPS) utilise regional and terrain information for maximising the efficiency of vehicle performance. These algorithms utilise data from the GPS to adapt control techniques according to road conditions and driving habits, resulting in a substantial enhancement in overall efficiency. They employ complex methods, like as artificial neural networks (ANNs), to identify driving patterns and choose the most suitable control algorithms from a collection of optimum driving modes [71].

In summary, a wide variety of control methods and algorithms are incorporated into the high-level supervisory control of EVs to guarantee maximum efficiency and performance. By integrating adaptive and predictive elements with rule-based control and advanced optimisation strategies, the above approach provides a comprehensive approach for managing EV systems' dynamic and complex environment. By implementing this comprehensive approach, not only are the immediate operational needs met, but the long-term viability and effectiveness of EVs are also enhanced [71].

Table 2.6 - Comparison of Global Optimisation Algorithms [12] [70]

	Computation Intensity	**Robust**	**Real-time**	**Analytical Solution**	**Compile Structure**
Linear Programming	+ +	-	- -	-	-
Optimal Control	- -	- -	-	+	-
DP	-	-	-	-	+
Stochastic DP	- -	-	-	-	+
Genetic Algorithm	-	+	-	-	+ +

++ Very High, + High, - Low, -- Very Low

2.5) Regenerative Braking

Most car manufacturers are currently prioritising the development of EVs, motivated by government incentives and backing for specific technology. Conventional braking systems employ mechanical friction to convert kinetic energy into heat, decelerating the vehicle. Nevertheless, the adoption of advances in technology has eradicated the necessity for mechanical friction in vehicle braking systems [72].

Traditionally, brakes have been designed to stop a vehicle by converting kinetic energy into heat. Studies indicate that braking can utilise from 33% to 50% of the energy needed to operate a vehicle, especially in urban locations where there is frequent stopping and starting [72]. When an electric motor reaches a state of full rest, the accumulated energy is usually dissipated into the surroundings as heat, resulting in a loss of valuable energy from the system.

Regenerative braking technology reduces this inefficiency by catching the kinetic energy that would otherwise be lost as heat during braking and turning it into electrical power that can be used by the vehicle. This cutting-edge technology is smoothly incorporated into the braking systems of EVs, enabling the retrieval and reutilisation of energy during deceleration [72]. The efficacy of regenerative braking depends on the driving conditions, with urban contexts often providing more energy recovery potential due to the more frequent occurrence of brake events compared to highway driving [72].

Regenerative braking improves the energy efficiency of EVs and boosts their overall sustainability by reducing energy waste and increasing their driving range. This technology signifies crucial progress in the search for transportation solutions that are both more efficient and environmentally sustainable.

Regenerative braking systems are essential for maximising efficiency and minimising the environmental effect of EVs by capturing and converting the energy that would otherwise be wasted during braking into electrical energy. This progress highlights the continuous efforts to develop within the automobile sector, to achieve significant enhancements in energy efficiency and environmental preservation. Table 2.7 illustrates the pros and cons of regenerative braking.

Table 2.7 - Pros and Cons of Regenerative Braking [72], [73]

Pros	Cons
Greater command of the braking system	Only applied to the motor-driven axle
Efficient in stop-and-go traffic	Cannot produce required braking torques for emergency stops on its own.
Reduces brake strain	When the SOC of a battery exceeds a certain threshold, it cannot be charged throughout regeneration.
Fuel efficiency	
Reducing the use of energy	

2.5.1) Operation of Regenerative Braking

EVs utilise advanced motor control strategies to optimise both their performance and efficiency. Analysing the operating dynamics of these vehicles requires studying the interplay between the motor, torque, and energy transfer in different situations. The operation can be generally classified into two distinct conditions: forward motion and regenerative deceleration.

The vehicle's speed characteristics are thereby enhanced by the amplification of the magnetic field's intensity by this resistance. The motor generates more torque, which facilitates better overall performance and quicker acceleration, by increasing the strength of the electromagnetic field. The energy conversion is more efficient as a result of the interaction between the vehicle's drivetrain and the increased magnetic field, which directly contributes to the improved speed characteristics [72], [74].

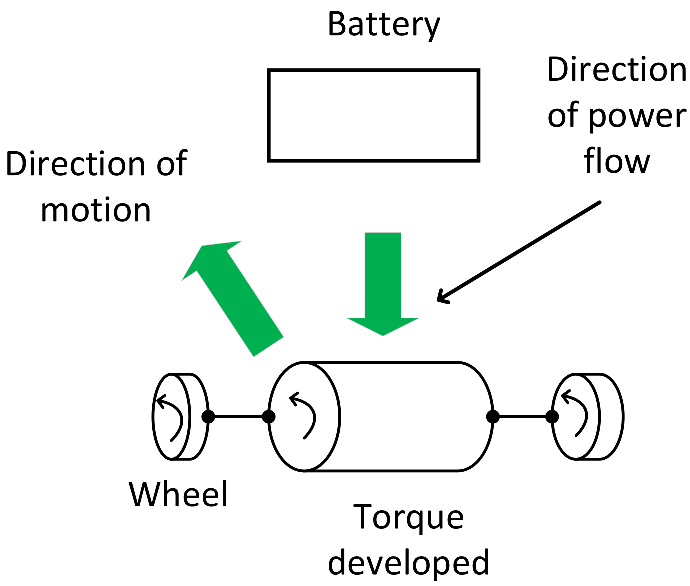

Figure 2.15 - Forward driving condition [75]

On the other hand, Figure 2.16 demonstrates the regenerative braking process, in which the motor functions as a generator. This process attenuates the magnetic field, resulting in a decrease in speed. Under these circumstances, the motor produces a torque that opposes the direction of wheel rotation. Furthermore, this procedure exemplifies the transfer of energy back to the battery, in contrast to the forward-driving scenario where the battery functions as the energy supply.

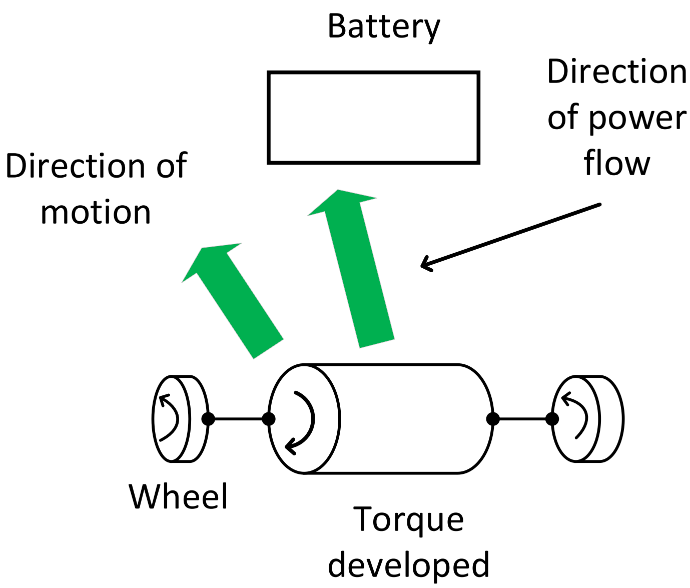

Figure 2.16 - Regenerative braking condition [75]

The outlined dynamics above emphasise the core concepts of electromagnetic induction and energy conversion in the operation of EVs, highlighting the effectiveness and functionality of regenerative braking in recovering energy and controlling speed.

2.5.2) Control Strategy

The control approach for the regenerative braking system is primarily reliant on a sophisticated three-phase inverter circuit. This system is dependent on a range of power electronic components, such as Metal Oxide Semiconductor Field Effect Transistors (MOSFETs), diodes, resistors, capacitors and inductors. These components collaborate to facilitate effective energy regeneration and control inside the vehicle's electrical system. The following is a detailed description of the main components of the regenerative braking system's control circuit [72], as illustrated in Figure 2.17.

- Resistance and inductance of the armature (R and L): The resistance and inductance of the armature are crucial factors that impact the motor's dynamic performance during braking and driving situations.
- Armature back electromotive forces (e_a, e_b, e_c) : The back EMFs are generated in the motor's windings while it is running and are crucial for determining the amount of energy that can be used for regeneration.
- Armature current (i_a, i_b, i_c): The currents passing through the windings of the motor in phases a, b, and c are observed and regulated to enhance performance and efficiency.

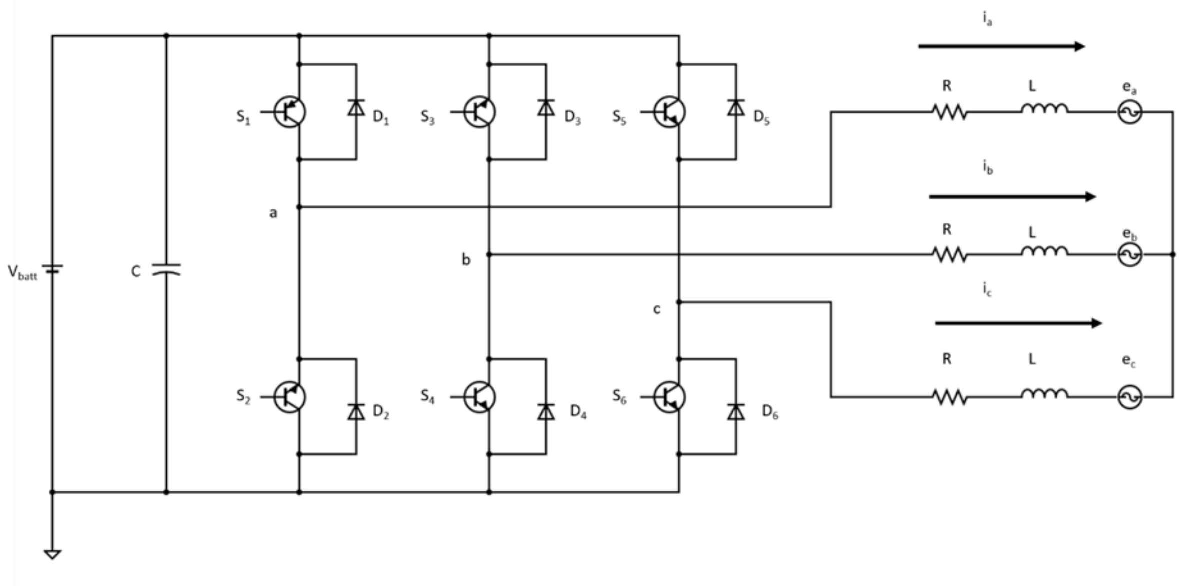

Figure 2.17 - Three-phase inverter [76]

2.5.3) Enhancement of Regenerative Braking System

Regenerative braking systems are crucial for enhancing the efficiency and sustainability of EVs. These devices transform the energy of motion, which is usually dissipated as thermal energy during the process of braking, into electrical energy that can be stored and subsequently utilised. Although there have been notable breakthroughs, studies have discovered certain areas that require additional improvement to optimise the efficiency and effectiveness of regenerative braking systems. The key elements being evaluated for improvement are the brake controller, the utilisation of flywheels, and the incorporation of SCs.

2.5.3.1) Flywheel

A flywheel functions as an electrochemical battery that relies on inertia, as depicted in Figure 2.18. This mechanism efficiently absorbs and stores mechanical energy. The magnetically-supported flywheel efficiently transfers electrical energy into kinetic energy and vice versa by utilising a single motor/generator. Technically, it functions by storing excess energy when there is more supply than demand, and then releasing that stored energy when there is more demand than supply [72], [74], [77]. To further understand the energy dynamics within a vehicle, we examine the derivation of the vehicle's kinetic energy. In Equation 2.7, the kinetic energy (KE) of a vehicle is derived from fundamental principles of classical mechanics [74]. The kinetic energy of an object is expressed as:

$$KE = \frac{1}{2} mv^2 \tag{2.7}$$

Where

m: Total mass of the vehicle

v: Velocity/Speed of the vehicle

The flywheel is essential in managing fluctuations in shaft speed produced by torque during regenerative braking. The system functions whenever there are fluctuations in the driving torque or load torque. By increasing the angular velocity of the flywheel and decreasing its speed, the stored energy is efficiently released. The specific energy of the flywheel is directly proportional to the decrease in mass of the spinning material, assuming the mechanical strength remains constant [72], [74], [78]. The mass can be reduced by using high-strength, low-density materials like carbon fibre composites or titanium alloys.

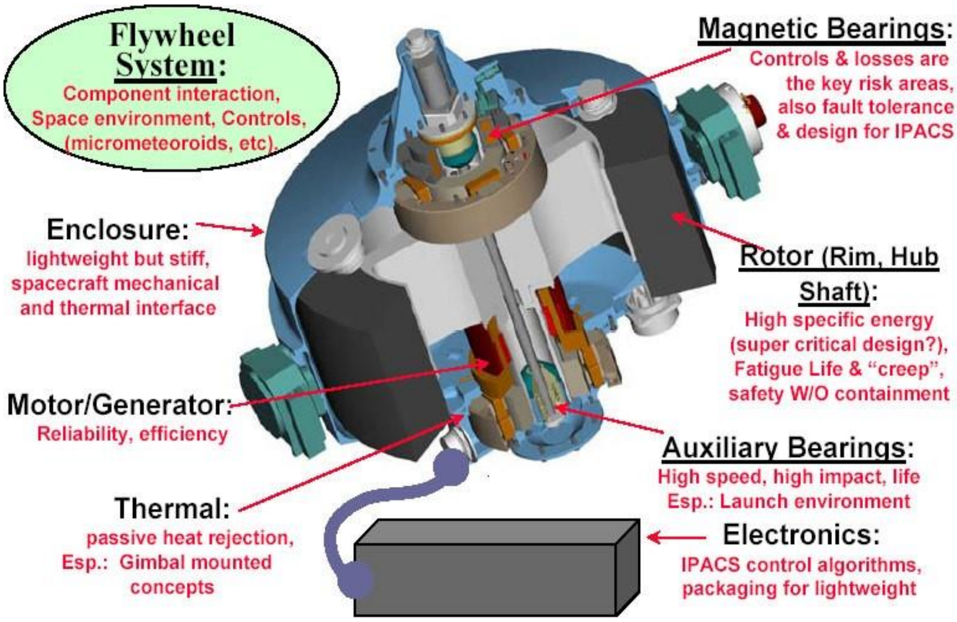

Figure 2.18 - Flywheel Mechanism [78]

2.5.3.1.1) Characteristic of Flywheel

Flywheels possess several qualities that make them suitable for energy storage and management in vehicular systems [72], [74], [77]:

1) Higher energy density
2) Durable cycle lifetime
3) Adaptability in both the structure and the functioning
4) It is a purely mechanical gadget that receives no power from outside sources.

Flywheels provide a lot of benefits, but they also have a few drawbacks. Their dependence on mechanical parts opens them up to the possibility of wear and tear, which is a major drawback. Additionally, it can be bulky and requires ensuring balance and stability at high rotational speeds [72], [74], [77].

2.5.3.2) Supercapacitors

By incorporating SCs into electric vehicles EVs, their energy storage capacity is greatly improved, resulting in an increased driving range for these vehicles. The next section will offer an extensive and precise elucidation of SC technology, with a particular emphasis on its technical components and operational capabilities.

2.6) Overview of Supercapacitors and Energy Storage

Capacitors operate as a different method of storing energy by utilising the separation of charges to generate a voltage in a setup consisting of parallel plates. This technique comprises two opposed plates that are kept apart by a dielectric substance, enabling capacitors to function without any chemical interactions, in contrast to batteries. SC, often referred to as ultracapacitors, are distinct from standard capacitors due to the fact they utilise an electrolyte and a thin insulator, typically composed of materials such as cardboard or paper, instead of a conventional dielectric [79].

SC have become an important part of energy storage systems because of their high power density, long lifespan, and very high capacitance compared to conventional capacitors. SCs still have a lower energy density than lithium-ion batteries, even with all these benefits. As a result of this quality, HESS has been developed, which combines the advantages of SCs and lithium-ion batteries while reducing their disadvantages. The integration of the SC technology in HESS will be elaborated on further [80]. SCs can be categorised into three primary types: Electrostatic Double-Layer Capacitors (EDLCs), pseudo-capacitors, and hybrid capacitors.

2.6.1) Electrostatic Double-Layer Capacitor

This type of SC has a phenomenon called the Helmholtz double-layer, where layers in between electrodes are made thinner, which leads to idiocies having a much higher energy density, however, compared to batteries this is still quite low [81]. A schematic representation of EDLC can be seen in Figure 2.19. The process of charging an EDLC involves the transfer of positive ions towards the negative electrode and negative ions towards the positive electrode. This flow is prompted by the application of a power source. At the point where the electrolyte meets the activated carbon electrodes, an electric double layer forms due to the ion migration. Figure 2.20a demonstrates that the activated carbon electrodes can store more charge because their micropores greatly enhance their surface area [82]. Figure 2.20b depicts the process of discharging an EDLC. When the capacitor is connected to a load, the charges stored in the electric double layer are discharged, resulting in the generation of an electric current that supplies power to the load. EDLCs are characterised by their ability to rapidly charge and discharge, which allows them to efficiently offer high power density [82].

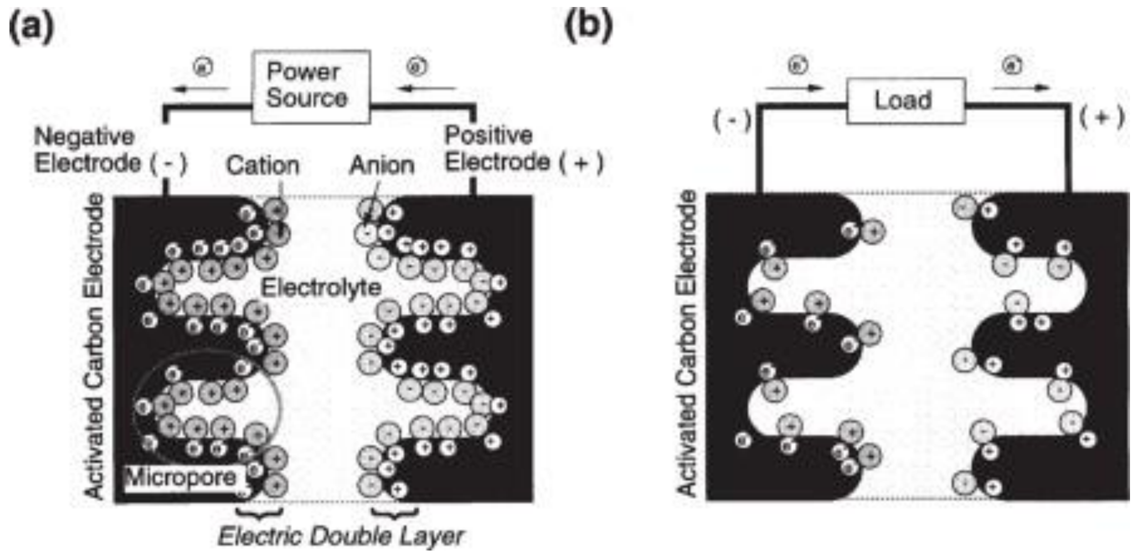

Figure 2.19 - Schematic representation of EDLC. (**a**) Charge state. (**b**) Discharge state [82]

2.6.2) Pseudo Capacitor

There are two distinct methods by which this particular SC can function. Energy is stored electrostatically in the first method, which is comparable to EDLCs. In the second approach, energy is stored electrochemically, as electron charge shifts occur between the electrode and the electrolyte. The electrodes are capable of hosting a rapid sequence of redox reactions, which enables the electrochemical storage of energy. This is achieved through the use of carefully chosen materials [83].

See Figure 2.20 for a schematic illustration of pseudo capacitors. As demonstrated, pseudo capacitors are composed of pseudocapacitive electrode materials that stimulate the redox reactions required for the storage of electrochemical energy. The pseudo capacitor's operability is contingent upon the presence of a separator, electrolyte, and current collector in the structure. Electrode materials are essential for energy storage as they endure reversible redox reactions, which lead to the accumulation of charge. Pseudo capacitors are capable of achieving higher energy densities than traditional EDLCs as a result of this distinctive mechanism, making them appropriate for a diverse array of high-performance energy storage applications [83].

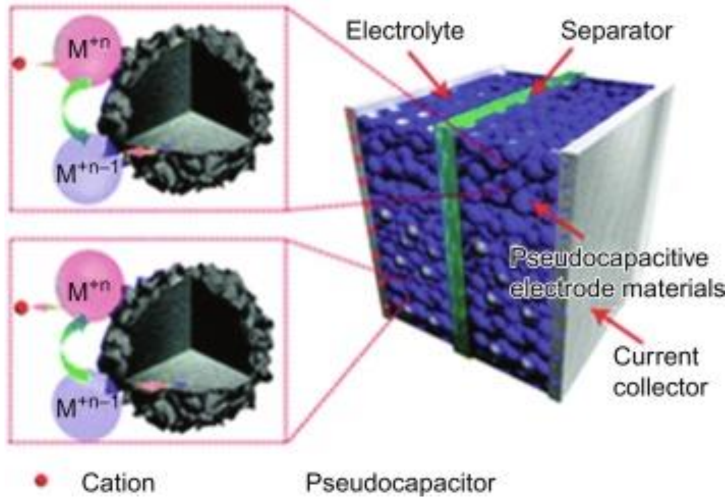

Figure 2.20 - Schematic representation of pseudo-capacitor [83]

2.6.4) Energy Storage

There is an increasing demand for EVs to support the decarbonisation of transportation. The increased demands drive the development of stored electrical energy to be re-used in driving the EV sector. EV batteries are always advised to have a shorter recharge time and longer time to use before recharge. Two types of electrical energy storage devices are particularly attracting great attention, these are SC and lithium-ion batteries.

The relationship between energy density and power density is illustrated in Figure 2.21 [79]. SCs demonstrate a moderate energy density and a high power density, while lithium-ion batteries display a low power density and a high energy density. The objective of an energy storage system is to simultaneously achieve enhanced energy and power, referred to as a HESS. A HESS synergistically combines SCs and lithium-ion batteries, leveraging the advantages of both technologies into a single, cohesive system.

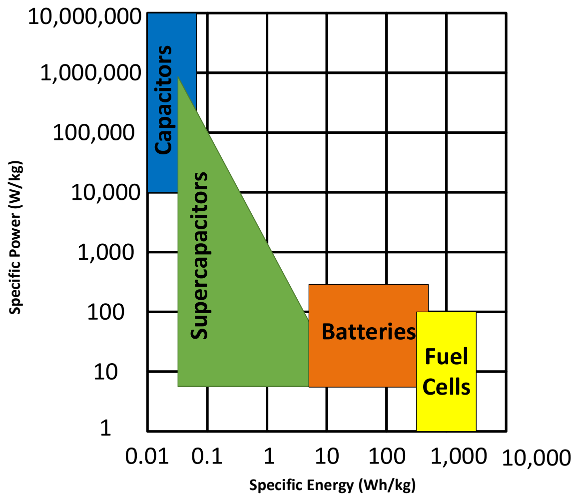

Figure 2.21 - Comparison of Energy Storage Devices [12]

The battery and SC systems are given a lot of attention, with an energy-dense battery functioning as a long-range energy source and an SC pack functioning as a peak power source, releasing bursts of high power during acceleration and recovering regenerated energy during brake [99]. Many HESS topologies that combine both battery and SC are commonly employed. The following are the details:

2.6.4.1) Passive

The most basic configuration for integrating battery and SC energy storage systems is the passive parallel connection, illustrated in Figure 2.22a. In this arrangement, both the battery pack and the SC are directly linked to the motor [12], [86], [87], [88]. This topology is preferred due to its straightforwardness and simplicity in its execution. Nevertheless, the absence of regulation on the DC side is a notable disadvantage. As the SC is linked in parallel with the motor drive, its control parameter needs to be calibrated to match the requirements of the motor drive. Hence, the amount of energy that can be obtained from the SCs is restricted by the working range of the motor drive. This limitation has a direct effect on the overall efficiency and effectiveness of the energy storage system.

It is important to acknowledge that the passive parallel connection simplifies the system architecture, but it also restricts the dynamic management and optimisation of energy distribution between the battery and the SC. Hence, in situations when accurate energy management and control are of utmost importance, alternate configurations or supplementary control methods may be necessary to improve performance and dependability.

2.6.4.2) Semi-Active

Semi-active HESS designs typically involve a controlled SC and a controlled battery. These configurations address several limitations inherent in passive parallel HESS designs.

2.6.4.2.1) Controlled SC

The controlled SC HESS design, as depicted in Figure 2.22b, enhances passive parallel HESS by directly connecting the battery pack to the DC bus. This direct connection guarantees a consistent voltage supply from the battery, while the power contribution from the SC is regulated by a DC/DC converter [12], [86], [87], [88]. This configuration effectively mitigates the primary drawbacks of passive parallel HESS, including inadequate power management and inefficiencies in power distribution. Nevertheless, this method is significantly hampered by the requirement for the DC/DC converter to be rated for the system's maximal power demand [12], [86], [87], [88]. This leads to a decrease in system efficacy and an increase in costs as more power is transferred through the interface converter.

2.6.4.2.2) Controlled Battery

On the other hand, the controlled battery HESS layout, as illustrated in Figure 2.22c, controls the battery independently via a DC-DC converter. In the controlled battery system, it is essential for the DC-DC converter to be rated for the system's maximal power demand. This ensures reliable operation under peak load conditions, prevents overloading, and maintains system stability and efficiency during high-demand scenarios. The SC is directly connected to the DC bus, where it functions as a low-pass filter [12], [86], [87], [88]. With this configuration, the SC is capable of absorbing high-frequency components of the load demand and stabilising power fluctuations. However, the DC-link voltage may fluctuate as a result of the SC's direct connection to the DC bus [12], [86], [87], [88]. In order to preserve the DC-link voltage's stability, it is imperative to implement a high-capacity SC, which may result in an increase in the overall system's complexity and cost [12], [86], [87], [88].

2.6.4.3) Fully Active

The fully active topology, seen in Figure 2.22d, utilises two DC-DC converters to separate the battery and SC from the DC bus [27], [28]. This setup offers numerous noticeable benefits. Firstly, it permits the separate modification of the battery and SC voltages to values below the direct current bus voltage, thus maximising the utilisation of the SC. By implementing this autonomous regulation, the energy efficiency and performance of the SC are optimised, resulting in notable advantages in energy density and power transmission.

Moreover, the fully active topology provides more flexibility in managing the energy storage system. By autonomously regulating the power distribution from the battery and SC, the system can potentially be fine-tuned for different operational situations, such as instances of high power requirements and regenerative braking events. This adaptability can result in enhanced overall system efficacy and extended battery lifespan, since the battery receives protection from high-power fluctuations that might induce wear and deterioration [94], [95], [96].

Despite the control technique for this configuration is more complex than simpler configurations, the potential advantages in terms of energy management and system efficiency are significant. While employing two full-sized converters may lead to greater initial expenses and potential decreases in system performance due to increased intricacy, these disadvantages can be alleviated by the substantial operational benefits offered by the fully active architecture [94], [95], [96].

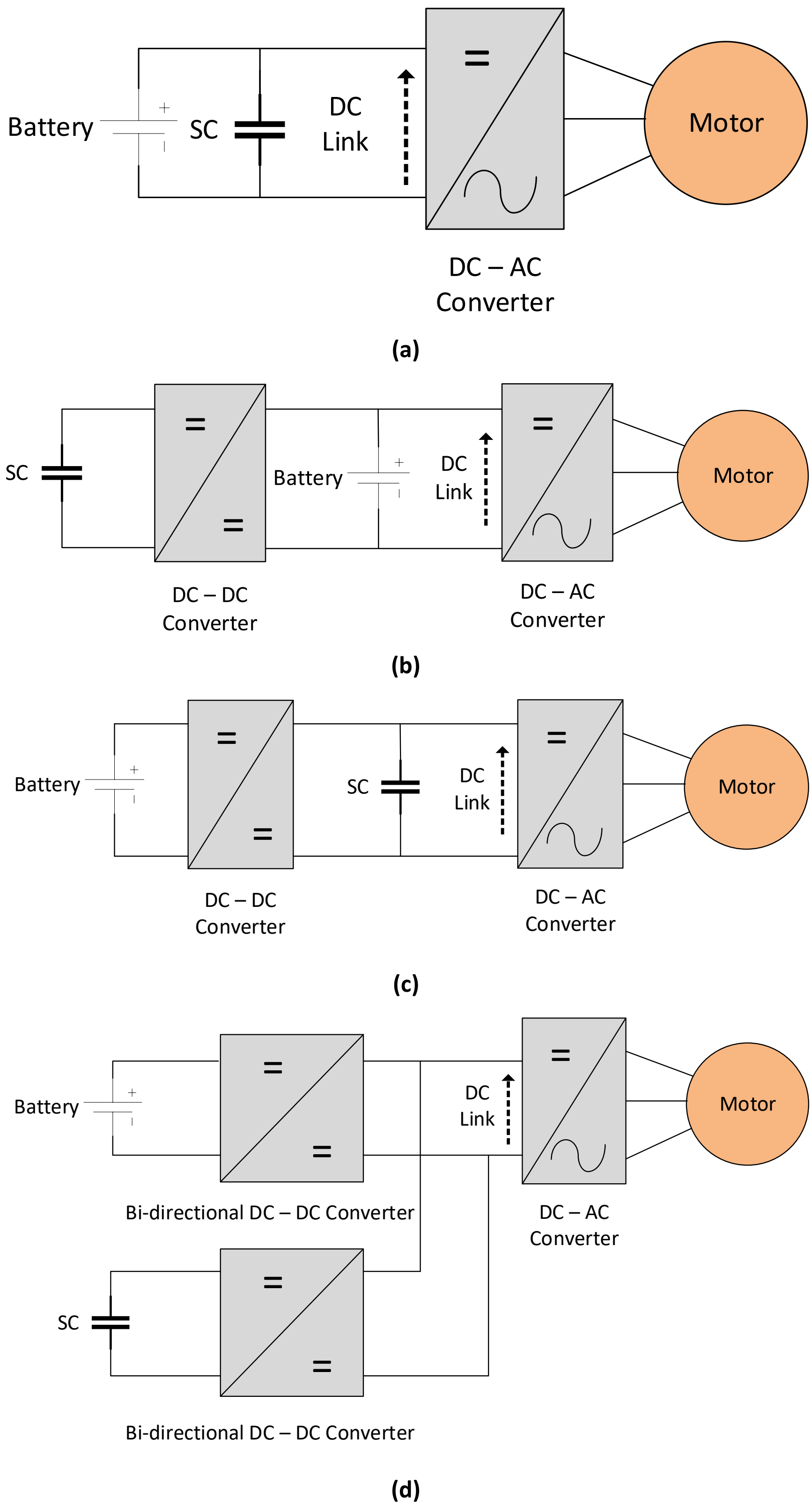

Figure 2.22 - HESS configurations: (**a**) passive parallel, (**b**) controlled SC, (**c**) controlled battery, (**d**) fully active [12]

2.7) Traction Motor Selection

In EVs, the generation of power is a physical process that entails the generation of a current to create a magnetic field within the stationary component of the machine, commonly referred to as the stator. A displacement is induced by this magnetic field, which starts the rotation of the rotor, another component of the machine. To operate electric motors, this rotation is essential, as it converts electrical energy into mechanical energy. Gaining a comprehensive understanding of the functioning of electric motors is crucial for the progress of EV technology. Electric motors can be categorised into different types according to their construction and operating principles. Figure 2.23 depicts many categories of AC and DC traction motors [89]. Recent research [90], [91], [92] have identified brushless DC motors (BLDC), AC induction motors (IM), permanent magnet synchronous motors (PMSM), and switching reluctance motors (SRM) as the most often utilised electric motors in EVs.

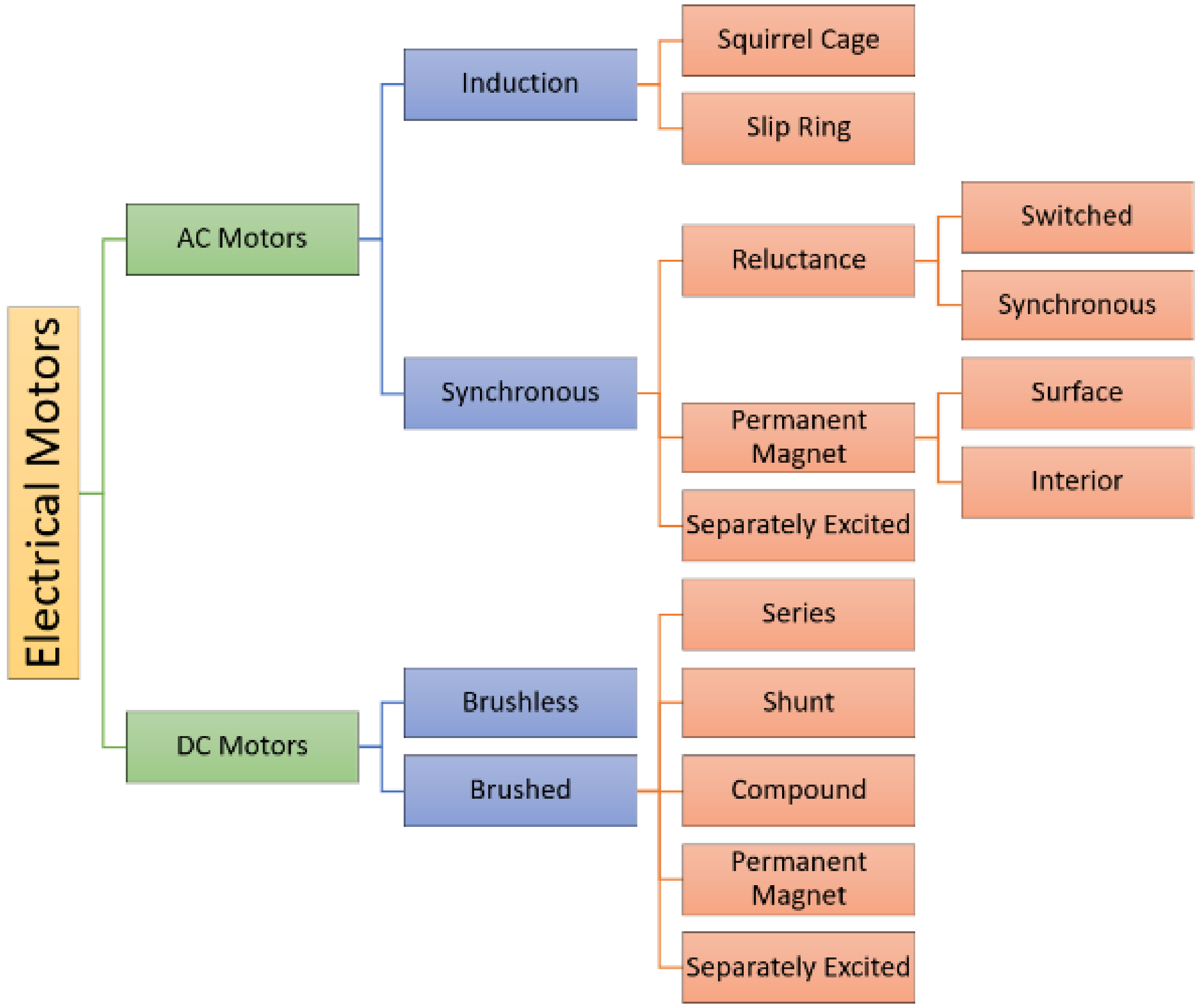

Figure 2.23 - Types of electrical motors [89]

2.7.1) DC Brushless Motor

DC motors, which have been traditionally used in EVs because of their uncomplicated speed regulation, advanced development, and economical manufacturing expenses, have now progressed to incorporate brushless designs [93], [94], [95] [96] . BLDC motors are commonly used in control applications due to their simple design, robustness, and cost-efficiency [97], [98]. The motors are available in single-phase, two-phase, and three-phase variants. BLDC motors are characterised by their high speed-to-torque ratios and their reliance on rotor position inputs for electronic commutation [99]. The rotor, which is fitted with a permanent magnet, and the stator poles wound with wire, generate a consistent density of magnetic flux in the space between them. Hall effect sensors are used to determine the position of the rotor, which is important for providing necessary feedback for commutation. BLDC motors provide exceptional power density, increased torque, minimised noise, elimination of electromagnetic interference, and excellent efficiency, making them the preferred option for EV applications [100].

2.7.2) Induction Motor

IM function by supplying the stator with a sinusoidal AC current, resulting in the creation of a spinning magnetic field and the generation of a current in the rotor [101]. Torque is generated by the interaction of the magnetic fields of the rotor and stator. Induction motors are preferred due to their affordable price, durability, and reduced maintenance needs, as they do not have brushes and commutators. Nevertheless, the requirement for converting AC into DC introduces complication into their control systems. However, their robust durability and cost-efficiency make them well-suited for EVs [102].

2.7.3) Permanent Magnet Synchronous Motor

PMSMs incorporate characteristics of both induction and BLDC motors. These motors have rotors equipped with permanent magnets and stators with windings specifically engineered to generate sinusoidal flux density. These motors have a greater power density compared to induction motors of same size because they do not consume power in the stator for developing the magnetic field [95] [96]. PMSMs exhibit excellent efficiency, substantial torque even at zero velocity, and remarkable power density. However, to achieve best performance, they necessitate the use of variable frequency drives (VFDs). Although this control system improves torque and efficiency, it also increases complexity and cost [103].

2.7.4) Switched Reluctance Motor

SRMs feature rotors without coils, meaning they do not produce magnetic fields or reactive torque. torque is produced by the alignment of stator and rotor pole pairs when the stator phases are energised [104]. Acoustic noise and vibration are the result of the high torque ripple that SRMs generate, despite their simple and cost-effective design. The torque output of these motors is inferior to that of other motor types, which restricts their use in EVs [95] [96].

2.7.5) Study of Motor Drives Efficiency

Every type of motor has unique benefits and drawbacks that affect its applicability for certain uses in the field of electric cars. DC brushless motors are favoured due to their great efficiency and impressive torque-to-speed ratios, but induction motors are highly regarded for their durability and minimal maintenance requirements. Permanent magnet synchronous motors have superior power density and efficiency, albeit at a greater expense and intricacy. Switched reluctance motors, despite their cost-effectiveness and reliability, are not widely utilised in EVs due to their lower torque output and the resulting noise and vibration problems.

The categories and characteristics outlined here offer a thorough understanding of the various roles and capabilities of electrical motors within modern EV technology. Table 2.8 presents the researcher's evaluation of the performance of the main traction motors, using a grading scale from 1 (lowest) to 5 (highest) [93], [96], [105], [106], [107][108].

Table 2.8 - Motor Drives Performance Evaluation [93], [96], [105], [106], [107][108]

Motor features	BLDC	IM	PMSM	SRM
Power density	2.5	4	5	3.5
Efficiency	2.5	4	5	4.5
Controllability	5	5	4	3
Reliability	3	5	4	5
Torque density	3	4	5	4
Speed range	2.5	4	4.5	4.5
Required maintenance	3	4	4	4
Torque ripple/noise	3.5	4.5	4.5	3
Overload capability	3	4	4	4
Complexity	5	4.5	4	3.5
Lifetime	3.5	5	4	4.5
Size and weight	3	4	5	4
Thermal management	5	3	3	5
Cost	4	5	3	4

2.8) Driving Cycles

Driving cycles, comprised of data that shows the relationship between speed and time, play a vital role in assessing a vehicle's performance across several variables. These cycles have multiple essential applications, which include [109]:

- Evaluation of the vehicle's capability
- Evaluation of the battery's capacity
- Evaluation of the vehicle's energy usage
- Modelling of the vehicle before its advancement

Efficient and cost-effective vehicles require careful consideration of materials during the design and manufacturing process. When it comes to EVs, this requires a careful choice of motor power electronics components, batteries, and mechanical elements. The selection process necessitates thorough computation and optimisation to minimise costs and energy losses [109].

2.8.1) Types of Driving Cycles

Driving cycles are subject to three conditions: dynamic, distance, and region. Table 2.9 depicts many sorts of driving cycles [110]. Dynamic situations have been favoured due to their combination of unpredictable and forceful accelerations, as well as sustained high speeds over a prolonged duration. Dynamic driving circumstances can be categorised into two types of driving cycles: model and transient. A model driving cycle is defined by a consistent velocity, so it does not accurately reproduce real-world driving conditions. This specific driving cycle is employed for a specific reason, such as conducting an emission test [111]. An instance of the New European Driving Cycle (NEDC) is depicted in Figure 2.24 [111]. In contrast, transient driving cycles are derived from actual driving patterns that encompass both acceleration and deceleration, as well as periods of constant speed. An illustration of a temporary driving pattern can be observed in the Federal Test Procedure (FTP 75) as depicted in Figure 2.25 [111].

Table 2.9 - Different Driving Cycle Categories [110]

Conditions	Category	Features
Dynamics	Model driving cycle	Steady state
	Transient driving cycle	Rapid acceleration
Distance	Short	Distance range 0 – 9 miles
	Medium	Distance range 9 – 20 miles
	Long	Distance range above 20 miles
Region	Urban	Speed range 0 – 25 mph
	Mixed	Speed range 25 – 45 mph
	Highway	Speed range above 45 mph

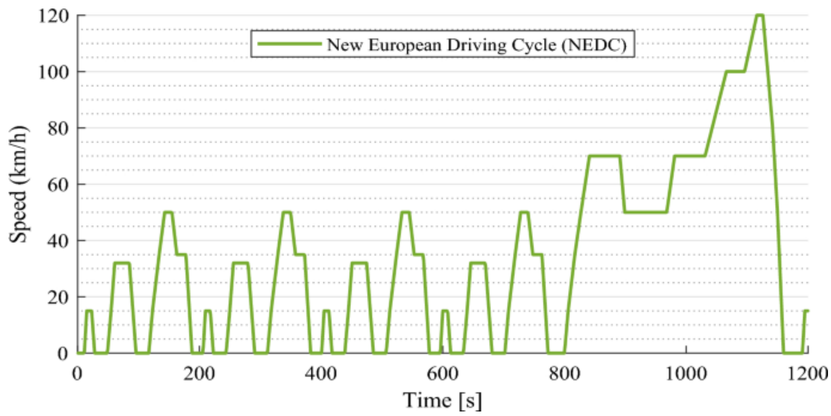

Figure 2.24 - New European Driving Cycle [111]

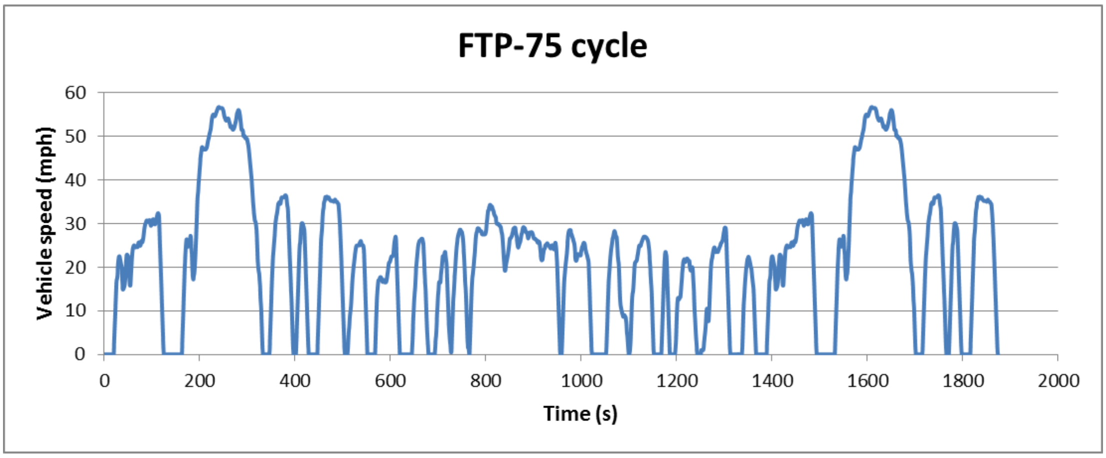

Figure 2.25 - Federal Test Procedure Cycle [111]

2.8.2) Developing Driving Cycle

Driving cycles are useful for forecasting a car's performance. Various methodologies can be employed to construct the driving cycle for urban areas, highways, or rural regions, among others. To design a driving cycle, the following phases must be conducted during the study [112]:

1. Route decision
2. Data gathering
3. Data categorisation
4. Development of drive cycles

2.9) Summary

In conclusion, Chapter 2 literature review has provided a comprehensive examination of the critical components and systems that support the operation and efficacy of EVs, with a particular emphasis on battery technologies and BMS. The review emphasised the various battery types utilised in EVs, including lead-acid, nickel-cadmium, nickel-metal-hydride, and lithium-ion batteries. It also evaluated their distinctive characteristics, advantages, and constraints. The critical parameters that influence battery performance, such as energy density, power density, charging rates, and lifecycle, were the primary focus.

The review also addressed the intricacies and advancements of BMS, including their function in monitoring and managing battery health, estimating SOC and SOH, thermal management, and maintaining cell balance. The significance of incorporating advanced control strategies and real-time tracking to improve battery safety and performance was emphasised.

Furthermore, the review investigated the concept of HESS, which integrates batteries and SCs to capitalise on the complementary capabilities of each technology. The challenges and research opportunities in this field, as well as the prospective advantages of HESS in enhancing the efficiency, reliability, and lifespan of EVs, were addressed.

Overall, this literature review establishes a thorough foundation for comprehending the present state of battery technologies and management systems in EVs, thereby facilitating additional research into the optimisation of these systems to improve their sustainability and performance.

Chapter 3 Control Strategies for Hybrid Energy Storage Systems in Electric Vehicles

3.1) Brief

This chapter explores the development and advancement of HESS designed for EVs. This technology tackles the difficulties linked to conventional lithium-ion batteries, including their restricted power density, shorter lifespan, and high manufacturing cost. The chapter addresses the potential benefits of combining SCs with lithium-ion batteries, including improved energy efficiency, longer lifespan, and enhanced performance. The essential elements comprise the HESS's structural framework, dynamic vehicle modelling for power and energy consumption prediction, and comprehensive models for both batteries and SCs. In addition, the chapter explores different control systems, such as PI, MPC, RBF, to enhance power distribution and enhance the overall performance of EVs.

3.2) Background

EVs are at the forefront of the global transition to sustainable transportation, with their success heavily reliant on the efficacy of their energy storage systems (ESS). The primary challenge in EV development is optimising these systems to ensure maximum energy efficiency, longevity, and performance. The most widely used ESS in EVs is the lithium-ion battery, prized for its high energy density. However, lithium-ion batteries come with significant drawbacks, including limited power density, reduced cycle life, and high costs. These limitations have spurred research into HESS that integrate lithium-ion batteries with SCs. SCs offer high power density and excellent cycle life, providing rapid energy discharge and absorption, which complements the slower but more energy-dense lithium-ion batteries.

3.3) Designing and Modelling a Hybrid Energy Storage System

The effective design and modelling of a HESS for EVs require a comprehensive approach that considers both the individual components and their interactions within the system. An adequately organised HESS not only guarantees the most effective utilisation of energy but also improves the overall performance and durability of the vehicle's energy storage components. This subsection explores the fundamental elements of system design, including as the structural framework, the behaviour of vehicles, and the intricate representation of batteries and SCs. The goal is to achieve a smooth equilibrium between energy efficiency and strong performance in different operational settings by incorporating innovative control systems.

3.3.1) Structural Framework

HESS utilises the advantageous qualities of both lithium-ion batteries and SCs to improve the efficiency and longevity of EVs. HESS can enhance the energy efficiency and lifespan of EV components by properly managing their dynamic power demands. Multiple configurations of HESS have been investigated, each possessing distinct benefits and difficulties. The completely active architecture is distinguished by its exceptional capacity to precisely regulate energy distribution and adjust to different load requirements. Section 2.6.4.3 contains a comprehensive discussion of the fully active topology.

3.3.2) Vehicle Model

The study focuses on analysing the dynamic forces affecting a vehicle's performance, which include aerodynamic force (F_{aero}), rolling resistance (F_{roll}), grading force (F_{grad}), and inertial force (F_{acc}). These forces are pivotal in developing a robust model that predicts a vehicle's power and energy consumption under various driving conditions. A comprehensive model of these forces, as illustrated in Figure 3.1, is the foundation for optimising the energy efficiency of the vehicle's drivetrain. Notably, this study excludes the grading force from the analysis, as its impact is minimal on the primary objective of examining driving resistance and power demands. This exclusion ensures a more focused and effective evaluation of the vehicle's performance under appropriate conditions without adding unnecessary complexity. Equation 3.1 determines the total force acting on a vehicle [113] [114].

$$F_{Total} = F_{aero} + F_{roll} + F_{grad} + F_{acc} \tag{3.1}$$

When a vehicle is in motion, it encounters various forces, one of which is aerodynamic drag. This force results from the interaction between the incoming and outgoing airflow. The aerodynamic force can be calculated using Equation 3.2 [113] [114].

$$F_{aero} = 0.5\, \rho\, C_d\, A_f\, v^2 \tag{3.2}$$

where ρ is air density, C_d represents the drag coefficient, A_f represents the frontal area of the vehicle, and v denotes velocity. The main cause of rolling resistance is the interaction between the road surface and the tyre. Both the friction of ball bearings and the power transmission system are factors that contribute to the rolling resistance. Rolling resistance increases in direct correlation with the mass of the vehicle. Equation 3.3 represents the force of horizontal road rolling resistance [113] [114].

$$F_{roll} = C_{rr}\, m\, g \tag{3.3}$$

where C_{rr} is the coefficient of rolling resistance, m represents the mass of the vehicle in kilogrammes, and g represents the acceleration due to gravity in metres per second. Equations 3.4 and 3.5 are utilised for calculating the gradient force and acceleration force [113] [114].

$$F_{grad} = m\ g\ \sin\ (\theta) \tag{3.4}$$

$$F_{acc} = m\ a \tag{3.5}$$

where a represents the acceleration. The power required for an EV can be determined and expressed using Equation 3.6. Where it calculates the sum of all forces exerted on the vehicle and combines it with the vehicle's velocity to determine the total power required in different driving scenarios [113] [114].

$$P_{Req} = F_{Total} * v \tag{3.6}$$

By thoroughly understanding and modelling these forces, the study aims to develop a reliable framework for predicting vehicle performance.

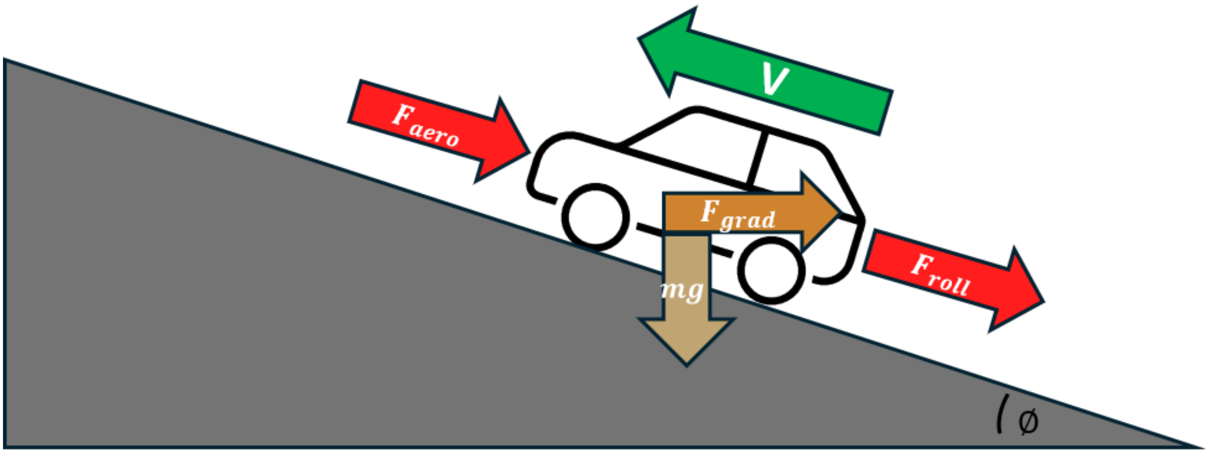

Figure 3.1 – Vehicle Forces

3.3.3) Battery Model

An equivalent circuit model is a widely used representation that utilise electrical elements to replicate the battery's activity. There are several ways to depict the electrical equivalent circuit model for the battery. Most of these representations can be categorised into two basic types: electrochemical models and equivalent circuit models, as explained in Section 2.3.6. [115].

The battery model depicted in Figure 3.2 has two integral equations to regulate the charging and discharging operations, effectively capturing the operational dynamics of a lithium-ion battery. Equation 3.7, which is crucial to the functioning and is illustrated in the selector switch mechanism Sel, is expressed as [113]:

$$\frac{Exp\ (s)}{Sel\ (s)} = \frac{A}{(\frac{1}{B} * i(t) * s + 1)} \tag{3.7}$$

The given formula employs an exponential smoothing function $Exp\ (s)$ to regulate the current $i(t)$, ensuring the system responds smoothly and progressively to changes in load and charging conditions. Derived from the battery model, this equation is intended to enhance efficiency and longevity by preventing abrupt current fluctuations. This smoothing mechanism balances power demand, battery energy degradation, and Equation 3.7, thereby modulating the battery's response to power requirements. The constants A and B, along with the variable s (from the Laplace transform domain) and the current $i(t)$, dynamically adjust the input current's influence. This dynamic adjustment aligns with the operational mode determined using the $Sel\ (s)$ switch. The battery model incorporates key parameters such as filtered current, short circuit current, and self-discharge current to accurately reflect its operational dynamics and align with the circuit's principles. Battery model uses Equations 3.8 and 3.9 to illustrate both charging and discharging scenarios [113].

$$E_{charge} = f_1\ (it, i^*, Exp.BattType) \tag{3.8}$$

$$E_{discharge} = f_2(it, i^*, Exp.BattType) \tag{3.9}$$

Equations 3.8 and 3.9 are essential for determining the energy required for charging and discharging. They consider various factors, such as the actual current (it), the filtered current (i^*), the exponential smoothing factor (Exp), and the battery type ($BattType$). By incorporating these parameters, the equations enable the battery management system to accurately regulate energy distribution, enhancing efficiency and extending the battery's lifespan in different operational conditions. Properly deriving and integrating these equations with the battery model's elements is vital for effectively controlling energy flows, as shown in the battery model schematic [113].

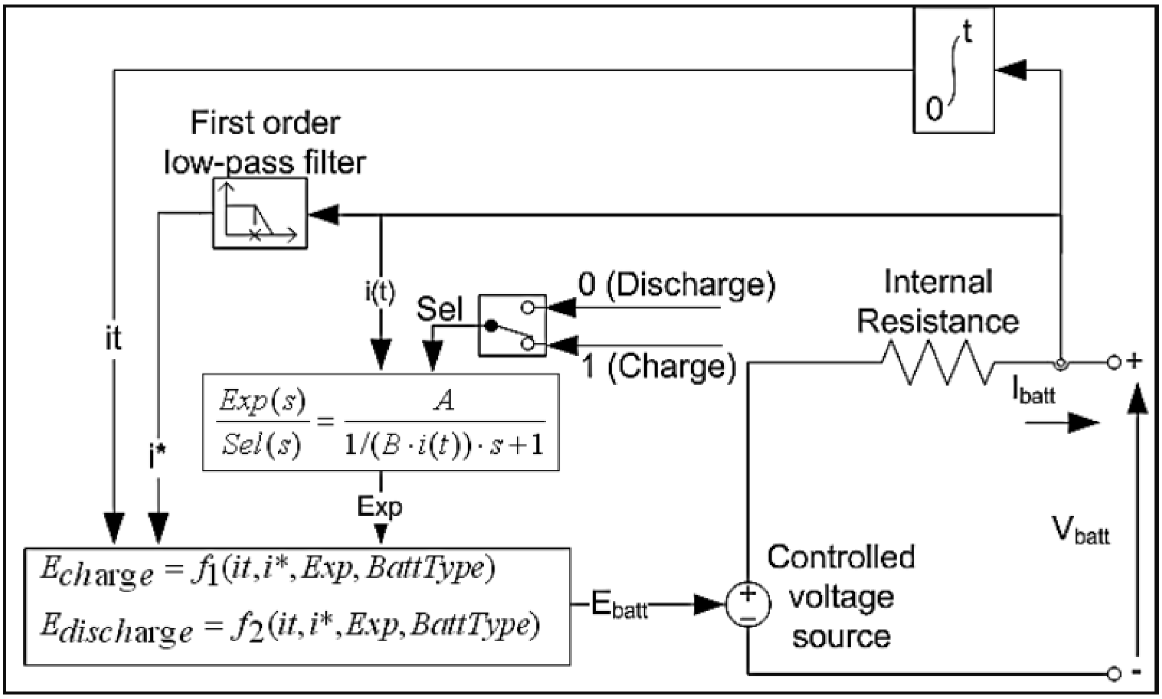

Figure 3.2 - Battery Equivalent Circuit [116]

3.3.4) Supercapacitor Model

Figure 3.3 illustrates the SC model, which portrays the equivalent circuit of a SC. This circuit includes a controlled voltage source connected to the SC, which features an internal resistance. Two essential mathematical equations that are fundamental to comprehending the operational behaviour of the system are also depicted in the schematic. Equation 3. 10 describes the total current i [113].

$$i = i_{sc} * \left(1 - u(t)\right) + \; i_{self_{dis}} * u(t) \tag{3.10}$$

where i_{sc} is the short circuit current, $i_{self_{dis}}$ is the self-discharge current, and $u(t)$ is the unit step function that controls the transition between normal operation and self-discharge. This configuration allows for a comprehensive examination of how the SC responds to different operational conditions, accounting for both internal chemical processes and external circuit parameters influencing electric current flow. Equation 3.11 determines the floating potential V_T of the SC when it is not actively supplying current to an external load [113].

$$V_T = \frac{N_s\; Q_T\; d}{N_p\, N_e\;\; \in\in_0\;\; A_i} + \frac{2\; N_e\; N_s\; R\; T}{F}\; arsinh\left(\frac{Q_T}{N_p\; {N_e}^2\; A_i\; \sqrt{8RT\; \in\in_0\; c}}\right) \tag{3.11}$$

In this equation, N_s and N_p denote the number of series and parallel connections of the SC cells respectively, Q_T is the electric charge (C), d is the molecular radius, N_e represents the number of electrode layers, $\in$ and $\in_0$ denote permittivity of the material and free space, A_i is the interfacial area between electrodes and electrolyte (m^2), R is the ideal gas constant, T is the operating temperature (K), F is the Faraday constant, and c is the molar concentration (mol/m^3) [113].

Equations 3.10 and 3.11 are essential for accurately predicting the performance characteristics of SCs, particularly in applications requiring detailed analysis of power distribution and storage behaviours under various electrical loads and conditions. This knowledge is critical for optimising battery management systems, enhancing reliability, and extending the lifespan of battery-powered devices [113].

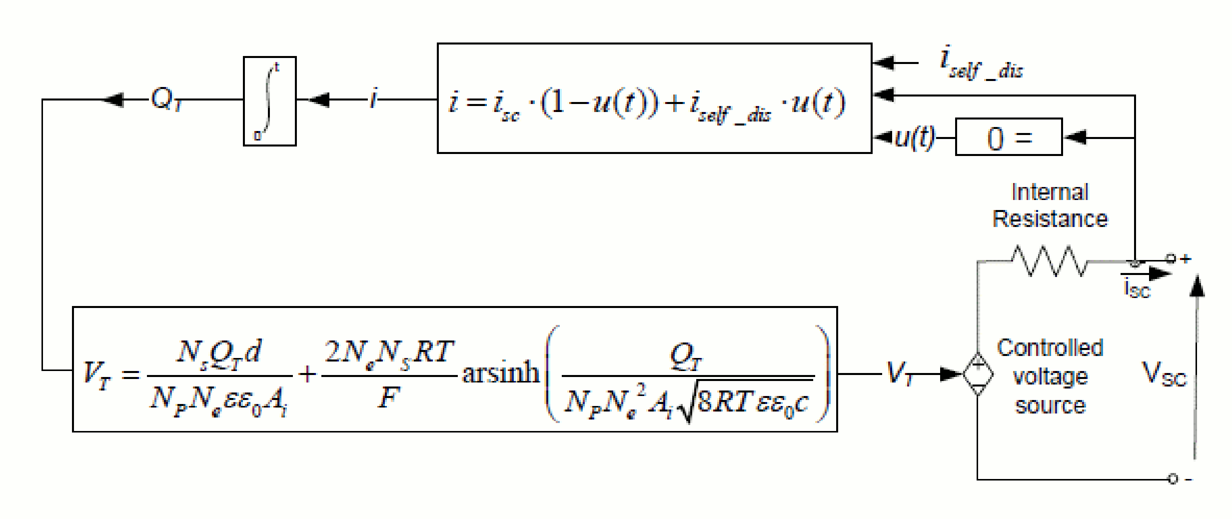

Figure 3.3 - SC Equivalent Circuit [116]

3.4) Controller Design

An efficient regulator is crucial for maximising energy transfer inside a HESS in EVs, improving dynamic performance and prolonging battery lifespan. The controller must properly regulate the allocation of power between the battery and SC to secure the battery against unexpected power fluctuations and enhance vehicle performance. The HESS combines a battery with a SC, and incorporates a rate limiter to provide smooth power changes. Figure 3.4 illustrates the structure of the system used in this study. The system utilises a boost converter to charge the battery and a buck-boost converter to charge/discharge the SC to fulfil the power needs of the EV. Three control systems, including PI control, MPC, and RBF neural network-based control, are utilised to attain optimal performance. These strategies optimise the distribution of power by considering real-time demand and using prediction models. They make use of the high energy storage capacity of batteries and the fast charging and discharging abilities of SCs. This comprehensive strategy tackles the drawbacks of independent energy storage systems and provides to the sustainable and effective use of energy in contemporary transportation [113].

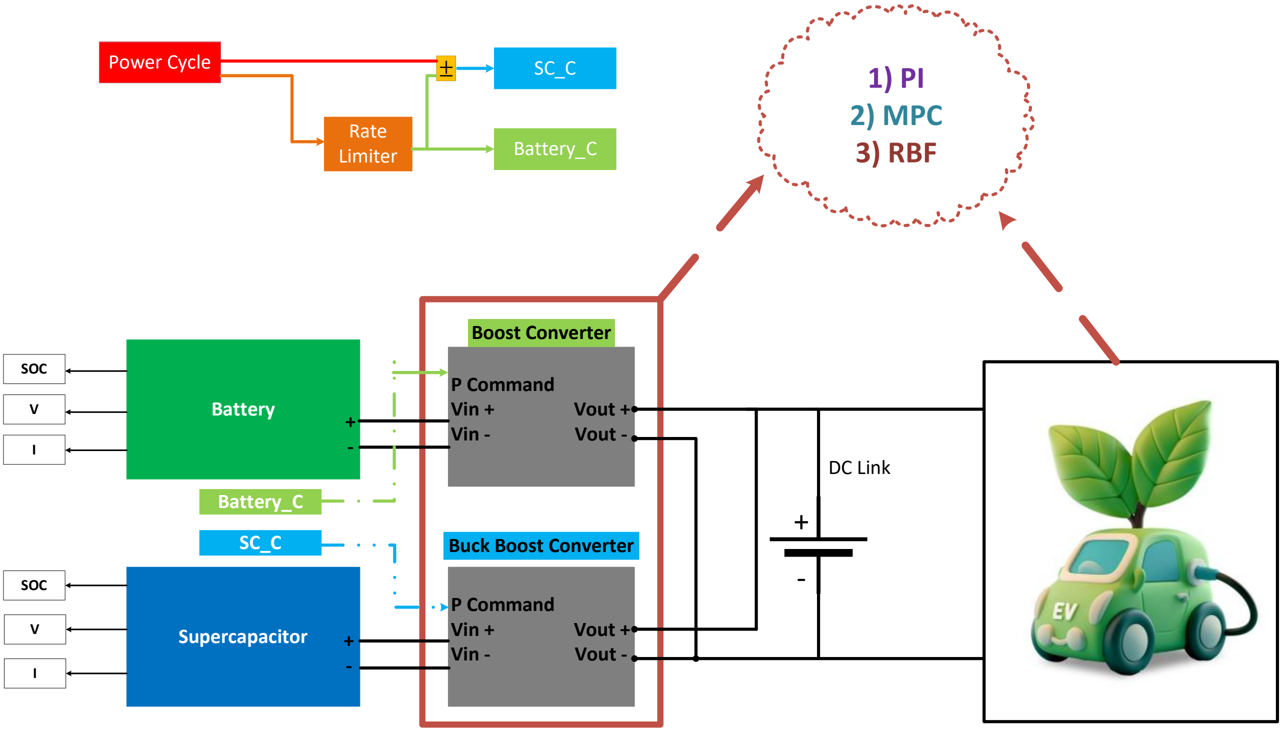

Figure 3.4 - Construction of the Proposed System

3.4.1) Proportional-Integral Control

The simplicity and convenience of the implementation of PI control make it a popular choice for industrial applications. It ensures constant operation by adjusting the control signals by the discrepancy between the desired and actual performance. Nevertheless, PI controllers may encounter performance degradation as a result of system unpredictability and parameter variations.

One notable application of the PI regulator is in optimising power allocation among batteries and SCs to ensure efficient system operation. The primary objective of this regulator is to minimise the difference between the desired reference value and the actual result, as mathematically represented in Equation 3.12 [113].

$$e(t) = r(t) - y(t) \tag{3.12}$$

Where $r(t)$ denotes the setpoint, the target value that the system aims to achieve, while $y(t)$ signifies the actual measurement, the observed value. The error signal $e(t)$, which is the difference between these two values, serves as the critical input for the PI regulator. The controller addresses this error by adjusting the control action, as expressed in Equation 3.13 [113].

$$u(t) = K_p * e(t) + K_i \int e(t)dt \tag{3.13}$$

Where K_p and K_i represent the proportional and integral gains, respectively. These gains are pivotal in ensuring the stability and precision of the system. The resultant control action $u(t)$ is employed to modulate the pulse-width modulation (PWM) signal, which in turn controls the switching operations of the converter within the HESS [113].

The practical consequences of these adjustments are substantial. The PI controller effectively adjusts the charge and discharge cycles of the batteries and SCs in response to changing power needs, ensuring consistent performance levels. This feature is especially vital in EV uses, where maximising energy efficiency and guaranteeing quick response times are of utmost importance. The system's constant feedback mechanism enables the controller to adjust its operations in real-time, guaranteeing that the energy storage system performs with maximum efficiency [113].

3.4.2) Model Predictive Control

MPC is an advanced control method that uses a system model to predict future behaviour and optimise control actions. It can efficiently handle control challenges and constraints related to several variables, making it ideal for complex systems such as the HESS in EVs. The MPC algorithm reliably integrates up-to-date data into its model, ensuring optimal performance and adaptability in the face of changing conditions.

MPC is one of the most effective control strategies in the context of power conversion in a HESS, with a particular emphasis on DC–DC converters. It is specifically designed to optimise a cost function to predict future system states by evaluating the future state of the inductor current ($I_{L,k+1}$), as outlined in Equation 3.14 [113].

$$I_{L,k+1} = \left(\frac{t_s}{L}\right) * \left(V_{in} - I_L * R_L - V_{out} * (1 - State_n)\right) + I_L \tag{3.14}$$

Where t_s is the sampling time, L is the inductance, R_L is the load resistance, $State_n$ indicates the converter mode (Buck or Buck-Boost), V_{in} is the input voltage, V_{out} is the output voltage, and I_L is the inductor current. $State_n$ alternates between the Buck and Buck-Boost modes depend on the voltage needs of the DC bus in comparison with the input voltage. To systematise this procedure, Equation 3.15 represents an inequality condition that can be used to dynamically ascertain the suitable state of the converter, guaranteeing the most efficient voltage adjustment, whether it be a raise or decrease, based on the requirements of the system [113]. Equation 3.15 is derived from the operational principles of the booster and buck-booster circuit shown in Figure 3.4, where illustrates the functionality of both configurations, demonstrating how they achieve efficient voltage regulation through precise control of the duty cycle. By dynamically adjusting the input and output voltage relationship, the system ensures optimal power delivery under varying load conditions.

$$State_n = \begin{cases} 'Buck' & if\ V_{in} > V_{out} \\ 'Buck - Boost' & if\ V_{in} \le V_{out} \end{cases} \quad (3.15)$$

This formula ensures that the converter mode is selected to either increase or decrease the voltage based on the current power requirements. To be more explicit, the Buck mode is used to reduce the voltage when the input voltage (V_{in}) from the energy storage exceeds the voltage required by the output load. Conversely, if the output load requires a voltage that is greater than the stored voltage, the Buck-Boost mode is activated to increase the voltage. This technique optimises the energy efficiency of the system by adjusting the voltage levels to match the specific needs at any given time, hence minimising energy waste and enhancing the overall system performance. The cost function is optimised using the MPC outline, as is expressed in Equation 3.16 [113].

$$J = \left|I_{L_{ref}} - I_{L,k}\right| + w_f * |State_n - State_{old}| \quad (3.16)$$

Where variables $I_{L_{ref}}$, $I_{L,k}$, w_f, $State_n$, and $State_{old}$ represent the reference inductor current, predicted inductor current at step k, weighting factor, and current and previous states of the converter, respectively. w_f imposes a penalty on the cost involved with transitioning between states. The MPC algorithm assesses possible future states by computing the cost associated with each state, considering the deviations from the current reference state and the cost of transitioning between states. It then chooses the control action that leads to the lowest overall cost. This optimisation guarantees effective power management and minimises energy wastage inside the system.

3.4.3) Radial Basis Function Control

RBF controllers are highly advanced type of neural networks that are well-known for their capacity to handle non-linear input and complex dynamic systems. Their capacity to adjust makes them extremely efficient for use in HESSs in EVs. RBF controllers provide adaptive architecture and learning mechanisms that adapt to varying inputs, facilitating accurate control and optimisation [113].

The structure of the RBF network comprises three primary layers, as illustrated in Figure 3.5:

1. Input layer: Receives the external input signals.
2. Hidden layer: Consists of neurons that apply a radial basis function (typically Gaussian) to the inputs. This transformation into a higher-dimensional space facilitates easier pattern recognition and separation.
3. Output layer: Produces the final output based on the transformed data from the hidden layer.

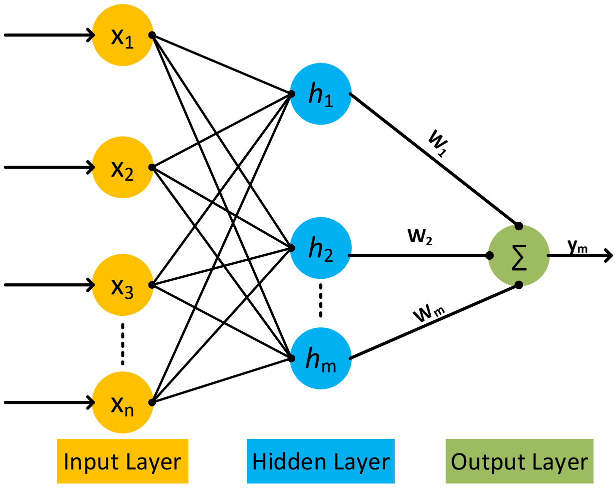

Figure 3.5 – Simple RBF Structure [117]

The network output is given by the Equation in 3.17 in Figure 3.6 plays a crucial role in the model predictive performance.

$$a_2 = B_2 + W * \Phi(x, \mu, \sigma) \tag{3.17}$$

Where B_2 is the bias, W is weight, σ is the spread. Every neuron in the radial basis layer assesses the Euclidean distance between the centre vector (μ) and the network input vector (x), and then applies a non-linear function to this result. Figure 3.7 depicts several different non-linear activation functions. In this investigation, the Gaussian function is utilised. The function exhibits normalisation, and radial symmetry with respect to its centre, and has the ability to approximate any power integrable function accurately.

The output of the radial basis layer is determined by the distance of the input vector to each neuron's center. Consequently, a radial basis network with centers that are significantly different from the input vector will yield an output close to zero. In contrast, a radial basis neuron whose center is near the input vector will produce an output value close to one. The output from the hidden layer is then scaled and adjusted using the W and B_2, respectively, to generate the final network output.

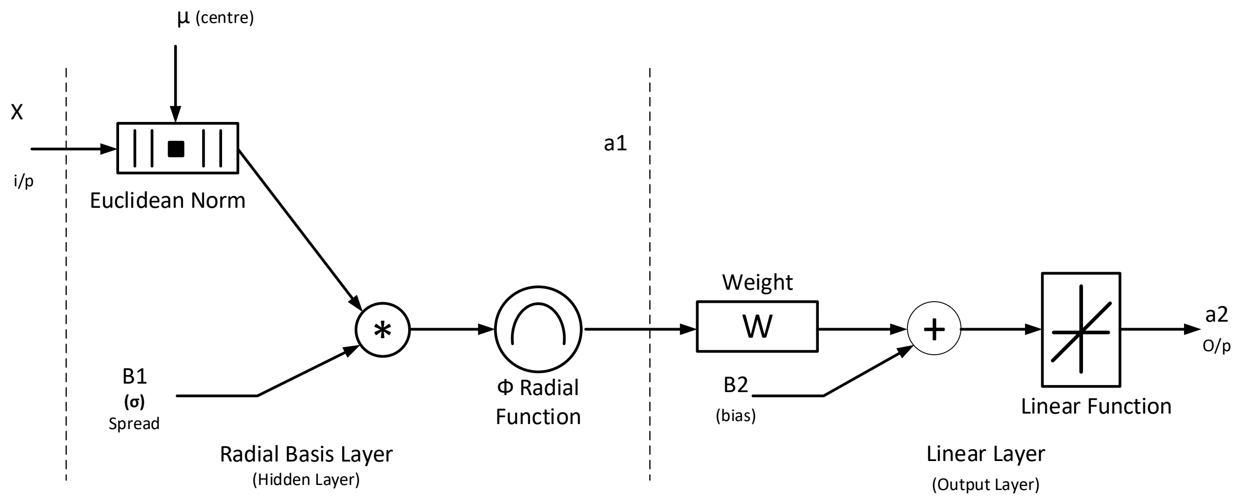

Figure 3.6 – Detailed RBF Network

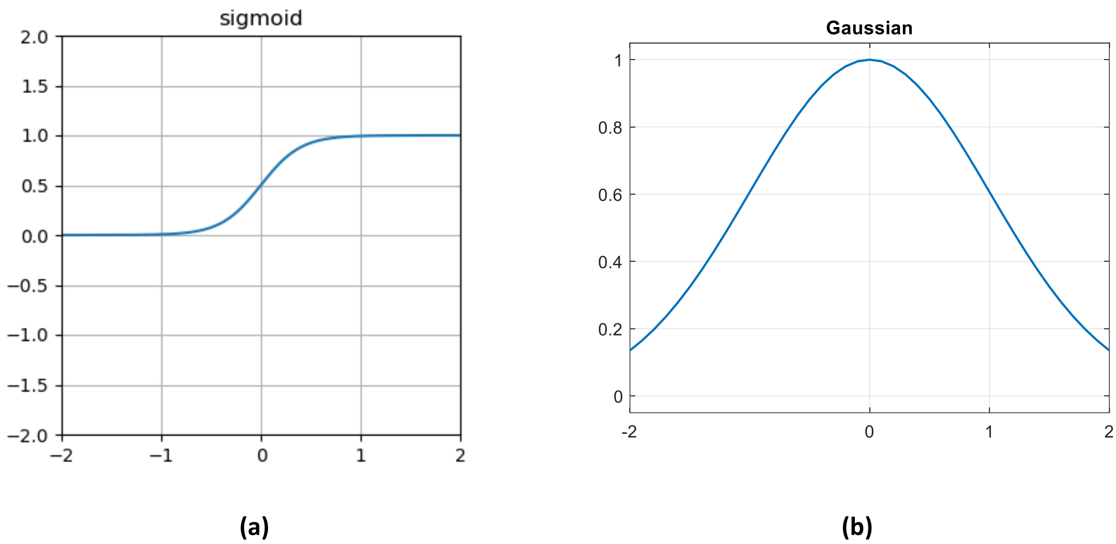

Figure 3.7 - Different Activation Functions: (**a**) Sigmoid, (**b**) Gaussian [117]

3.4.3.1) Leaning Strategies

The structure of the RBF network comprises three primary layers [118]:

1. Hidden layer parameters
   - Centres of each neuron
   - σ
2. Output parameters
   - W
   - B_2

3.4.3.2) Gaussian Activation Function

Activation function plays a vital part in determining the controller's response to changes in input, effectively modifying the system's behaviour to minimise errors and enhance reliability. A Gaussian activation function $\Phi(x, \mu, \sigma)$, is used in the hidden layer and is defined in Equation 3.18 [113].

$$\Phi(x, \mu, \sigma) = e^{-(|\frac{x-\mu}{\sigma}|)^2} \tag{3.18}$$

3.4.3.3) Parameter Adjustment Using Gradient Descent

W, μ, and σ parameters in the RBF are adjusted using the gradient descent technique. This approach improves these parameters by using the error obtained from the system's output, as shown in Figure 3.8. The weight update rule is expressed in Equation 3.19 [113].

$$\Delta W = \lambda_w \, E\Phi(x, \mu, \sigma) \tag{3.19}$$

Where variables ΔW, λ_w and E represents the change in weight, the learning rate and the error. This update is essential for fine-tuning the impact of the input features on the network's output. Equation 3.20 expresses the updated weight, guaranteeing that the system adjusts gradually [113].

$$W_k = \lambda_w E \emptyset_k(x, \mu, \sigma) + W_{k-1} \tag{3.20}$$

μ is adjusted using the formula shown in Equation 3.21.

$$\Delta\mu = \lambda_\mu WE \frac{(x-\mu)}{\sigma^2} \, \Phi\,(x, \mu, \sigma) \tag{3.21}$$

where $(x - \mu)$ represents the distance between the data point and the centre. This formula modifies the midpoint of the Gaussian activation function, enabling the function to maintain its responsiveness to the input data near the updated average. It is essential to update μ, in order to ensure that the Gaussian distribution appropriately represents the most significant data points. This adjustment maintains the precision of the model when handling various inputs, and strengthens the performance and dependability of the control system by enhancing its capacity to adjust to new conditions. The updated centre is determined using Equation 3.22 [113].

$$\lambda_\mu WE \, \frac{(x-\mu)}{\sigma^2} \, \Phi(x, \mu, \sigma) + \mu_{k-1} \tag{3.22}$$

σ represents the spread of the Gaussian bell curve, and can be obtained using Equation 3.23 [113].

$$\Delta\sigma = \lambda_\sigma \, WE \, \frac{(x-\mu)^2}{\sigma^3} \, \Phi(x, \mu, \sigma) \tag{3.23}$$

The update rule plays a crucial role in regulating the responsiveness of the output to variations in the input. This enables the model to improve its ability to make generalisations or concentrate more specifically based on the specific driving conditions. Equation 3.24 expresses the new spread [113].

$$\sigma_k = \lambda_\sigma WE \frac{(x-\mu)^2}{\sigma^3} \Phi(x,\mu,\sigma) + \sigma_{k-1} \tag{3.24}$$

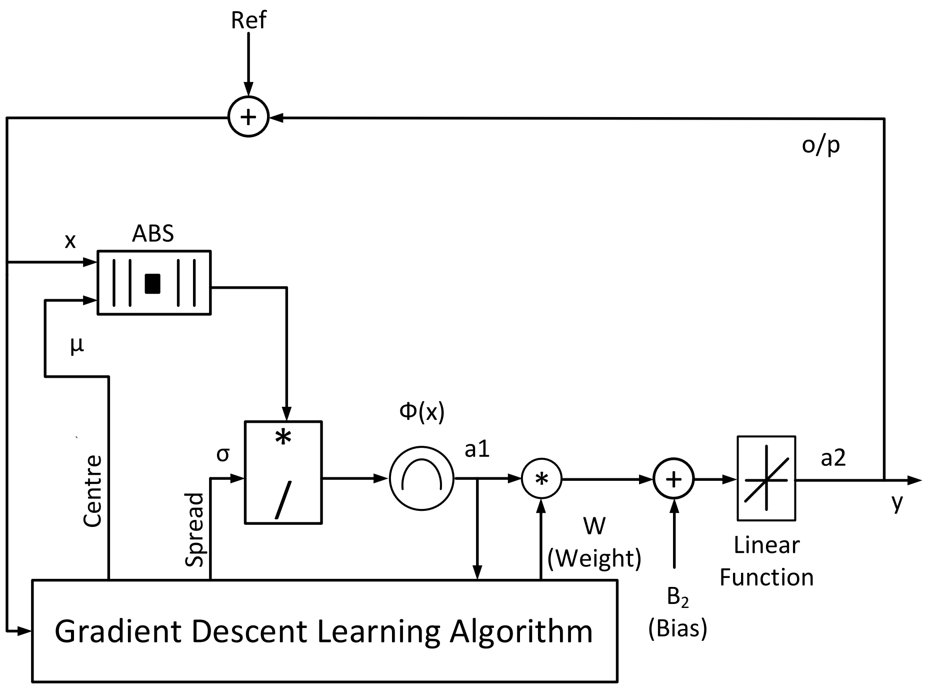

Figure 3.8 - RBF Controller Schematic with Gradient Descent Parameter Optimisation

3.4.3.4) Adaptive Leaning Rate

In gradient descent learning algorithms, the learning rate coefficient (λ) is a critical parameter that influences the overall rate of convergence by determining the magnitude of weight adaptations made during each iteration. λ is a significant value due to the potential for significant variations in the learning rate to result in varying outcomes. If the value of λ is excessively large, the network response may oscillate around the steady-state value, resulting in slowing convergence. Conversely, the total time to convergence will be substantially increased if the selected value of λ is too small, as the descent will proceed in very small steps. As a result, the optimal value of λ is dependent on the specific problem and may necessitate a period of trial and error to determine a suitable choice [118].

The learning rate is adjusted throughout the training process to obtain the best possible results. The current study introduces a simple adaptive mechanism that is intended to ascertain the most efficient learning rate. This mechanism functions by perpetually monitoring the error during training and adjusting the λ_i values of each ($i = w, \mu, \sigma$) to more closely align with the local descent region. The relationship between the learning rate and the error is represented by an exponential function, as illustrated in Figure 3.9. The learning rate is increased to compensate for the excessively cautious nature of its current value for local minima when network parameters reduce the error. Thus, the function's logic is as follows. Conversely, the learning rate is reduced to prevent overshooting by swiftly diminishing the influence of past parameter values if the error is excessively high [118].

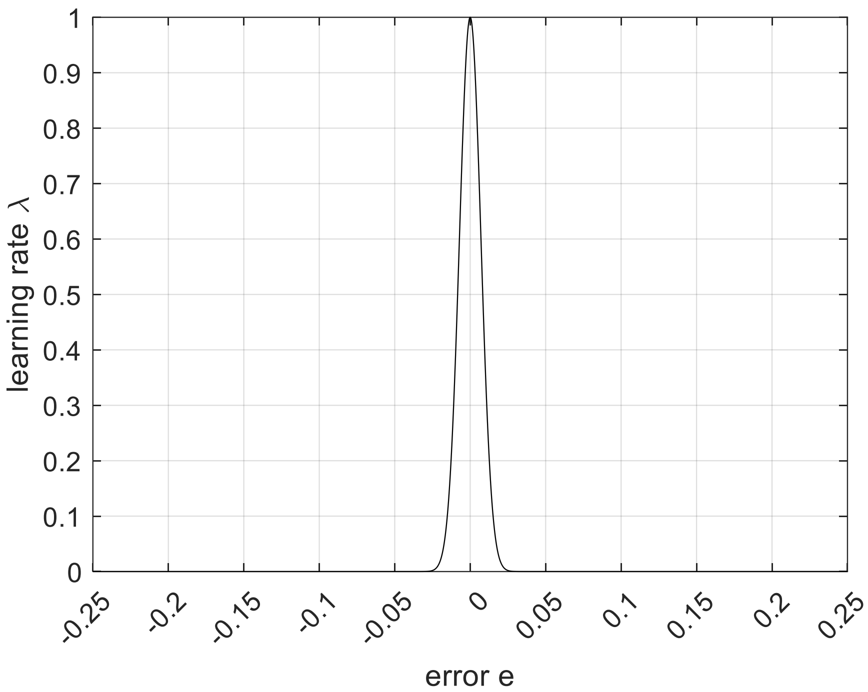

Figure 3.9 - Exponential Function for Adaptive Learning Rate

3.4.3.5) DC-DC Converter Optimisation

For this work, the RBF performs a crucial role in optimising the operation of the DC–DC converter, which is essential for regulating the energy flow between batteries and SCs. The inputs of this controller include voltage levels (input and output), current measurements, and error signals (W, μ, and σ). The outputs are control commands for converter settings and parameter adjustments. The control commands executed using the RBF controller assure a flawless alignment between the power sourced from the battery or SC and the power produced from the converter side. Ensuring synchronisation is essential for preserving the effectiveness and steadiness of the energy transfer in the HESS, hence improving the overall efficiency of the EV. These tasks involve enhancing the learning rate and adjusting the controller parameters to more accurately align with the characteristics of the EVs energy components [113].

3.4.3.6) Adaptive Mechanisms and Efficiency

These adjustments guarantee that the RBF controller adequately tackles the distinct obstacles presented by the EV environment, thereby enhancing both performance and energy efficiency. The

RBF controller utilises these methods to dynamically adjust its parameters, hence optimising the control approach for real-time energy management. The controller's capacity to continuously adjust these settings depending on the system's feedback loop makes it very efficient in handling the intricate dynamics of EVs, hence improving vehicle responsiveness. This adaptive mechanism guarantees that the EV functions at its best in various driving situations, utilising the maximum capabilities of its energy storage system [113].

3.5) Comparative Analysis of Control Strategies

To summarise, the PI controller offers simplicity and robustness for predictable situations, whereas MPC is particularly effective in optimising complicated systems by predicting future states. On the other hand, the RBF controller provides great precision in dynamic and unexpected contexts. By integrating various controllers, the unique advantages of each one are utilised to achieve optimal performance and reliability. Table 3.1 illustrates an overview of control strategy performance in EVs.

Table 3.1 - Overview of control strategy performance in EVs [113]

Type	Key Findings	Merits	Demerits	Ref
	Proposed controller boosts EVs with HESS operating efficiency, energy efficiency, and stability.			[119]
PI	Proposed controller improves fuel cell system performance and reliability for automotive applications, according to the research.	• Simple, stable performance.	• Adequate dynamic response; • Nonlinearities present a challenge.	[120]
	Highlights how the proposed controller improves hybrid EV power system efficiency and stability.			[121]
	Energy flow between storage components is dynamically adjusted based on the battery's SOC to improve energy efficiency and battery life.			[122]
MPC	MPC improves hybrid system efficiency and performance by dynamically modifying control actions based on vehicle mass estimates, according to the study.	• Effectively manages constraints • Predicts future states	• High computational burden • Implementation complexity	[123]
	Demonstrates that recognising driving patterns improves MPC systems' prediction accuracy and energy management efficiency			[124]
RBF	Simulations show improved transition smoothness and system robustness during mode transitions.	• Highly proficient at managing nonlinearities • Demonstrates exceptional adaptability with learning mechanisms	• Necessitates a significant amount of training data • Carries the risk of overfitting, which can be mitigated with appropriate tuning	[125]
	Research shows that adaptive strategies enhance fuel efficiency and pollution			[126]

3.6) Summary

This chapter focuses on the difficulties of optimising ESS for EVs, with a particular emphasis on the drawbacks of lithium-ion batteries, including their restricted power density, shorter cycle life, and elevated costs. To address these problems, the chapter examines HESS, which integrate lithium-ion batteries with SCs to take advantage of their superior power density and long cycle life. The chapter discusses the structural design of HESS, the modelling of vehicle dynamics for power and energy consumption prediction, and the thorough modelling of batteries and SCs. The analysis also explores advanced control techniques such as PI, MPC, and RBF in order to enhance energy management efficiency. In summary, the chapter offers a thorough strategy for improving the effectiveness, functionality, and longevity of EVs.

Chapter 4 Comparative Analysis of Hybrid Energy Storage Systems and Brushless DC Motor Speed Control Methods

4.1) Brief

This chapter has two main goals: firstly, to compare the discharge characteristics of batteries and SCs in a HESS using MATLAB/Simulink simulations, and secondly, to assess the performance of PI and RBF controllers in regulating the speed of BLDC motors. Specifically, the focus is on how these controllers respond to a reference speed of 3000 RPM, chosen because it is a speed that is frequently utilised in BLDC motor applications and provides a useful foundation for performance comparison.

The early sections of the chapter explore the energy storage components, primarily focusing on batteries and SCs. Analytical simulations were performed to examine the discharge characteristics of the subject under the same conditions. The battery and SC were first adjusted to a voltage of 12V, and a load resistance of 1 ohm (Ω) was used. The battery had a capacity of 1000 ampere-hours (Ah), while the SC had a capacitance of 10 farads (F). The simulations, conducted over a duration of 10 seconds with a time interval of 0.01 seconds, demonstrated that batteries maintain a consistent voltage level, which is ideal for continuous energy generation. On the other hand, SCs experience a rapid decrease in voltage, suggesting their suitability for delivering brief bursts of energy.

The chapter proceeds with a comprehensive examination of BLDC motors, focusing on their structure, functioning, and the benefits they offer in comparison to traditional DC motors. BLDC motors are well regarded for their low maintenance needs, dependability, and exceptional efficiency. The text discusses the building of BLDC motors, which consist of three-phase synchronous motors with permanent magnets and electronic commutation. The discussion is backed by circuit diagrams and mathematical models.

The chapter assesses the effectiveness of PI and RBF controllers through MATLAB/Simulink simulations in a comparative analysis. The simulations are designed to achieve a target speed of 3000 RPM for BLDC motors, using a PI controller that is optimised to minimise overshoot, settling time, and steady-state error. On the other hand, the RBF controller utilises a neural network that has been trained on the dynamic behaviour of the motor. The results demonstrate that although the PI controller successfully attains the target speed, it has substantial overshoot and extended settling times. Contrarily, the RBF controller provides enhanced adaptability and durability while minimising overshoot and achieving faster response times.

4.2) Energy Storage Components and Discharge Characteristics

To assess the performance attributes of batteries and SCs, first simulations were carried out in MATLAB/Simulink to understand their discharge patterns under identical circumstances. Validating this aspect is essential in the process of constructing an efficient HESS, as it verifies the anticipated fast discharge of SCs in comparison to batteries under the same conditions.

A MATLAB simulation was set up to compare the discharge characteristics of a battery and a SC under the same initial voltage and load resistance. The initial voltage for both the battery and the SC was set to 12 volts (V), with a load resistance of 1 Ω. The battery capacity was 1000 Ah, and the SC capacitance was 10 F. The simulation was run for 10 seconds with a time step of 0.01 seconds to provide a detailed observation of the discharge process. The MATLAB code used for this simulation, along with the setup details, is provided in **Appendix A** to facilitate reproducibility and further analysis. .The following plots in Figure 4.1 illustrate the discharge characteristics of the battery and the SC over the 10-second simulation period:

1. Battery voltage versus time:
   The battery voltage shows minimal decline during the simulation period, maintaining near stability around 12V. This behaviour highlights the battery's ability to deliver a consistent and sustained energy supply over an extended duration. The plot demonstrates that even after 10 seconds, the voltage remains nearly unchanged, reflecting the battery's suitability for tasks requiring long-term energy delivery.
2. Supercapacitor voltage versus time:
   The SC exhibits a rapid decline in voltage, demonstrating its characteristic of quick discharge. The graph depicts a rapid decrease in voltage within a short period of time, emphasising the SCs ability to rapidly discharge stored energy. The swift decline in voltage demonstrates that the SC is well-suited for applications that require fast surges of energy.
3. Battery power versus time:
   The battery's power output is stable throughout simulation period, indicating its consistent energy supply. This steadiness indicates the battery's reliability for continuous energy supply.
4. Supercapacitor power versus time:
   The SC experiences a significant decrease in power output, indicating its rapid depletion of energy. The plot illustrates a rapid decline in power output within a few seconds, highlighting the SCs ability to deliver instant power surges, but also its restriction in maintaining energy over extended durations.

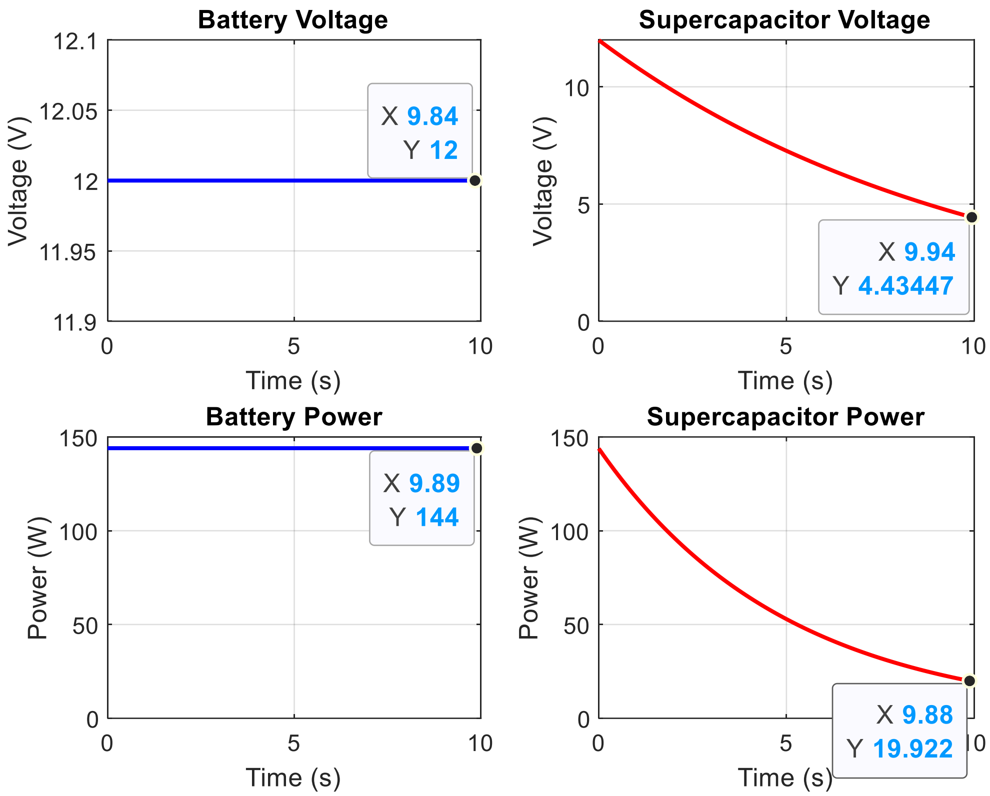

Figure 4.1 - Discharge Characteristics of the Battery and the Supercapacitor

4.3) BLDC Motor Overview

In numerous contemporary applications, BLDC motors are the preferred choice due to their minimal maintenance, reliability, and high efficiency. In terms of precision control and dynamic performance, these motors surpass conventional DC motors.

4.3.1) Architecture

BLDC motors are constructed similarly to three-phase synchronous motors. The stator contains three separate windings, while the rotor is equipped with permanent magnets. The motor operates using a semiconductor-based electronic commutation circuit [127]. By turning electronic components on and off, this circuit delivers electric power to the motor. The circuit diagram for a BLDC motor driving system is presented in Figure 4.2.

Figure 4.2 illustrates the circuit diagram of the BLDC motor driving system, which operates through a combination of control signals and power conversion stages. The DC power supply provides energy to the inverter, which converts it into three-phase AC signals required to drive the BLDC motor. The inverter's switching signals are generated by the control system based on the rotor position and the desired speed or torque commands. Rotor position information is typically obtained from sensors such as Hall effect sensors, ensuring precise phase commutation.

The BLDC motor driving system employs a six-step commutation process, where the inverter sequentially energizes the motor windings to produce a rotating magnetic field. This field interacts with the rotor's permanent magnets to generate torque, enabling smooth operation across varying load conditions. The control system dynamically adjusts the switching sequence and duty cycle of the inverter to regulate motor speed, optimise efficiency, and minimise torque ripple. This configuration ensures robust and efficient operation of the BLDC motor under different performance requirements.

Hall effect detectors analyse the rotor's location to establish the order of switches. The rotor will revolve due to the torque created as current flows through the windings. The controller analyses the rotor's current orientation to decide where the power switches should be moved (Decoder). Figure 4.3 depicts the rotation of the rotor because of the six-step synchronisation. Table 4.1 depicts the hall sensors and switches that modify position values while the rotor is turned [128]. The rotor's interaction with the push and attract depends on its current location. The rotor's rotation is maintained using quick switching operations [117].

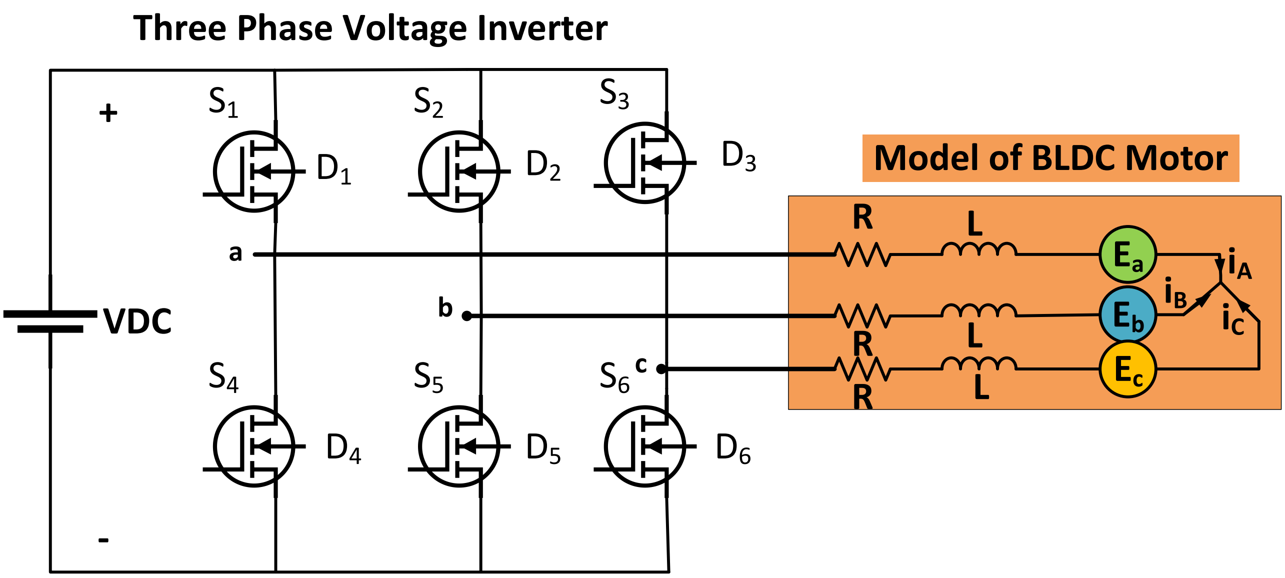

Figure 4.2 - Three-phase voltage Inverter for BLDC Motor Control [117]

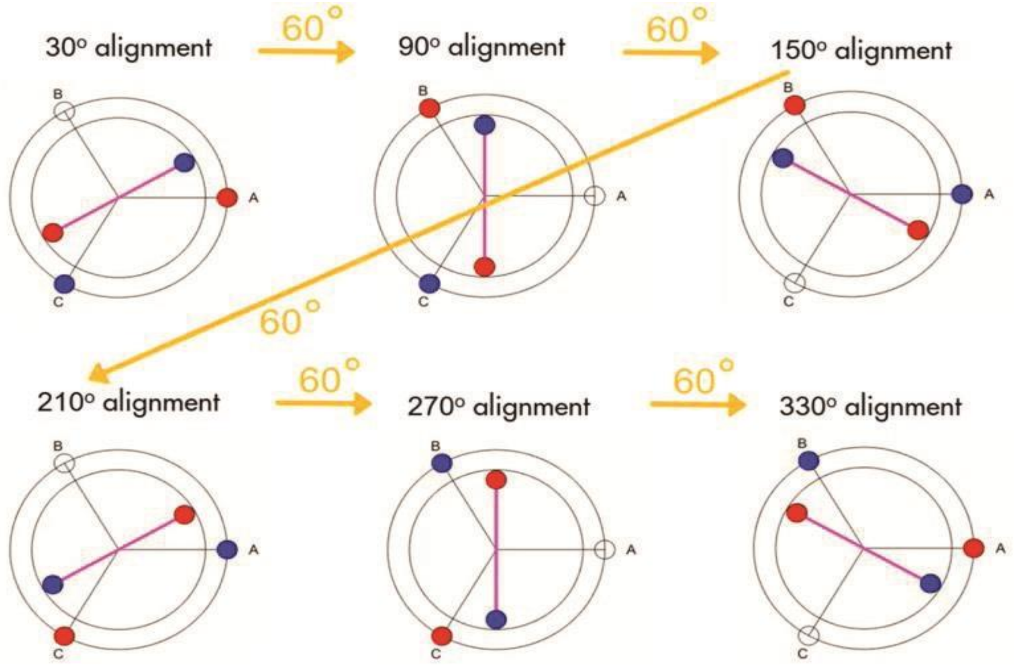

Figure 4.3 - BLDC Motor with Six Step Commutation [117]

Table 4.1 - Truth table for the Gate Pulse and Decoder [128]

Back Emf			Hall sensors			Location of switches					
E_a	**E_b**	**E_c**	**H_1**	**H_2**	**H_3**	**S_1**	**S_2**	**S_3**	**S_4**	**S_5**	**S_6**
0	0	0	0	0	0	0	0	0	0	0	0
0	-1	+1	0	0	1	0	0	0	1	1	0
-1	+1	0	0	1	0	0	1	1	0	0	0
-1	0	+1	0	1	1	0	1	0	0	1	0
+1	0	-1	1	0	0	1	0	0	0	0	1
+1	-1	0	1	0	1	1	0	0	1	0	0
0	+1	-1	1	1	0	0	0	1	0	0	1
0	0	0	1	1	1	0	0	0	0	0	0

4.3.2) Mathematical Modelling of BLDC

The BLDC motor is characterised by a symmetrical and balanced three-phase configuration. The permanent magnet's high resistance value results in the rotor current being ignored [129].The BLDC motor is trained because of the interaction that occurs between the permanent magnet and its coils [130], [131]. Figure 4.2 displays the corresponding circuit model of a BLDC motor. The matrix representation of the phase voltage mathematical equations is presented in Equation 4.1 [131].

$$\begin{bmatrix} E_a \\ E_b \\ E_c \end{bmatrix} = \begin{bmatrix} R & 0 & 0 \\ 0 & R & 0 \\ 0 & 0 & R \end{bmatrix} \begin{bmatrix} i_A \\ i_B \\ i_C \end{bmatrix} + \frac{d}{dt} \begin{bmatrix} L-M & 0 & 0 \\ 0 & L-M & 0 \\ 0 & 0 & L-M \end{bmatrix} \begin{bmatrix} i_a \\ i_b \\ i_c \end{bmatrix} + \begin{bmatrix} E_a \\ E_b \\ E_c \end{bmatrix} \tag{4.1}$$

Where E_a, E_b *and* E_c represent the voltages of each phase. i_A, i_B and i_C denote the currents of each phase in amperes (A). R stands for the resistance of each winding, measured in ohms (Ω). $L - M$ signify Mutual and self-inductances measure in Henries (H). An expression for the electromagnetic torque produced by a BLDC motor is given in Equation 4.2 [131].

$$T_e = \frac{E_a\, i_a + E_b\, i_b + \ E_c\, i_c}{\Omega} \tag{4.2}$$

Where T_e represents electromagnetic torque measure in newton meters (Nm) and Ω represents the angular velocity. Mathematical model of the electromechanical system that is associated with the action of the motor is presented in Equation 4.3.

$$T_e - T_L = J\frac{dw}{dt} + \beta_v \tag{4.3}$$

Where T_L represents Load torque (Nm), J is moment of inertia of the motor and the load it drives and β_v is the damping constant (Ns/m).

4.4) Comparative Study

The performance of motor controllers is a crucial factor in the design and functioning of BLDC motors. PI controllers are commonly employed because of their simplicity and straightforward setup. Nevertheless, they may be inadequate in managing non-linearities and parameter fluctuations in intricate systems. RBF neural network controller provide enhanced adaptability and robustness by utilising machine learning techniques to successfully handle non-linearities and fluctuations. This section presents an in-depth comparison analysis of PI and RBF controllers using rigorous simulations and analyses. The focus is on their practical implications for controlling the speed of BLDC motors [117].

4.4.1) Simulation Setup

The comparative analysis was conducted using MATLAB/Simulink, a versatile simulation tool widely used in control systems research. The setup aimed to evaluate the performance of PI and RBF controllers in maintaining a reference speed of 3000 RPM for BLDC motors. To ensure a comprehensive evaluation, the simulation environment was meticulously configured with appropriate parameters and conditions. The simulations were performed in MATLAB/Simulink, utilising its powerful modelling and simulation capabilities to create a realistic representation of the BLDC motor control system. The motor model included precise parameters such as inductance, resistance, back EMF constant, and inertia to accurately reflect the physical characteristics of a typical BLDC motor, as detailed in Table 4.2 [117].

Table 4.2 - Parameters Used in the Simulation [117]

Parameters	Value
Number of poles	4
Back EMF waveform	Trapezoidal
Stator phase resistance (Ω)	2.8750
Stator phase inductance (H)	8.5e-3
Flux linkage	0.175
Back EMF flat area (°)	120
K_p	1
K_i	318.4
Controlled Voltage Source	100 V DC

The PI controller was configured with finely tuned proportional and integral gains to achieve the desired speed response. The tuning process involved iterative adjustments to minimise overshoot, settling time, and steady-state error. The RBF controller was designed using a neural network with radial basis function neurons. The network was trained using a dataset generated from the motor's dynamic behaviour, enabling it to adaptively adjust the control inputs to maintain the target speed. Simulation parameters included a reference speed of 3000 RPM, chosen to evaluate the controllers' performance under steady state operation, to assess the robustness and adaptability of each controller.

The model blocks in Figure 4.4 depict the fundamental elements of the BLDC motor system, demonstrating the transmission of information and power throughout the system. The control system receives inputs including the speed reference signal, which specifies the target motor speed, and feedback signals such as rotor position, phase currents, and voltages. These inputs enable the control system to assess the motor's present operational status and implement requisite modifications to sustain optimal performance. The control system's outputs comprise switching signals for inverter control and current instructions that govern the power supplied to the motor windings. The inverter block is essential for transforming control signals into suitable electrical power by producing three-phase AC from the DC power source. This connection guarantees accurate speed control, effective torque generation, and seamless motor performance under diverse load circumstances, emphasising the synchronised working of the system's essential components.

The simulation findings offer a comprehensive evaluation of the controllers' performance, emphasising critical parameters such speed response, overshoot, settling time, and stability. The results illustrate the interaction between the inputs and outputs of the model blocks, affecting the overall performance of the BLDC motor system across various control schemes [117].

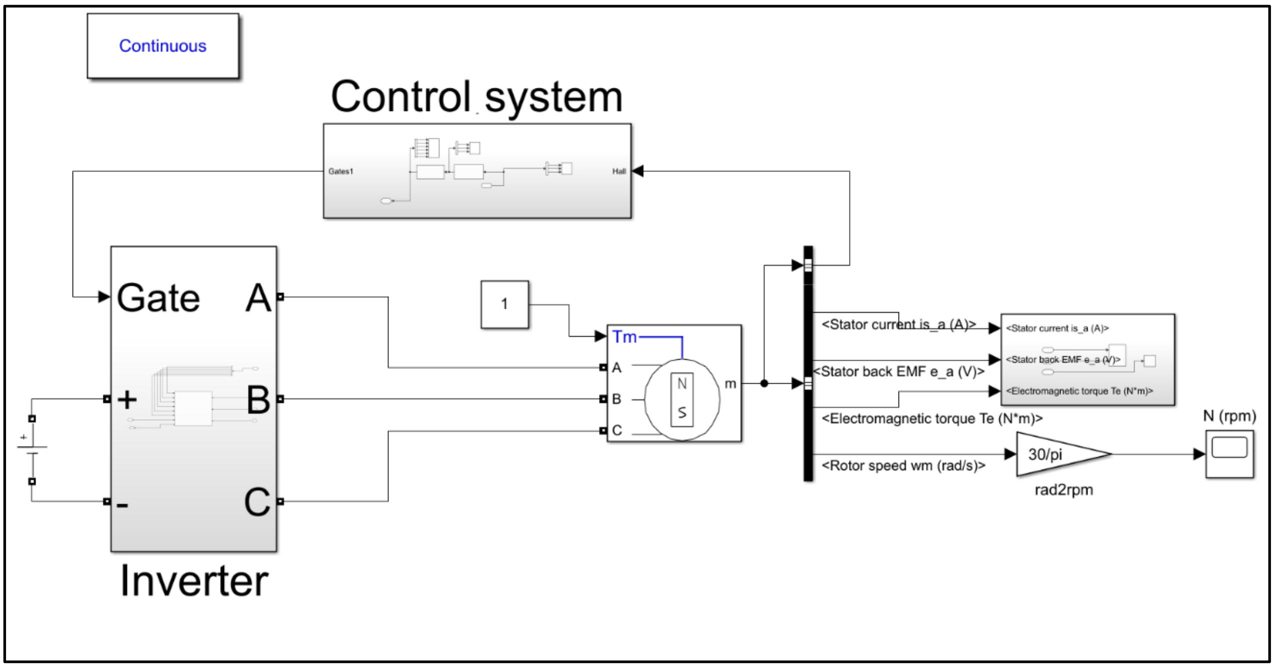

Figure 4.4 - Simulink BLDC Motor Model [117]

4.4.2) Results

The study thoroughly analyses the comparative performance of a traditional PI controller and an RBF neural network controller for BLDC motor speed control. Figures 4.5 & 4.5 are pivotal in illustrating the differences in the speed response capabilities of these two control strategies [117].

Figure 4.5 illustrates the speed response of the BLDC motor controlled by a PI controller. The graph demonstrates that the PI controller successfully achieves the desired speed of 3000 RPM. Nevertheless, it demonstrates significant overshoot and requires a longer duration to reach a stable state at the target velocity. More precisely, the PI controller attains stability in around 0.027 seconds. The presence of initial overshoot and prolonged settling time suggests that although the PI controller can achieve the desired speed, it is not as effective in ensuring precise and stable speed control, particularly when faced with fluctuating load conditions. This behaviour indicates possible difficulties in applications that necessitate quick adjustment to changes in speed and a high level of accuracy.

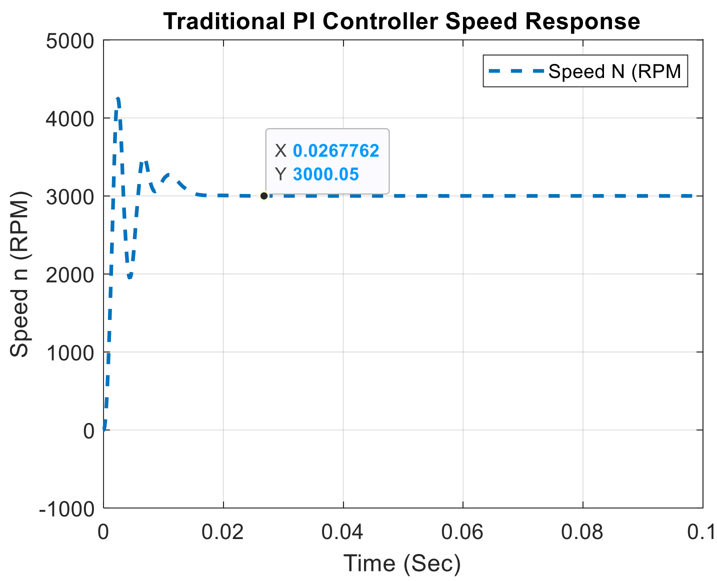

Figure 4.5 - Traditional PI Controller Speed Response

Figure 4.6 illustrates the speed response of the BLDC motor when controlled by an RBF controller. The performance of the RBF controller is considerably enhanced in comparison to that of the PI controller, as it achieves the reference speed with minimal overshoot and a settling time of approximately 0.039 seconds. The improved RBF controller's ability to adapt to real-time speed changes and effectively manage the motor's nonlinear dynamics is emphasised by the reduced overshoot and faster response time. The RBF controller is made more suitable for applications that require high precision, adaptability, and stability in varying operational conditions as a result of this enhanced performance [117].

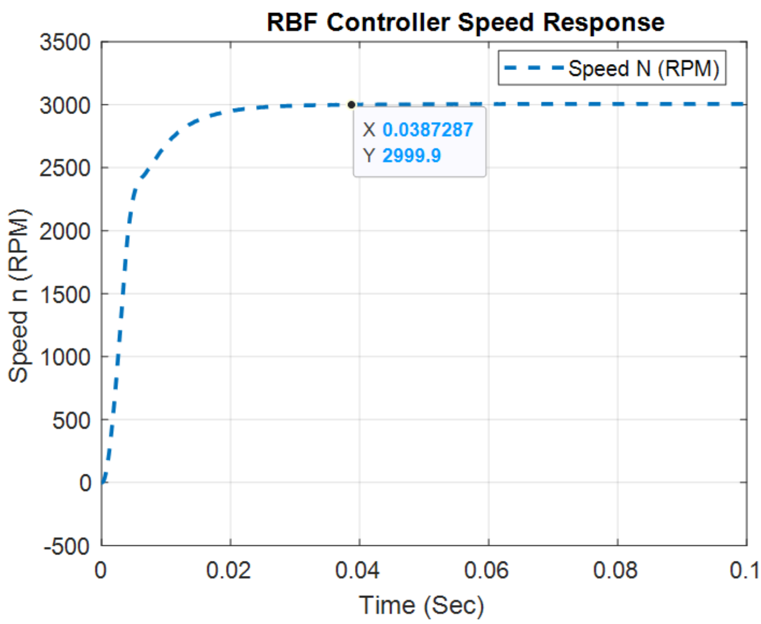

Figure 4.6 - RBF Controller Speed Response

4.4.3) Discussion

Comparative analysis of Figures 4.5 & 4.6 emphasises the unique advantages and constraints of each control method. The PI controller experiences prolonged settling periods and overshoot, despite its ability to achieve a faster initial speed response. These characteristics can result in inefficiencies in systems that require precision, stability, and speed. In contrast, the RBF neural network controller, which boasts superior adaptability and robustness, offers a more consistent speed response with minimal overshoot, despite a slightly longer response time. The RBF controller is now more capable of managing the intricacies and nonlinearities that are inherent in BLDC motor control, particularly in dynamic and unpredictable environments [117].

4.5) Summary

Chapter 4 examines the discharge characteristics of batteries and SCs and evaluates the effectiveness of PI and RBF controllers in regulating the speed of BLDC motors using MATLAB/Simulink simulations. The study demonstrates that batteries maintain a consistent voltage level that is appropriate for providing sustained energy, whereas SCs have a rapid decrease in voltage, demonstrating their capacity to release energy quickly. The distinction emphasises the mutually supportive functions of batteries and SCs in HESS.

The chapter also offers a comprehensive examination of BLDC motors, highlighting their high efficiency, dependability, and low maintenance needs. The motor's detailed details encompass its three-phase synchronous architecture, permanent magnet rotor, and electronic commutation method. Mathematical models and circuit diagrams provide more clarity on how the motor works.

Comparative simulations of PI and RBF controllers reveal substantial disparities in their performance. The PI controller exhibits significant overshoot and prolonged settling time, indicating reduced precision and stability in response to changing conditions, although achieving the required speed. On the other hand, the RBF controller, utilising its adaptive neural network methodology, reduces overshoot and improves response time, making it more efficient in handling the nonlinear dynamics of the motor.

In summary, the chapter emphasises the need of choosing suitable energy storage components and control approaches to maximise the performance and efficiency of HESS and BLDC motor systems. The results indicate that RBF controllers provide improved adaptability and resilience, rendering them more suitable for applications that demand accurate and stable speed control in dynamic conditions.

Chapter 5 Optimising Energy Efficiency in Electric Vehicles through Hybrid Energy Storage Systems and Advanced Control Strategies

5.1) Brief

The growing adoption of EVs involves improving ESS to optimise their effectiveness and durability. This chapter examines the incorporation of lithium-ion batteries and SCs to create a HESS. The objective is to enhance energy efficiency and enhance the performance of EVs. The work investigates a HESS topology that is completely active and guarantees accurate control of energy flow. It compares the performance of PI and RBF controllers through simulations utilising typical driving cycles. The findings demonstrate that the RBF controller surpasses the PI controller in minimising power losses and ensuring consistent SoC profiles. This highlights the vital significance of control techniques in attaining optimal energy management. In order to simulate the motor for HESS, a DC source has been used for compensation. A flowchart illustrates the dynamic process in an EV mechanism. In this process, the battery supplies power to satisfy the average demand, while a DC source sends power to the SC during acceleration and stores energy during deceleration. This enables consistent and optimised power delivery [132].

5.2) Analysis and Performance Modelling of a Hybrid Energy Storage System

HESS combines the high energy density of lithium-ion batteries with the high-power density and long cycle life of SCs. The objective of integrating these two storage technologies is to mitigate battery strain during dynamic driving situations, hence prolonging the battery's longevity. In this study, a fully active topology was chosen for the HESS configuration. This configuration demonstrates that by utilising parallel converters, it is feasible to enable a negative power flow exclusively in the SCs, which are known for their substantial charge and discharge capabilities. For the SC system, a buck-boost converter is utilised, connected to the SC to serve a dual purpose: discharging as a boost converter and charging as a buck converter. The adoption of a buck-boost converter for the SC ensures efficient energy transfer during both charging and discharging phases, allowing for versatile operation and effective utilisation of the SC's high charge and discharge capacities. Additionally, a boost converter is used for the battery, participating only in the discharge phase [132]. A DC source serves to provide compensation to the motor in the HESS. Figure 5.1 depicts the system. The battery fulfils the typical power need, while the DC source supplies power to the SC during acceleration and saves energy during deceleration, ensuring consistent and efficient power distribution [132].

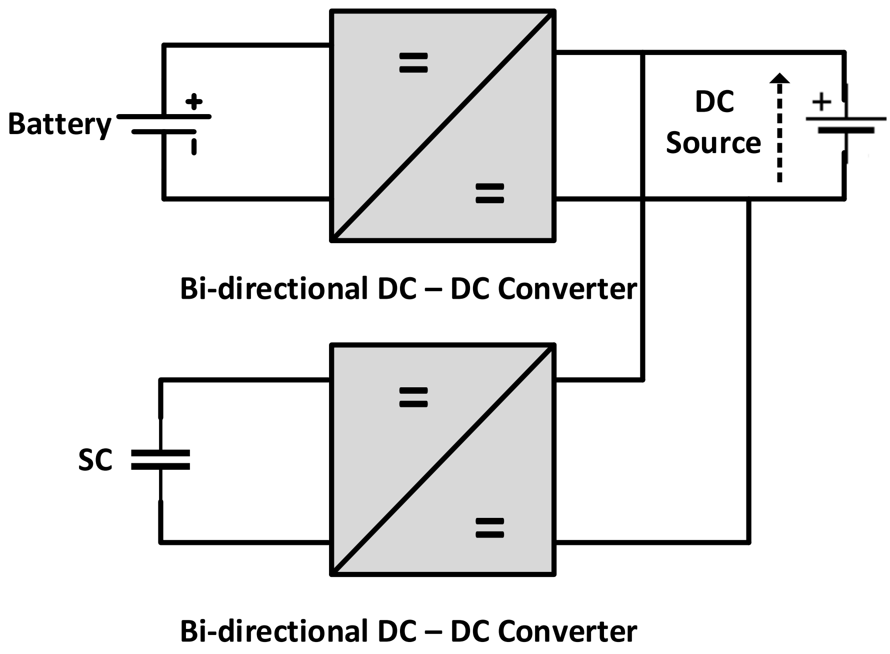

Figure 5.1 - Proposed Fully Active HESS Topology

5.2.1) Vehicle Dynamics Model

The vehicle dynamics model considers various forces acting on the vehicle, including aerodynamic drag, rolling resistance, gravitational force, and acceleration force. These forces are crucial for simulating realistic driving scenarios and understanding the vehicle's performance [132]. The equations and models used to simulate these dynamics can be referred back to in Chapter 3. Table 5.1 provides a comprehensive overview of the precise parameters that were implemented during the simulations for the proposed vehicle. A thorough sensitivity analysis was performed to confirm the reliability of the simulation results. This analysis played a crucial role in evaluating the selected parameter values and identifying the key variables that affect the performance of the HESS. The parameters used in this study were based on well-established values found in existing literature and then modified to fit the specific needs of the simulation framework. The approach used was dictated by the findings published in previous research, which provide a strong basis for selecting and adjusting parameters.

5.2.2) Battery and Supercapacitor Models

The thesis fully covers the intricate modelling of battery and supercapacitor systems, encompassing its internal resistances and control mechanisms. For more detailed information, consult Sections 3.3.3 and 3.3.4, which discuss the equivalent circuit models for the battery and SC, respectively. These sections provide insights into the mathematical equations and operational behaviours that are fundamental to understanding and managing these components.

Table 5.1 - Simulation Module-Specific Parameters

Module	Parameter	Value
EV	C_{rr}	1
	C_d	1
	m	1567 kg
	A_f	1 m^2
Battery	Nominal Voltage of the Cell	3.7 V
	Rated capacity	47 Ah
SC	Nominal Voltage	16 V
	Rated Capacitance	500 F
	Number of Series Capacitors	6
	Number of Parallel Capacitors	1

5.3) Control Strategies for HESS

The control strategies for HESS, including PI and RBF controllers, have been discussed in detail earlier in the thesis. For more comprehensive information on these controllers and their effectiveness, refer back to Sections 3.4.1, 3.4.3 and 3.5 where the control algorithms and their applications are thoroughly examined.

5.4) Simulations and Results

The performance of PI and RBF controllers were assessed using MATLAB/Simulink simulations, with a focus on different driving cycles, namely US06 and SC03. The simulations included accurate representations of vehicle dynamics and models of both the battery and SC to thoroughly evaluate the system's performance. Figure 5.2 depicts the flowchart of HESS's operation, providing insight into the dynamic interactions inside the system [132]. The flowchart depicts the dynamic process of an EV mechanism that incorporates a HESS. The process commences with the battery providing sufficient power to fulfil the typical energy requirements of the vehicle. While accelerating, the system verifies whether extra assistance is required. If necessary, a DC source (SC) supplies additional power to help the battery handle the intense power requirement. This guarantees that the vehicle accelerates seamlessly without placing excessive strain on the battery. On the other hand, when the vehicle is slowing down, the system harvests the extra energy and stores it in the DC source via regenerative braking. This technique not only enhances power efficiency but also facilitates energy storage for future acceleration requirements. The flowchart illustrates the dynamic collaboration between the battery and DC source to enable continuous and optimised power supply, assuring the efficient operation of the electric vehicle.

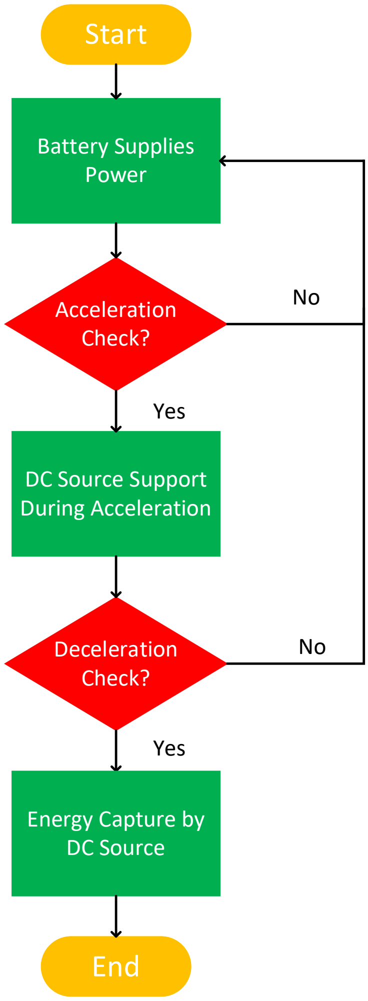

Figure 5.2 - Flowchart of Operation of HESS

5.4.1) Chosen Driving Cycles

The simulations incorporate the US06 cycle, which is known for its fast speeds and strong accelerations, as well as the SC03 cycle, which represents urban driving with frequent stops and mild accelerations. The attributes of both cycles are depicted in Table 5.2. The driving cycles' profiles are illustrated in Figures 5.3 [132].

Table 5.2 - Attributes of each Driving Cycle

Driving Cycle	US06	SC03
Average Speed (km/h)	Varies (Aggressive)	25.7
Type	Aggressive Urban	Urban
Stops and Starts	Frequent	Frequent
Acceleration Patterns	Rapid	Moderate
Speed Variability	High	Moderate
Duration (s)	600	600
Traffic Condition	Heavy	Moderate

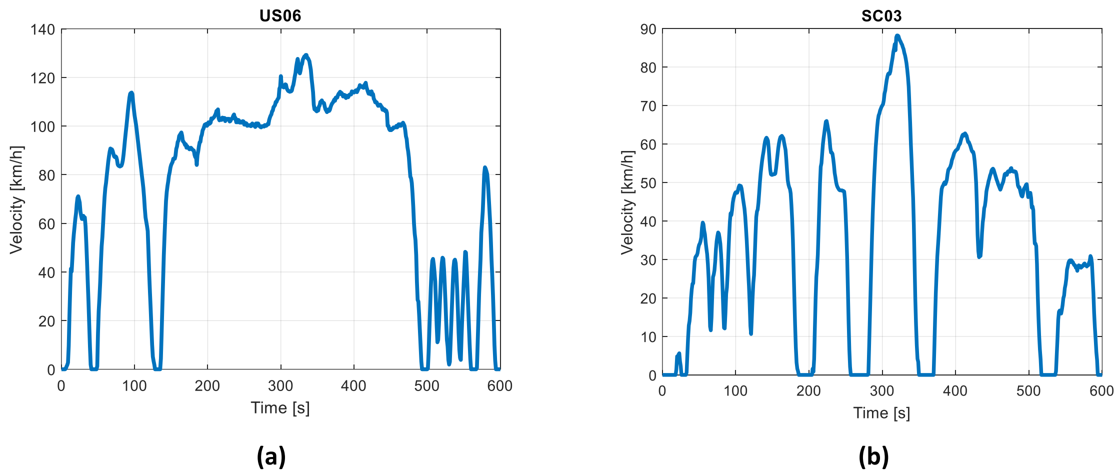

Figure 5.3 - Selected driving cycles: (**a**) US06, (**b**) SC03

5.4.1.1) US06

The US06 driving cycle is widely utilised to evaluate the effectiveness of a HESS for EV in a variety of real-world scenarios. The power demand profile of the proposed vehicle, discussed in Table 5.1, can be calculated based on the mathematical equations provided in Chapter 3, specifically Equations 3.1 to 3.6. Power demand profile can be seen in Figure 5.4 [132].

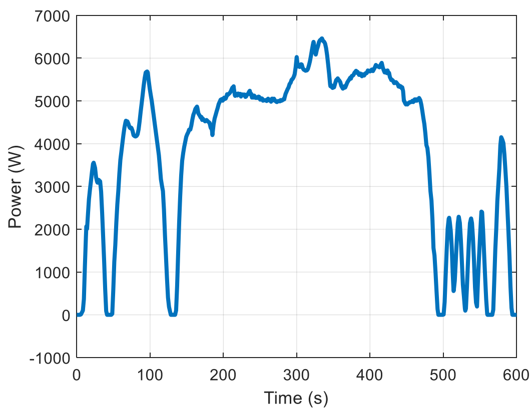

Figure 5.4 - Power Demand of US06 Cycle

Outcomes results of US06 cycle are displayed in Figure 5.5, providing insight into the behaviour of the vehicle, ensuring the proposed vehicle's performance is optimised for typical driving conditions represented by the US06 cycle [132].

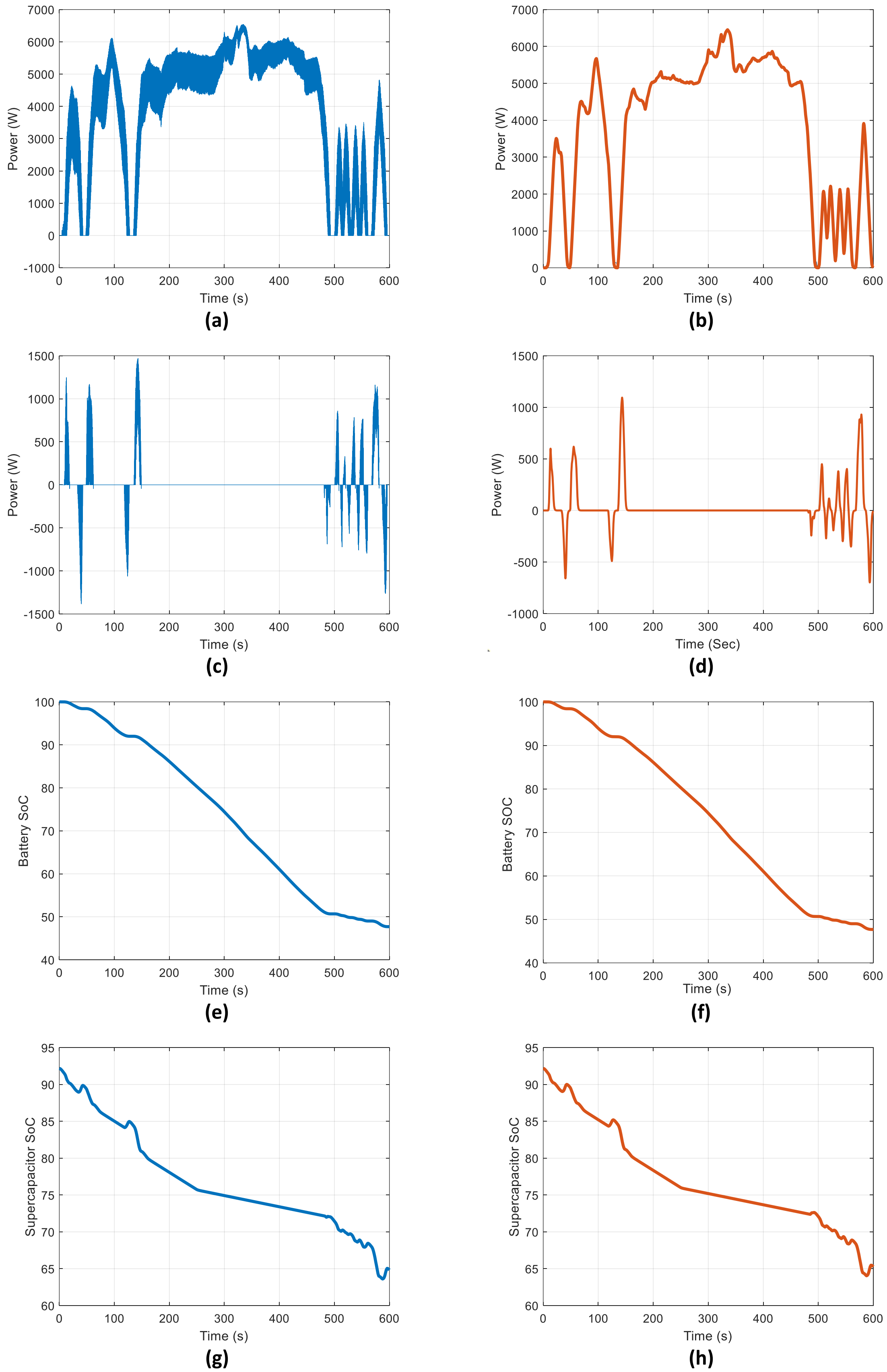

Figure 5.5 – Outcome Results of US06 Cycle: (**a**) Battery Profile using PI, (**b**) Battery Profile using RBF, (**c**) SC Profile using PI, (**d**) SC Profile using RBF, (**e**) Battery SOC using PI, (**f**) Battery SOC using RBF, (**g**) SC SOC using PI, (**h**) SC SOC using RBF

5.4.1.2) SC03

The SC03 driving cycle is also another famous cycle that is widely used to evaluate the effectiveness of a HESS strategy for EVs in a variety of real-world scenarios. The power demand profile of the proposed vehicle, discussed in Table 5.1, can be calculated based on the mathematical equations provided in Chapter 3, specifically Equations 3.1 to 3.6. Power demand profile can be seen in Figure 5.6. Outcomes results of SC03 cycle are displayed in Figure 5.7, providing insight into the behaviour of the vehicle, ensuring the proposed vehicle's performance is optimised for typical driving conditions represented by the US06 cycle [132].

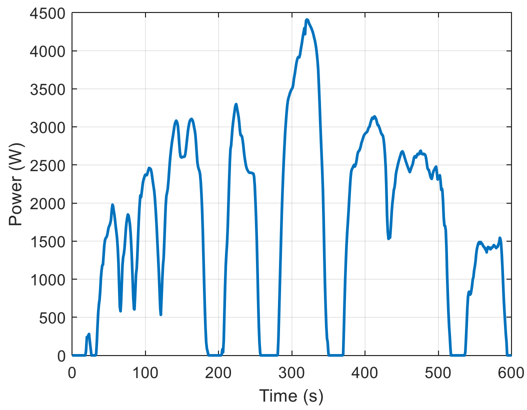

Figure 5.6 - Power Demand of US06 Cycle

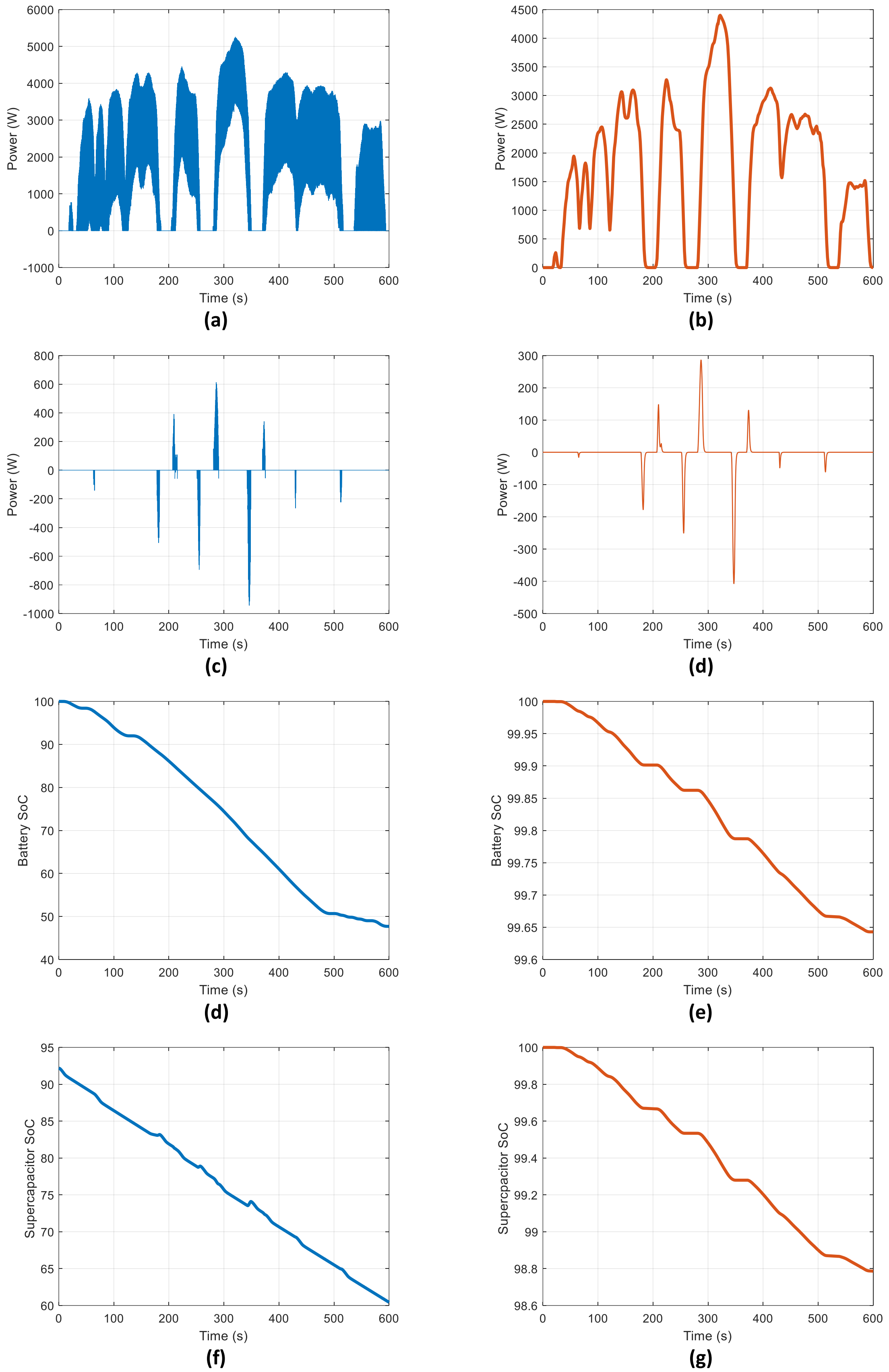

Figure 5.7 - Outcome Results of SC03 Cycle: (**a**) Battery Profile using PI, (**b**) Battery Profile using RBF, (**c**) SC Profile using PI, (**d**) SC Profile using RBF, (**e**) Battery SOC using PI, (**f**) Battery SOC using RBF, (**g**) SC SOC using PI, (**h**) SC SOC using RBF

5.4.1.3 Discussion

5.4.1.3.1 Battery Power Profile

A closer look of the battery power profiles illustrated in Figures 5.5a, 5.5b, 5.7a, and 5.7b verifies that the battery power adequately fulfils the standard power requirements for both vehicle controllers. The major role of the DC source is to provide power to the battery during acceleration and to capture energy during deceleration. Although the battery power profiles of both controllers are comparable, the RBF controller exhibits a more consistent power profile. The stability of the system is a result of its efficient adjustment of control inputs according to the system's present condition. However, the PI controller demonstrates significant power variations [132].

5.4.1.3.2 Supercapacitor Power Profile

Figures 5.5c, 5.5d, 5.7c, and 5.7d depict the utilisation of the SC for power management. The PI controller increases the rate at which the SC charges or discharges, promptly adapting to immediate faults and system fluctuations. The high level of responsiveness can put excessive pressure on the supercapacitor, resulting in increased fluctuations in its charging and discharging speeds. Conversely, the RBF controller exhibits a reduced rate of charging and discharging for the supercapacitor. This is because of its superior ability to adapt and regulate inputs, leading to a more stable and less strained operation for the SC [132].

5.4.1.3.3 State of Charge

The variations in the SOC between the PI controller and the RBF controller throughout the US06 and SC03 cycles result from their distinct control strategies for managing the battery and supercapacitor. In the US06 cycle, both controllers demonstrate consistent SOC patterns, as depicted in Figures 5.5e, 5.5f, 5.5g, and 5.5h. However, in the SC03 cycle, the PI controller shows significant power dissipation due to its inability to adapt effectively to the high-frequency transient power demands. This limitation results in a substantial reduction in SOC, with the battery experiencing a 50% decrease and the supercapacitor showing a 34% decrease, as shown in Figures 5.7d and 5.7f

In contrast, the RBF controller leverages its predictive and adaptive capabilities to handle intricate and nonlinear system dynamics more effectively. This is evident in Figures 5.7e and 5.7g, where the RBF controller achieves a dramatic reduction in power losses—0.35% for the battery and 1.2% for the supercapacitor. These improvements highlight the RBF controller’s ability to optimise energy flow and minimise dissipation, particularly during the high-demand SC03 cycle.

The results underscore the critical role of control system selection in influencing the energy management and overall performance of the HESS. By effectively reducing power losses and maintaining SOC stability, the RBF controller not only enhances system efficiency but also contributes to the long-term durability of the battery and supercapacitor. This demonstrates the advantages of using advanced control algorithms like the RBF controller in handling complex operational scenarios with greater precision and adaptability [132].

5.4.1.4 Conclusions

The analysis presented for Figures 5.5 and 5.7 is in good agreement with the supplied interpretations. Both controllers exhibit effective power profiles, but, the RBF controller's capacity to optimise control inputs leads to a more stable and efficient functioning. As a consequence, there is a decrease in power fluctuations and a reduction in stress on the SC. The comparisons of SOC further emphasise the superior performance of the RBF controller, especially during the SC03 cycle, by consistently retaining higher efficiency and reduced power losses. The RBF controller offers notable benefits in efficiently controlling energy and improving overall system performance [132].

5.5) Summary

This study offers a thorough examination and computer modelling of a HESS that integrates lithium-ion batteries with SCs to improve the efficiency and lifespan of EVs. The study utilises active topology and bidirectional DC-DC converters to efficiently control the flow of energy between the battery and supercapacitor. The models for vehicle dynamics, battery, and SC were created and simulated using MATLAB/Simulink. The focus was on two specific driving cycles, US06 and SC03, in order to assess the performance of the system under various driving situations.

The simulation findings demonstrate that both the PI and RBF controllers successfully regulate the energy distribution inside the HESS. However, the RBF controller outperforms the PI controller by maintaining a more stable power profile and minimising energy losses. The simulations of the US06 cycle consistently showed similar SOC patterns for both controllers. However, during the SC03 cycle, it became evident that the RBF controller had an edge in reducing power losses and improving stability.

In summary, combining SCs with lithium-ion batteries in a HESS and controlling them with advanced techniques results in notable enhancements in energy management, system efficiency, and battery lifespan specifically for EV applications. This study underscores the potential of HESS to meet the dynamic power demands of EVs and provides a robust framework for future research and development in hybrid energy storage solutions.

Chapter 6 Improving the Efficiency of Electric Vehicles: Advancements in Hybrid Energy Storage Systems

6.1) Brief

This chapter examines the incorporation of HESS into EVs in order to improve their efficiency and dependability. The study examines the performance evaluation of three distinct control strategies—PI control, MPC, and RBF control—using fully active structure for operational of HESS installed in a Nissan Leaf. The goal is to enhance energy management in different driving scenarios by efficiently integrating the high energy density of lithium-ion batteries with the high-power density of SCs. The control techniques are evaluated by simulation using MATLAB/Simulink on three distinct driving cycles: Artemis rural, Artemis motorway, and US06 [113].

6.2) Contributions

This work presents significant contributions to the field of EV energy management. It evaluates the performance of different control strategies in a fully active HESS and demonstrates notable improvements in battery SOC management and system responsiveness, particularly under real-world driving cycles such as Artemis Rural, Artemis Motorway, and US06.

Key contributions of this chapter include:

- The development of a hybrid energy storage model that integrates SCs and batteries to handle dynamic load conditions efficiently.
- Introduction of the RBF controller, which surpasses conventional control methods by optimising energy flow, stabilising SOC, and enhancing energy recovery during regenerative braking.
- Detailed comparative analysis of control strategies under varying driving scenarios, showcasing the superiority of the RBF controller in improving system performance metrics.
- Emphasis on the role of supercapacitors in enhancing power density and reducing battery stress, resulting in increased energy efficiency and durability.

This research provides a foundation for further development in EV technology, emphasising the importance of advanced control algorithms in enhancing the efficiency and durability of HESS [113].

6.3) Hybrid Energy Storage Systems and Control Models

HESS integrates the high energy density of lithium-ion batteries with the high-power density and extended cycle life of SCs to reduce the stress on batteries during dynamic driving situations. For this work fully active topology was chosen. This helps to extend the lifespan of the batteries and enhance the overall energy efficiency. The vehicle dynamics model incorporates fundamental factors such as aerodynamic drag, rolling resistance, and acceleration, while the battery and SC models utilise similar circuit representations to accurately depict their dynamic behaviours [113]. For in-depth analysis of these models, refer to Chapter 3.

The study assesses three main control systems for regulating energy distribution within HESS: PI control, MPC, and RBF control. The advantages and challenges of each control approach are examined through MATLAB/Simulink simulations. The PI controller is well-known for its straightforwardness and stability in foreseeable conditions. It efficiently controls the transfer of energy between batteries and SCs, although it may encounter difficulties with non-linearities and fluctuations in parameters. MPC method that adapts control actions based on anticipated future conditions, which makes it well-suited for optimising intricate systems. Nevertheless, it necessitates substantial processing resources and can pose difficulties in its implementation. RBF controller, demonstrates exceptional performance in managing non-linearities and adjusting to real-time variations. It provides exceptional performance in dynamic and unpredictable settings, making it ideal for EV applications that demand great accuracy and consistency [113].

6.4) Results and Discussion

This section presents an evaluation of the outcome demonstrated by the three control strategies. MATLAB/Simulink has been used to implement the designed control system. The system parameters are detailed in Table 6.1, alongside the battery pack and SC parameters that have been studied in this work. The simulation profiles are derived from three distinct driving cycles, encompassing three unique environmental driving conditions to effectively test the controller performance of the optimised HESS [113].

Table 6.1 - Specifications for EV, battery, and SC modules [133], [134]

Module	Parameter	Value	Unit
EV	A_f	2.14	m^2
	C_d	0.28	-
	C_{rr}	0.01	-
	g	9.81	m/s^2
	m	1567	kg
Battery	Nominal Pack Voltage	360	Volts
	Nominal Pack Capacity	24	kWh
	Number of Cells	192	-
	Parallel Number	2	-
	Nominal Cell Voltage	3.75	Volts
	Cell Nominal Capacity	64	Ah
SC	Maxwell BMO3000	-	-
	Nominal Pack Voltage	24	Volts
	Nominal Pack Capacity	85	Faraday
	Number of Cells	89	-
	Parallel Number	1	-
	Nominal Cell Voltage	2.7	Volts
	Cell Nominal Capacity	3000	Faraday

The selected driving cycles are the Artemis rural cycle, the Artemis motorway with a speed differential of 150 km/h, and US06. These driving cycles are depicted in Figure 6.1. The Artemis rural cycle is designed to replicate driving conditions commonly found in rural areas, which are distinguished by reduced speeds and frequent stops and starts. This simulation accurately represents the stop-and-go aspect of country roadways. The motorway cycle represents high-speed motorway driving conditions, simulating sustained speeds of 150 km/h, typical of highway travel. Finally, the US06 cycle is a representation of rough driving circumstances, with its fast acceleration and deceleration patterns, which are typical of city driving in heavy traffic. The attributes of each driving cycle are detailed in Table 6.2 [135]. The next section presents a more comprehensive examination of the efficiency and effectiveness of HESSs in optimising battery SOC across various driving cycles, utilising the insight obtained from the controller analysis [113].

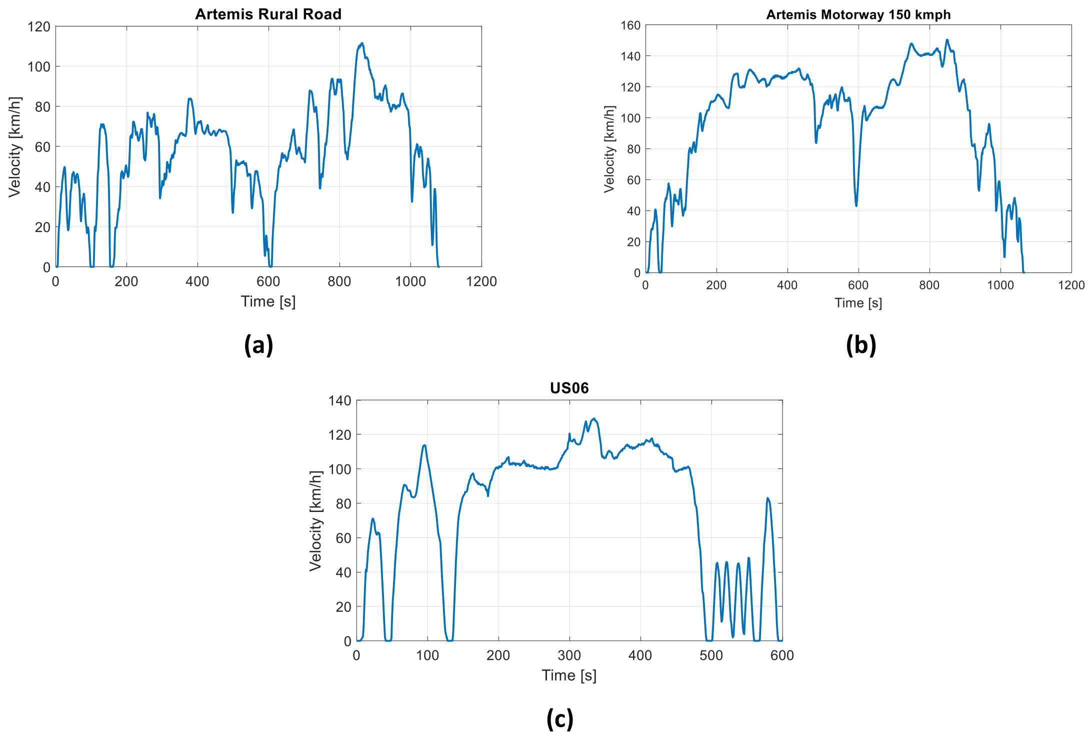

Figure 6.1 - Representation of Selected Driving Cycles: (**a**) Artemis Rural, (**b**) Artemis Motorway, (**c**) US06

Table 6. 2 - Characteristics of each Driving Cycle [135]

Driving Cycle	Artemis Rural	Artemis 150 km/h Motorway	US06
Average Speed (km/h)	70	150	34.2
Type	Rural Roads	High-Speed Motorway	Aggressive Urban
Stops and Starts	Frequent	Few	Frequent
Acceleration Patterns	Varied	Sustained	Rapid
Speed Variability	Moderate	Minimal	High
Duration (s)	1082	1068	596
Traffic Condition	Light	Smooth	Heavy

6.4.1) Impact of HESSs on Battery Performance

The implementation of the HESS brought about notable improvements in the management of battery SOC across all examined driving cycles. For this study, the analysis will concentrate on the initial 600 seconds of both Artemis driving cycle scenarios and the first 300 seconds of the US06 cycle. This specific focus is intended to provide a clear and straightforward presentation of the results. The choice to prioritise the first 600 seconds of the Artemis driving cycle scenarios and the first 300 seconds of the US06 cycle was made after careful consideration. This decision aims to capture critical moments in battery performance during dynamic and demanding driving phases [113].

This approach was used to ensure a comprehensive understanding of battery SOC management, especially during challenging start-up scenarios where there are significant interactions between energy demand and supply. The objective of this study was to facilitate a focused examination of these specific periods, offering valuable insights that can be directly applied to real-world situations. Ultimately, this approach aims to drive innovation and optimisation in battery technology for vehicle systems. The control system accurately determines the SOC of the battery by using real-time data from the battery management system, analysing variables such as voltage, current, and other relevant factors to provide a precise estimation of the SOC [113].

6.4.1.1) Artemis Rural Cycle

In the analysis of the Artemis rural cycle, Figure 6.2 reveals that the introduction of the HESS results in a very consistent battery SOC profile across all three controllers: PI, MPC, and RBF. The stability provided by the HESS showcases its ability to effectively manage the balance between energy storage and distribution, thereby minimising SOC fluctuations that could lead to losses and rapid wear. This improvement is largely due to the HESS's ability to leverage the high-power density of SCs for handling sudden power demands and transient loads. This capability reduces the strain on the battery, which is better suited for delivering a steady energy supply given its higher energy density but lower power density. By distributing the load between the battery and the supercapacitor, HESSs optimise battery longevity and performance, mitigating the rate and depth of battery discharges. Additionally, the HESS efficiently captures energy from regenerative braking by using the SC, which can rapidly charge and discharge. This mechanism helps maintain the battery's SOC and enhances overall energy efficiency [113].

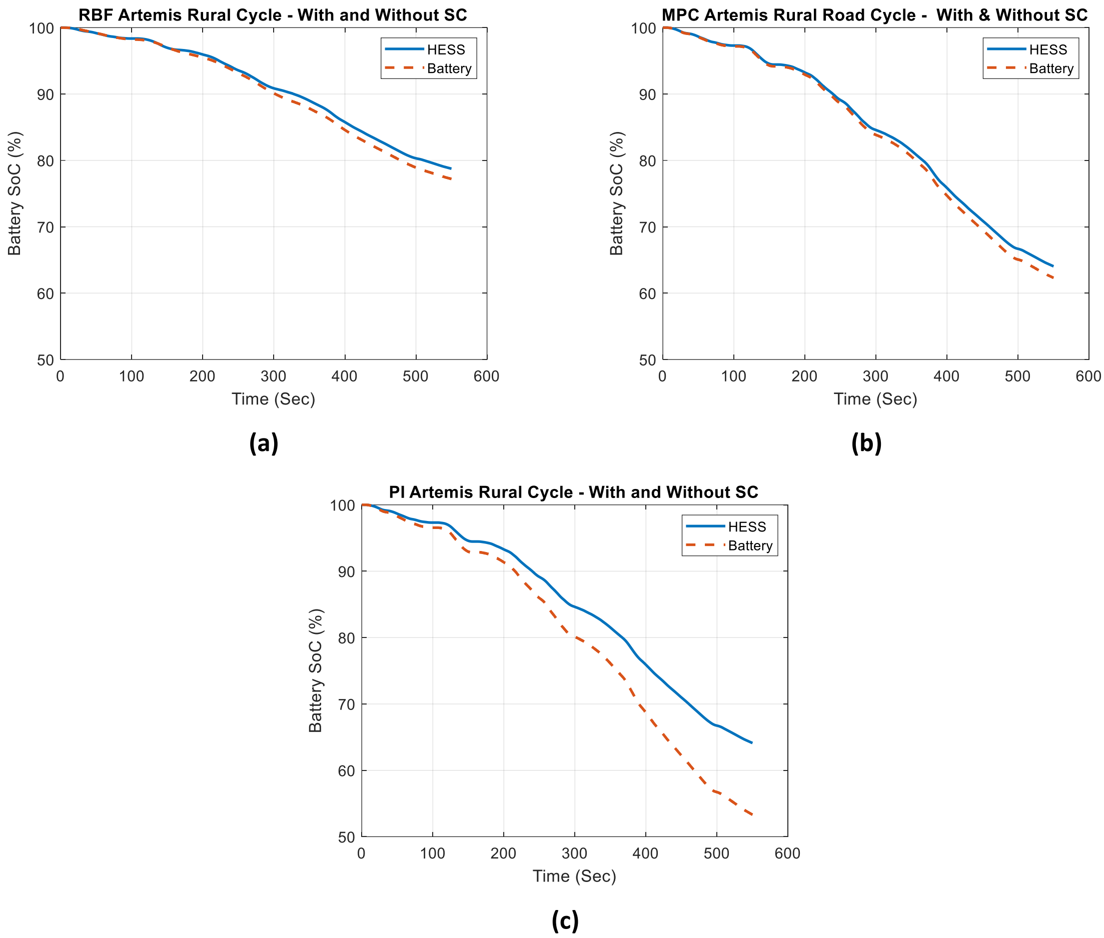

Figure 6.2 - Battery SOC comparison over time for an HESS versus a standalone battery across various control strategies for the Artemis rural cycle. (**a**) SOC decay under the RBF, (**b**) SOC decay under the MPC, (**c**) SOC decay under the PI

6.4.1.2) Artemis Motorway Cycle

The same principle applies to the Artemis motorway cycle, where the benefits of HESS integration remained evident. As shown in Figure 6.3, all three controllers demonstrated improved battery SOC control with the HESS, maintaining a consistent and optimised SOC profile throughout the cycle. This consistency is essential for EVs operating at high speeds, where rapid energy fluctuations can occur [113].

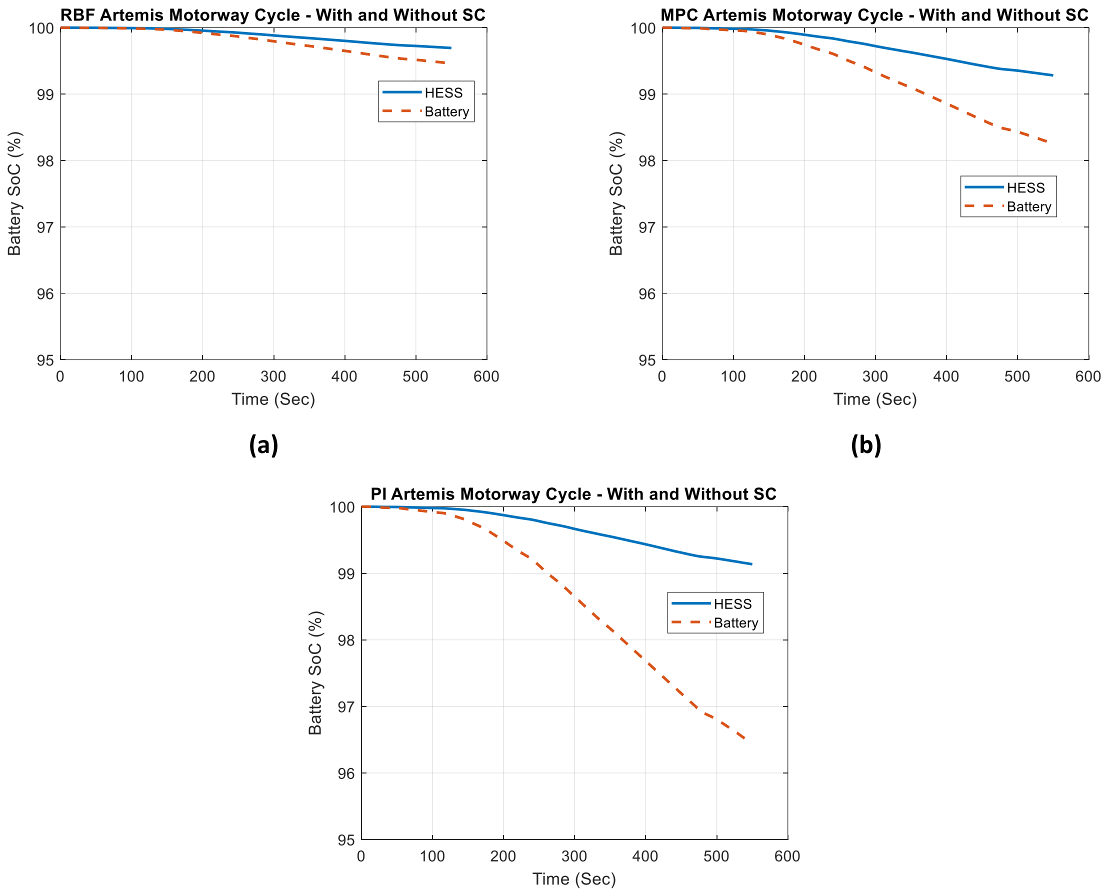

(a) **(b)**

(c)

Figure 6.3 - Battery SOC comparison over time for an HESS versus a standalone battery across various control strategies for the Artemis motorway cycle. (**a**) SOC decay under the RBF, (**b**) SOC decay under the MPC, (**c**) SOC decay under the PI

6.4.1.3) US06 Cycle

In the US06 cycle, all three controllers demonstrated stable and effective battery SOC management, as illustrated in Figure 6.4. During the interval of 100–150 seconds, the system experienced frequent fluctuations in power demand due to acceleration and deceleration phases, which are characteristic of the US06 cycle. The HESS effectively managed these fluctuations, as evidenced by the stable SOC profiles across all three controllers. This stability indicates the system's ability to adapt dynamically to transient power requirements, ensuring efficient energy utilisation. Such adaptability is vital for practical EV applications, where varying driving scenarios can significantly impact energy storage and usage [113]

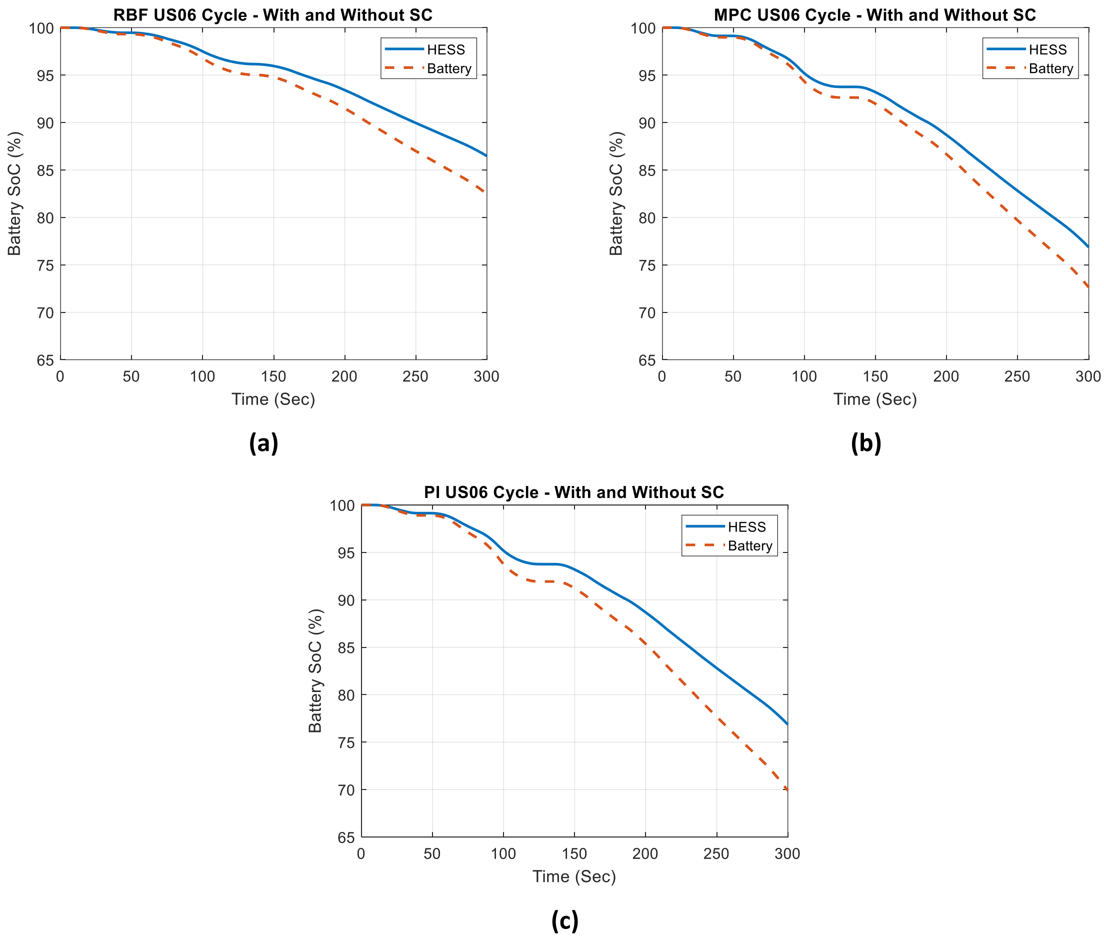

Figure 6.4 - Battery SOC comparison over time for an HESS versus a standalone battery across various control strategies for US06. (**a**) SOC decay under the RBF, (**b**) SOC decay under the MPC, (**c**) SOC decay under the PI

6.4.1.4) Energy Saved Calculation

In order to measure the amount of energy saved by proposed controller strategies, the following methodology was utilised. First, the difference in the SOC, denoted as ΔSOC between two control strategies needs to be calculated as expressed in Equation 6.1.

$$\Delta SOC \;=\; SOC_{Controller\ 1} \;-\; SOC_{Controller\ 2} \tag{6.1}$$

To calculate the energy savings, please refer to Equation 6.2

$$Energy\ Saved\ (kWh) \;=\; C_{battery}\ (kWh) \;*\; \left(\frac{\Delta SOC}{100}\right) \tag{6.2}$$

Where $C_{battery}$ is battery Nominal Pack Capacity.

6.4.1.4) Comment

The analysis of SOC across three distinct driving cycles offers valuable insights into how effectively various controllers manage energy usage. In the context of the Artemis rural scenario, as shown in

Table 6.3, the RBF regulator demonstrates higher efficiency compared to both the MPC and PI controllers, regardless of whether the system uses only a battery or an HESS. This is evident from the significantly improved SOC values achieved with the RBF controller, indicating reduced energy consumption. In contrast, the MPC and PI controllers show lower SOC values, with the MPC controller performing significantly better than the PI controller [113].

Table 6.3 - Comparison of Battery SOC for Artemis Rural

	RBF	MPC	PI	Energy Saved (kWh)	
				RBF_PI	MPC_PI
Battery only	77.27%	62.5%	53.49%	5.66	2.11
HESS	78.86%	64.41%	64.2%	3.452	0.05

In the Artemis Motorway scenario shown in Table 6.4, all controllers demonstrate high SOC values with only slight variations. However, it is noteworthy that the RBF controller shows exceptional energy efficiency, especially in the battery-only setup, highlighting its effectiveness in optimising energy utilisation [113].

Table 6.4 - Comparison of Battery SOC for Artemis Motorway

	RBF	MPC	PI	Energy Saved (kWh)	
				RBF_PI	MPC_PI
Battery Only	99.47%	98.26%	96.47%	0.54	0.39
HESS	99.69%	99.28%	99.14%	0.11	0.04

Table 6.5 illustrates the driving cycle of the US06, showing similar trends where the RBF controller achieves the highest SOC, followed by the MPC and PI controllers. In summary, the findings indicate that the RBF controller is highly effective in conserving energy across various driving conditions, making it an optimal choice for improving the efficiency of battery and HESS systems. The distinct urban driving characteristics of the US06 cycle, such as frequent starts and stops, rapid acceleration, and significant speed variability, largely account for this effectiveness. The RBF controller excels in these scenarios, which demand a highly responsive energy management system [113].

In comparison, the Artemis rural and motorway cycles, with their more consistent and stable driving patterns, show smaller SOC improvements. The battery system faces fewer dynamic challenges from the frequent stops and starts at lower speeds in the rural cycle and the continuous high-speed driving in the motorway cycle than in the US06 cycle. As a result, the US06 cycle sees a greater SOC increase due to the efficient use of regenerative braking and the advanced control techniques of the RBF controller, enhancing energy efficiency in these demanding driving conditions [113].

Table 6.5 - Comparison of Battery SOC for US06

	RBF	**MPC**	**PI**	**Energy Saved (kWh)**	
				RBF_PI	MPC_PI
Battery Only	82.91%	72.75%	70.2%	3.09	0.61
HESS	86.46%	77.1%	77.1%	2.67	0

6.4.2) Impact of HESSs on SC Performance

This subsection delves into the impact of SCs on HESSs, focusing on their effects on battery SOC. By evaluating how HESSs influence SC performance, significant insights emerge regarding the combined advantages of incorporating SCs alongside batteries in EVs. Integrating SCs with EV batteries is pivotal for optimising system efficiency. In practical driving scenarios, SCs can enhance vehicle performance by providing additional power during acceleration, thereby improving responsiveness, and ensuring a smoother driving experience. The rapid charge and discharge capabilities of SCs allow for swift power bursts necessary for rapid acceleration or climbing inclines. This responsiveness not only improves overall vehicle performance but also maintains efficiency. The analysis of SOC profiles of SCs under the influence of three different controllers during various driving cycles, alongside their corresponding charge and discharge profiles, yields valuable insights into the performance of each controller [113].

6.4.2.1) Artemis Rural Cycle

Throughout the Artemis rural driving cycle, the RBF controller consistently demonstrated superior efficiency, often achieving a higher SOC. This superior performance was notably observed during the intervals of 120–300 s, 380 s, and 500 s, as illustrated in Figure 6.5a. Additionally, the power profiles for charging and discharging highlighted the RBF controller's advantages, particularly within the first 200 s. The charging and discharging profiles for the three controllers reflect their adaptability to power requirements and effective use of regenerative energy, which are crucial for the acceleration and deceleration of EVs, as detailed in Figure 6.5b, where illustrates the power profiles for charging and discharging, wherein the RBF controller exhibits notable adaptability and efficiency, especially during the initial 200 seconds. The significant variations in the RBF power curve demonstrate its capacity to adapt swiftly to abrupt changes in acceleration and deceleration, rendering it exceptionally efficient for addressing transient power requirements. The more stable reactions of the MPC and PI controllers indicate their design prioritises stability over agility, potentially reducing energy recovery efficiency during transient events. In comparison to the battery charging/discharging profile shown in Figure 6.5c, the RBF controller's dynamic and responsive nature is evident from its frequent and substantial power output fluctuations. This indicates a control system that is highly sensitive and adept at managing complex and rapidly changing conditions with precision. While MPC and PI controllers offer smoother responses, the agility of the RBF controller is particularly beneficial in scenarios that demand flexibility and rapid adjustments [113].

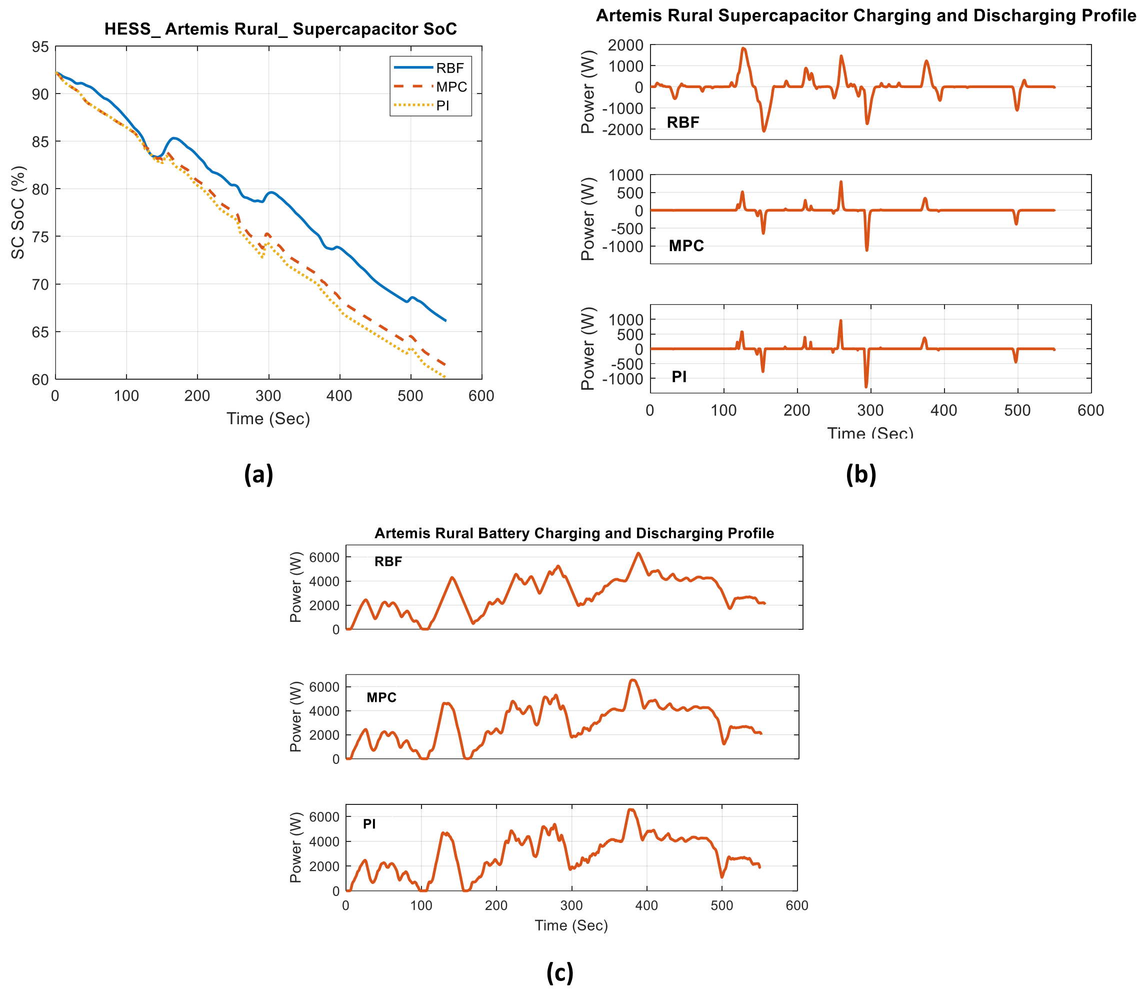

Figure 6.5 - Artemis Rural: (**a**) SOC of SC, (**b**) Charging/Discharging Profile of SC, (**c**) Charging/Discharging Profile of Battery

6.4.2.2) Artemis Motorway Cycle

The RBF controller demonstrated exceptional performance in managing the SC charge during the Artemis motorway cycle study, as illustrated in Figure 6.6a. Despite starting with a lower SOC, the RBF controller showed considerable improvements in efficiency, particularly noticeable between 300 s and 500 s. This interval coincides with periods of acceleration and deceleration, where the RBF controller effectively captures regenerative braking energy, allowing it to optimise energy storage and increase SOC stability.

In contrast, the PI controller shows a steady decline in SOC over the cycle, as seen in Figure 6.6a. The PI controller's lack of adaptive capability limits its responsiveness to dynamic load demands, resulting in lower SOC recovery and overall energy efficiency. The MPC controller, while maintaining relatively stable output, also demonstrates less adaptability in capturing regenerative braking energy compared to the RBF controller.

The charging and discharging patterns depicted in Figure 6.6b further emphasise the advantages of the RBF controller's design. It exhibits minimal oscillation in power output, reflecting a highly efficient energy flow management system capable of quickly adjusting to fluctuations in power demand. This stability is critical in motorway conditions, where consistent power availability supports steady driving at high speeds. The RBF controller's ability to anticipate and respond to rapid changes enables it to maximise energy recovery, minimising power losses and maintaining higher SOC levels.

As shown in Figure 6.6c, the RBF controller maintains a steady and near-maximum power output, reflecting its superior control accuracy and reliability. The MPC controller, though stable, shows slightly more variability, indicating effective but less precise control. Meanwhile, the PI controller displays significant oscillations, suggesting that it may be less suitable for applications where stable power delivery is crucial. Overall, the RBF controller's dynamic adaptability and predictive capability make it exceptionally well-suited for managing high-speed motorway conditions, enhancing both energy efficiency and regenerative braking effectiveness [113].

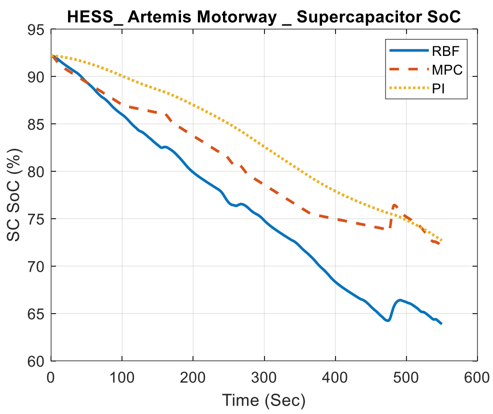

(a)

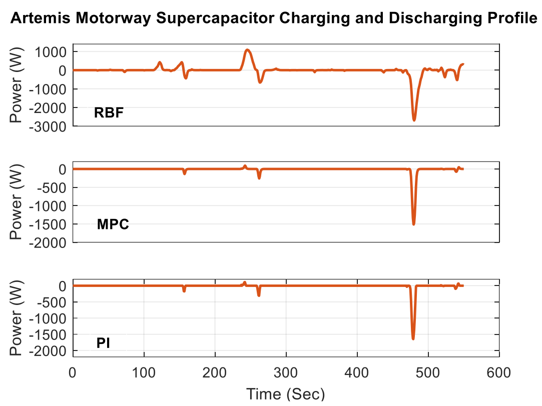

(b)

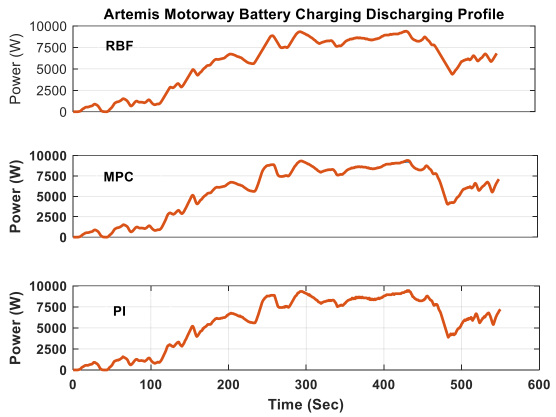

(c)

Figure 6.6 - Artemis Motorway: (a) SOC of SC, (b) Charging/Discharging Profile of SC, (c) Charging/Discharging Profile of Battery

6.4.2.3) US06 Cycle

In analysing the US06 cycle, the RBF controller initially showed a slightly lower SOC compared to the MPC and PI controllers. However, it demonstrated notable improvement within the first 100 seconds, as shown in Figure 6.7a, where MPC and PI controllers exhibit similar SOC performance due to their shared reliance on conventional control mechanisms that prioritise stability over adaptability. Both controllers regulate energy flow effectively under steady-state conditions but lack the dynamic responsiveness of the RBF controller during rapid changes in load demand. The similarity arises because the MPC's predictive capabilities are not fully utilised in the relatively less complex transient conditions of the US06 cycle, making its performance comparable to the simpler PI controller. The energy profile from the cycle highlighted the RBF controller's ability to quickly adapt to power fluctuations, which is crucial for managing the rapid acceleration and deceleration typical of the US06 cycle, as depicted in Figure 6.7b. Overall, the RBF controller outperformed both the MPC and PI controllers across all cycles, showcasing its superior energy management capabilities. This advantage enhances EV acceleration and optimises regenerative braking energy usage, which is vital for extending battery life and improving EV performance. When compared to the battery charging/discharging profile in Figure 6.7c, the RBF controller maintains a higher level of stability and consistently high power output throughout the entire period, especially after initial fluctuations. This indicates its superior ability to handle disruptions and adapt to varying conditions, underscoring its strength and effectiveness in maintaining target power levels. The RBF controller exhibits less instability and a more reliable power output profile than both MPC and PI, making it an excellent choice for EV applications that demand high dependability and precision [113].

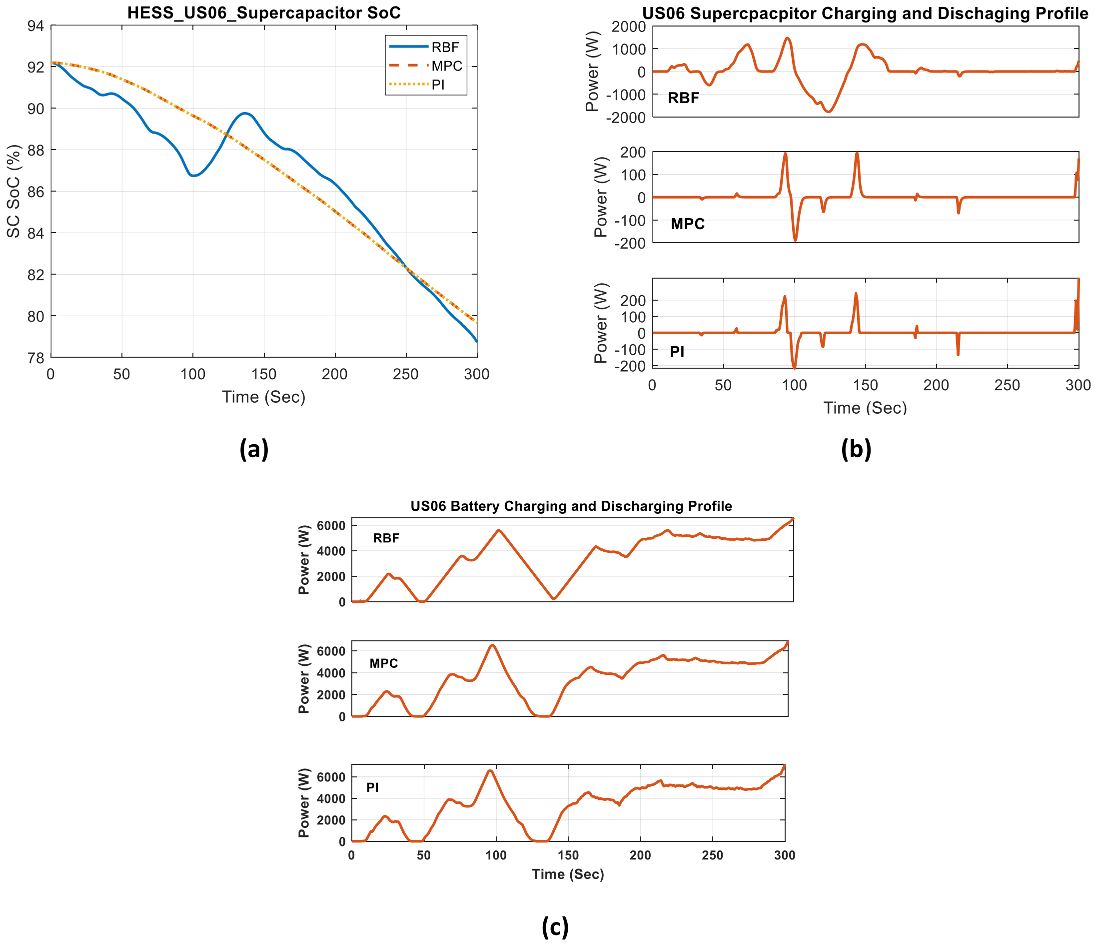

Figure 6.7 - US06: (**a**) SOC of SC, (**b**) Charging/Discharging Profile of SC, (**c**) Charging/Discharging Profile of Battery

6.4.3) Validation of Control Strategies

As shown in Figures 6.8 illustrates all control strategies (PI, MPC, and RBF) closely follow the reference speed for each driving cycle. This close adherence confirms both the accuracy of the simulation model and the effectiveness of the control strategies. The fact that all controllers successfully maintain the reference speed despite the varying conditions of the driving cycles highlights the robustness and reliability of the control systems used in the HESS [113].

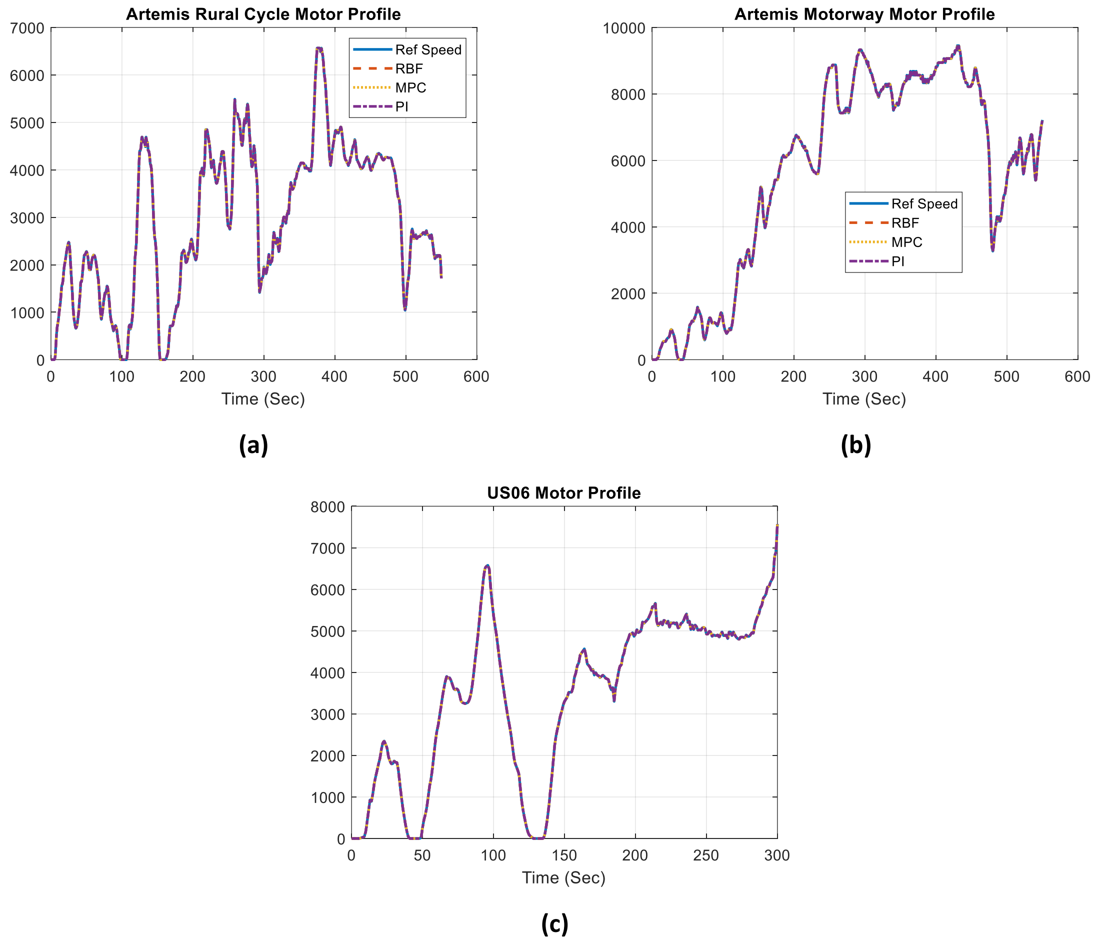

Figure 6.8 - Motor Profile of Selected Driving Cycles Motor (**a**) Artemis Rural, (**b**) Artemis Motorway, (**c**) US06

6.4.4) Overall System Efficiency and Performance

Integrating HESSs with EVs, as demonstrated with the Artemis rural, Artemis motorway, and US06 driving cycles, significantly enhances battery SOC management and SC efficiency. The HESS improves responsiveness and energy management across various driving scenarios, including high power demands, rapid acceleration, and fluctuating speeds. For instance, during periods of high acceleration, the SC provides quick bursts of power, easing the load on the battery and maintaining SOC stability, a benefit most evident in the US06 cycle. The Artemis rural cycle demonstrates how the HESS optimises energy distribution between the battery and SC, effectively handling frequent stops and starts while minimising energy loss and battery wear. On motorway cycles, the HESS maintains a steady SOC, which is essential for long-distance travel. While this study focuses on the Nissan Leaf, the described control strategies can be adapted for other EV models by adjusting parameters to suit their specific characteristics. This ensures that the benefits of HESSs, such as improved SOC management and SC performance, are transferable to different EVs. Overall, the use of HESSs enhances energy management, boosts vehicle performance, and extends battery life, highlighting the importance of advanced control algorithms for sustainable transportation [113].

6.5) Summary

This study assesses the efficiency of a fully active HESS in a Nissan Leaf. The HESS combines lithium-ion batteries and SCs to optimise energy management, enhance performance, and improve the dependability of EVs. The study utilises three control techniques, including PI, MPC, and RBF, on three different driving cycles: Artemis rural, Artemis motorway, and US06. The RBF controller demonstrated the most notable enhancement in effectively regulating the battery's SOC and improving the system's responsiveness. Integrating SCs with batteries in HESS efficiently reduces the burden on batteries, resulting in improved energy efficiency and prolonged battery lifespan. While all controllers effectively track the reference speed, the RBF controller excelled in battery SOC management and system responsiveness. This suggests that the RBF controller better optimises energy distribution between the battery and SCs, enhancing overall efficiency and extending battery life. In summary, the research showcases how proposed control algorithms have the power to greatly enhance the performance and longevity of EVs, hence promoting the broader acceptance of electric transportation alternatives [113].

Chapter 7 Conclusions and Future Work

7.1) Conclusions

This thesis has focused on the development and optimisation of a battery SC management system for EVs, addressing significant challenges in efficiency, integration, and control strategies. The results indicate that the performance, reliability, and energy efficiency of EVS can be significantly improved by the integration of batteries and SCs, which are regulated by advanced control algorithms.

It is important to highlight that this research was conducted exclusively in a simulation-based environment, utilising MATLAB/Simulink to model and evaluate the proposed HESS and associated control strategies. While the outcomes demonstrate the potential of the proposed system, these findings are limited to theoretical validation, and practical implementation remains a critical next step. Future research should focus on conducting comprehensive validation of these simulation results through hardware-in-the-loop (HIL) testing and real-world experimentation, benchmarking the proposed HESS and control strategies against state-of-the-art implementations and real-world performance metrics to demonstrate their robustness and applicability in practical scenarios.

The control algorithms, which include PI control, MPC control, and RBF control, were subjected to a comprehensive evaluation through exhaustive simulations in this thesis. The RBF controller's superior efficacy was demonstrated by a 3.09 kWh energy savings in the US06 cycle when compared to the PI controller, as revealed by statistical analysis. Additionally, the RBF controller demonstrated its efficacy in improving energy management by achieving a 5.66% enhancement in battery SOC over the PI controller during the Artemis rural cycle. The HESS's power flow control was significantly improved by these controllers, resulting in improved energy management. Among all the controllers, the RBF controller exhibited the most substantial improvement in the system's responsiveness and the efficient management of the battery's SOC. This controller's exceptional ability to manage non-linearities and adapt to real-time fluctuations made it the most effective in optimising energy allocation between the battery and SCs, thereby increasing overall efficiency and extending the lifecycle of the battery.

The results emphasise the efficacy of the suggested control mechanisms under different driving conditions, guaranteeing optimal performance and resilience of the EMS. The simulations encompassed various driving cycles, such as the Artemis rural, Artemis motorway, and US06 cycles. The RBF controller regularly outperformed the PI and MPC controllers in these situations by maintaining a steadier power profile and minimising energy losses. During periods of fast acceleration, the SC delivered rapid surges of power, reducing the strain on the battery and ensuring stability of the SOC. The US06 cycle showcased the exceptional performance of the RBF controller in effectively handling the rapid acceleration and deceleration patterns commonly encountered during city driving in congested traffic.

Integrating SCs with batteries in HESS efficiently reduces the burden on batteries, resulting in improved energy efficiency and prolonged battery lifespan. The research demonstrated that using the RBF controller led to significant energy savings compared to the PI and MPC controllers. In the Artemis rural cycle, the energy savings with the RBF controller were particularly pronounced. This was achieved by optimising the energy distribution between the battery and SCs, effectively handling frequent stops and starts while minimising energy loss and battery wear. On motorway cycles, the HESS maintained a steady SOC, which is essential for long-distance travel, thereby enhancing the overall efficiency and reliability of the EV.

The validation of the control methods' design and execution was conducted through MATLAB/Simulink simulations. The PI controller, renowned for its simplicity and consistent performance in predicted circumstances, faced difficulties with non-linearities and parameter changes. The MPC, due to its capacity to adjust control actions according to predicted future conditions, necessitated significant computer resources and presented implementation challenges. On the other hand, the RBF controller shown outstanding performance in handling non-linearities and adjusting to real-time changes, which makes it well-suited for EV applications that require precise and consistent results.

To summarise, this research demonstrates how the suggested control algorithms can significantly improve the efficiency and durability of EVs, hence encouraging the wider adoption of electric transportation options. The thesis enhances the development of sustainable transport technology by tackling significant technological challenges. It lays the groundwork for future research and development in the field of HESS, offering practical choices and valuable perspectives to enhance the effectiveness and dependability of EVs. The study demonstrates that the utilisation of HESS has a positive impact on energy management, vehicle performance, and battery longevity. The significance of sophisticated control algorithms for sustainable transportation is emphasised, emphasising their contribution to the wider acceptance of EVs.

7.2) Future work

Although this thesis has made substantial strides in the development and optimisation of HESS for EVs, several constraints present opportunities for future research.

1. Integration of Advanced Materials: One limitation of this research is the reliance on currently available battery and SC materials. Future studies could explore the integration of advanced materials such as solid-state electrolytes or graphene-based SC. These materials have the

potential to enhance energy density and power efficiency, addressing the limitations of current HESS configurations discussed in Chapter 5.

2. Extended Real-World Testing: The simulations and models utilised in this thesis are derived from conventional driving cycles and controlled conditions. Nevertheless, they fail to adequately account for real-world driving conditions' inherent variability. In future research, the control strategies devised in this thesis could be validated and refined through extended field testing in a variety of environmental conditions and driving habits. This would directly resolve the limitation identified in Chapter 6 concerning the adaptability of the control algorithms in various operational scenarios.
3. Enhanced Control Algorithms: While the thesis showcases the efficacy of several control systems, such as PI, MPC, and RBF controllers, there is still potential for additional enhancement. Subsequent research could prioritise the development of control algorithms that are more adaptable and learning-oriented, capable of dynamically adapting to the evolving conditions of the HESS in real-time. This enhancement has the potential to alleviate the constraint of fixed parameter modification, as emphasised in the comparative study presented in Chapter 4.

By focusing on these areas, future work can help make EVs better and more efficient for everyday use.

List of References

[1] "Global EV Outlook 2023 – Analysis - IEA." Accessed: May 16, 2024. [Online]. Available: https://www.iea.org/reports/global-ev-outlook-2023

[2] H. Ritchie and M. Roser, "Tracking global data on electric vehicles," *Our World in Data*, 2024.

[3] N. Novas *et al.*, "Global Perspectives on and Research Challenges for Electric Vehicles," *Vehicles*, vol. 4, no. 4, pp. 1246–1276, 2022, doi: 10.3390/vehicles4040066.

[4] J. A. Sanguesa, V. Torres-Sanz, P. Garrido, F. J. Martinez, and J. M. Marquez-Barja, "A Review on Electric Vehicles: Technologies and Challenges," *Smart Cities*, vol. 4, no. 1, pp. 372–404, 2021, doi: 10.3390/smartcities4010022.

[5] A. Albatayneh, M. N. Assaf, D. Alterman, and M. Jaradat, "Comparison of the overall energy efficiency for internal combustion engine vehicles and electric vehicles," *Rigas Tehniskas Universitates Zinatniskie Raksti*, vol. 24, no. 1, pp. 669–680, 2020.

[6] C. C. Chan, "The state of the art of electric, hybrid, and fuel cell vehicles," *Proceedings of the IEEE*, vol. 95, no. 4, pp. 704–718, 2007.

[7] J. Blazquez Lidoy and J. M. Martin Moreno, "Energy efficiency in automobiles. The electric car, a challenge of this present; Eficiencia energetica en la automoacion. el vehiculo electrico un reto del presente," *Economia Industrial*, vol. 377, 2010.

[8] T. Hofman, "18 - Hybrid drive train technologies for vehicles," in *Alternative Fuels and Advanced Vehicle Technologies for Improved Environmental Performance*, R. Folkson, Ed., Woodhead Publishing, 2014, pp. 567–581. doi: https://doi.org/10.1533/9780857097422.3.567.

[9] A. L. Dicks, "4.08 - PEM Fuel Cells: Applications," in *Comprehensive Renewable Energy*, A. Sayigh, Ed., Oxford: Elsevier, 2012, pp. 203–245. doi: https://doi.org/10.1016/B978-0-08-087872-0.00406-6.

[10] Íñigo Díez Olleros, "Analysis of different methodologies for the design of the electric vehicle's fast and ultrafast public charging network in Spain," Master Thesis , UNIVERSIDAD PONTIFICIA COMILLAS ESCUELA TÉCNICA SUPERIOR DE INGENIERÍA (ICAI), Madrid , 2019. Accessed: May 17, 2022. [Online]. Available: https://repositorio.comillas.edu/xmlui/bitstream/handle/11531/41452/TFM%20-%20Diez%20Olleros%2C%20IAigo.pdf?sequence=1&isAllowed=y

[11] M. Wahid, B. Budiman, E. Joelianto, and M. Aziz, "A Review on Drive Train Technologies for Passenger Electric Vehicles," *Energies (Basel)*, vol. 14, p. 6742, Oct. 2021, doi: 10.3390/en14206742.

[12] M. Farrag, C. S. Lai, and M. Darwish, "Overview of Electric Vehicle Interconnected Subsystems," in *2022 57th International Universities Power Engineering Conference (UPEC)*, 2022, pp. 1–6. doi: 10.1109/UPEC55022.2022.9917616.

[13] Q. Zheng, S. Tian, and Q. Zhang, "Optimal Torque Split Strategy of Dual-Motor Electric Vehicle Using Adaptive Nonlinear Particle Swarm Optimization," *Math Probl Eng*, vol. 2020, p. 1204260, 2020, doi: 10.1155/2020/1204260.

[14] C. Rossi, D. Pontara, M. Bertoldi, and D. Casadei, “Two-motor, Two-axle Traction System for Full Electric Vehicle,” *World Electric Vehicle Journal*, vol. 8, pp. 25–39, Mar. 2016, doi: 10.3390/wevj8010025.

[15] Pascal Fenner, “Efficient Use of the Existing Real Estate Infrastructure for Electric Vehicle Charging,” Master Thesis, Technical University Dortmund, 2019. Accessed: May 17, 2022. [Online]. Available: https://eldorado.tu-dortmund.de/bitstream/2003/38406/1/MSc_Thesis_Fenner_Pascal.pdf

[16] C. Unal, E. Yirik, E. Ünal, M. Cuma, B. Onur, and M. Tümay, “A REVIEW OF CHARGING TECHNOLOGIES FOR COMMERCIAL ELECTRIC VEHICLES,” *INTERNATIONAL JOURNAL OF ADVANCES ON AUTOMOTIVE AND TECHNOLOGY*, Jan. 2018, doi: 10.15659/ijaat.18.01.892.

[17] A. Bahrami, *EV Charging Definitions, Modes, Levels, Communication Protocols and Applied Standards*. 2020. doi: 10.13140/RG.2.2.15844.53123/11.

[18] Bob Johan Alexander Vrösch, “CONSUMER’ ACCEPTANCE OF ELECTRIC VEHICLES IN LISBON,” Master Thesis, University Institute of Lisbon Repository, Lisbon , 2018. Accessed: May 19, 2022. [Online]. Available: https://repositorio.iscte-iul.pt/bitstream/10071/18980/1/master_bob_alexander_vrosch.pdf

[19] Claude Ricaud and Philippe Vollet, “Connection method for charging systems – a key element for electric vehicles,” 2010. Accessed: May 19, 2022. [Online]. Available: https://www.elektropunjaci.com/wp-content/uploads/bsk-pdf-manager/Connection-method-for-charging-systems_18.pdf

[20] T. Bryden, “Overcoming the electricity grid capacity and battery thermal limitations of electric vehicle fast charging using stationary energy storage and cell thermal modelling,” 2019.

[21] Dwaramakki Gaurav and Harinarayanan Manimaran, “Impact of EV Charging Station on the Electric Distribution Grid,” Master Thesis, POLITECNICO DI MILANO, Milan, 2016. Accessed: May 19, 2022. [Online]. Available: https://www.politesi.polimi.it/bitstream/10589/120624/1/Thesis_LM.pdf

[22] Alexander Wanitschke, “Are battery electric vehicles the future? An uncertainty and robustness comparison with hydrogen fuel cell and internal combustion engine vehicles in Germany,” Master Thesis , Technical University of Berlin, Berlin, 2021. Accessed: May 18, 2022. [Online]. Available: https://www.reiner-lemoine-stiftung.de/pdf/dissertationen/Dissertation-Alexander_Wanitschke.pdf

[23] D. Rimpas *et al.*, “Energy management and storage systems on electric vehicles: A comprehensive review,” *Mater Today Proc*, vol. 61, pp. 813–819, 2022, doi: https://doi.org/10.1016/j.matpr.2021.08.352.

[24] P. Voelker and T. F. Scientific, “Trace degradation analysis of lithium-ion battery components,” *R&D Magazinde,(April 2014) http://www. rdmag. com/articles/2014/04/trace-degradation-analysislithium-ion-battery-components Search PubMed,(accessed August 2015)*, 2014, Accessed: May 24, 2022. [Online]. Available: https://tools.thermofisher.com/content/sfs/brochures/AR-Lithium-Ion-Battery-Degradation-RandD-Mag-042214.pdf

[25] Y. Miao, P. Hynan, A. von Jouanne, and A. Yokochi, “Current Li-Ion Battery Technologies in Electric Vehicles and Opportunities for Advancements,” *Energies (Basel)*, vol. 12, no. 6, 2019, doi: 10.3390/en12061074.

[26] M. Darwish, S. Ioannou, A. Janbey, H. Amreiz, and C. C. Marouchos, “Review of Battery Management Systems,” in *2021 International Conference on Electrical, Computer, Communications and Mechatronics Engineering (ICECCME)*, 2021, pp. 1–6. doi: 10.1109/ICECCME52200.2021.9590884.

[27] S. Shete, P. Jog, R. K. Kumawat, and D. K. Palwalia, “Battery Management System for SOC Estimation of Lithium-Ion Battery in Electric Vehicle: A Review,” in *2021 6th IEEE International Conference on Recent Advances and Innovations in Engineering (ICRAIE)*, 2021, pp. 1–4. doi: 10.1109/ICRAIE52900.2021.9703752.

[28] C. S. Lai, Y. Jia, L. L. Lai, Z. Xu, M. D. McCulloch, and K. P. Wong, “A comprehensive review on large-scale photovoltaic system with applications of electrical energy storage,” *Renewable and Sustainable Energy Reviews*, vol. 78, pp. 439–451, 2017, doi: https://doi.org/10.1016/j.rser.2017.04.078.

[29] D. K. Bhatt and M. El. Darieby, “An Assessment of Batteries form Battery Electric Vehicle Perspectives,” in *2018 IEEE International Conference on Smart Energy Grid Engineering (SEGE)*, 2018, pp. 255–259. doi: 10.1109/SEGE.2018.8499462.

[30] S. Nejad, “Adaptive Techniques for Estimation and Online Monitoring of Battery En ergy Storage Devices,”

[31] Junyi Shen, “Energy Management of a Battery-Ultracapacitor Hybrid Energy Storage System in Electric Vehicles,” PhD Dissertation, University of Maryland, 2016. Accessed: May 25, 2022. [Online]. Available: https://drum.lib.umd.edu/bitstream/handle/1903/18641/Shen_umd_0117E_17253.pdf?sequence=1&isAllowed=y

[32] M. Armand and J.-M. Tarascon, “Building Better Batteries,” *Nature*, vol. 451, pp. 652–657, Mar. 2008, doi: 10.1038/451652a.

[33] A. Burke, “Ultracapacitor Technologies and Application in Hybrid and Electric Vehicles,” *Int J Energy Res*, vol. 34, pp. 133–151, Feb. 2010, doi: 10.1002/er.1654.

[34] A. Ahmadian, M. Sedghi, A. Elkamel, M. Fowler, and M. Aliakbar Golkar, “Plug-in electric vehicle batteries degradation modeling for smart grid studies: Review, assessment and conceptual framework,” *Renewable and Sustainable Energy Reviews*, vol. 81, pp. 2609–2624, 2018, doi: https://doi.org/10.1016/j.rser.2017.06.067.

[35] Ali Milad Jarushi, “ANALYSIS AND MODELLING OF ENERGY SOURCE COMBINATIONS FOR ELECTRIC VEHICLES,” PhD Thesis, University of Manchester, Manchester, 2010. Accessed: May 24, 2022. [Online]. Available: https://www.escholar.manchester.ac.uk/api/datastream?publicationPid=uk-ac-man-scw:123309&datastreamId=FULL-TEXT.PDF

[36] A. K. Shukla, A. S. Aricò, and V. Antonucci, “An appraisal of electric automobile power sources,” *Renewable and Sustainable Energy Reviews*, vol. 5, no. 2, pp. 137–155, 2001, doi: https://doi.org/10.1016/S1364-0321(00)00011-3.

[37] E. Karden, P. Shinn, P. Bostock, J. Cunningham, E. Schoultz, and D. Kok, "Requirements for future automotive batteries - A snapshot," *J Power Sources*, vol. 144, pp. 505–512, Jun. 2005, doi: 10.1016/j.jpowsour.2004.11.007.

[38] P. van den Bossche, F. Vergels, J. van Mierlo, J. Matheys, and W. Autenboer, "SUBAT: An assessment of sustainable battery technology," *J Power Sources*, vol. 162, pp. 913–919, Nov. 2006, doi: 10.1016/j.jpowsour.2005.07.039.

[39] J. van . Mierlo, G. Maggetto, and Ph. Lataire, "Which energy source for road transport in the future? A comparison of battery, hybrid and fuel cell vehicles," *Energy Convers Manag*, vol. 47, no. 17, pp. 2748–2760, 2006, doi: DOI:101016/jenconman200602004.

[40] G. Zubi, R. Dufo-López, M. Carvalho, and G. Pasaoglu, "The lithium-ion battery: State of the art and future perspectives," *Renewable and Sustainable Energy Reviews*, vol. 89, pp. 292–308, 2018, doi: https://doi.org/10.1016/j.rser.2018.03.002.

[41] Gareth Dauley, "How it works: delving into the anatomy of a battery." Accessed: May 26, 2022. [Online]. Available: https://www.pacificgreen-group.com/articles/how-it-works-delving-anatomy-battery

[42] V. Vaideeswaran, S. Bhuvanesh, and M. Devasena, "Battery Management Systems for Electric Vehicles using Lithium Ion Batteries," in *2019 Innovations in Power and Advanced Computing Technologies (i-PACT)*, 2019, pp. 1–9. doi: 10.1109/i-PACT44901.2019.8959965.

[43] J. F. Peters, M. Baumann, B. Zimmermann, J. Braun, and M. Weil, "The environmental impact of Li-Ion batteries and the role of key parameters – A review," *Renewable and Sustainable Energy Reviews*, vol. 67, pp. 491–506, 2017, doi: https://doi.org/10.1016/j.rser.2016.08.039.

[44] M. Li, "Li-ion dynamics and state of charge estimation," *Renew Energy*, vol. 100, pp. 44–52, 2017, doi: https://doi.org/10.1016/j.renene.2016.06.009.

[45] S. Chacko and Y. M. Chung, "Thermal modelling of Li-ion polymer battery for electric vehicle drive cycles," *J Power Sources*, vol. 213, pp. 296–303, 2012, doi: https://doi.org/10.1016/j.jpowsour.2012.04.015.

[46] C. Pastor-Fernández, K. Uddin, G. H. Chouchelamane, W. D. Widanage, and J. Marco, "A Comparison between Electrochemical Impedance Spectroscopy and Incremental Capacity-Differential Voltage as Li-ion Diagnostic Techniques to Identify and Quantify the Effects of Degradation Modes within Battery Management Systems," *J Power Sources*, vol. 360, pp. 301–318, 2017, doi: https://doi.org/10.1016/j.jpowsour.2017.03.042.

[47] Y. Xing, W. He, M. Pecht, and K. L. Tsui, "State of charge estimation of lithium-ion batteries using the open-circuit voltage at various ambient temperatures," *Appl Energy*, vol. 113, pp. 106–115, 2014, doi: https://doi.org/10.1016/j.apenergy.2013.07.008.

[48] C. Edouard, M. Petit, C. Forgez, J. Bernard, and R. Revel, "Parameter sensitivity analysis of a simplified electrochemical and thermal model for Li-ion batteries aging," *J Power Sources*, vol. 325, pp. 482–494, 2016, doi: https://doi.org/10.1016/j.jpowsour.2016.06.030.

[49] S. Yang, C. Ling, Y. Fan, Y. Yang, X. Tan, and H. Dong, "A review of lithium-ion battery thermal management system strategies and the evaluate criteria," *Int J Electrochem Sci*, vol. 14, no. 7, pp. 6077–6107, 2019.

[50] W. Situ *et al.*, “Effect of high temperature environment on the performance of LiNi0.5Co0.2Mn0.3O2 battery,” *Int J Heat Mass Transf*, vol. 104, pp. 743–748, 2017, doi: https://doi.org/10.1016/j.ijheatmasstransfer.2016.09.005.

[51] J. Wu, Y. Wang, X. Zhang, and Z. Chen, “A novel state of health estimation method of Li-ion battery using group method of data handling,” *J Power Sources*, vol. 327, pp. 457–464, 2016, doi: https://doi.org/10.1016/j.jpowsour.2016.07.065.

[52] W. Zhou, Y. Zheng, Z. Pan, and Q. Lu, “Review on the Battery Model and SOC Estimation Method,” *Processes*, 2021.

[53] P. Shrivastava, T. K. Soon, M. Y. I. bin Idris, and S. Mekhilef, “Overview of model-based online state-of-charge estimation using Kalman filter family for lithium-ion batteries,” *Renewable and Sustainable Energy Reviews*, vol. 113, p. 109233, 2019, doi: https://doi.org/10.1016/j.rser.2019.06.040.

[54] C. Lin, A. Tang, and W. Wang, “A Review of SOH Estimation Methods in Lithium-ion Batteries for Electric Vehicle Applications,” *Energy Procedia*, vol. 75, pp. 1920–1925, 2015, doi: https://doi.org/10.1016/j.egypro.2015.07.199.

[55] C. Zhang, K. Li, S. Mcloone, and Z. Yang, “Battery modelling methods for electric vehicles - A review,” in *2014 European Control Conference (ECC)*, 2014, pp. 2673–2678. doi: 10.1109/ECC.2014.6862541.

[56] G. Saldaña, J. Martín, I. Zamora, F. Asensio, and O. Oñederra, “Analysis of the Current Electric Battery Models for Electric Vehicle Simulation,” *Energies (Basel)*, vol. 12, p. 2750, Jul. 2019, doi: 10.3390/en12142750.

[57] D. Lyu, B. Ren, and S. Li, “Failure modes and mechanisms for rechargeable Lithium-based batteries: a state-of-the-art review,” *Acta Mech*, vol. 230, no. 3, pp. 701–727, 2019, doi: 10.1007/s00707-018-2327-8.

[58] M.-K. Tran and M. Fowler, “A Review of Lithium-Ion Battery Fault Diagnostic Algorithms: Current Progress and Future Challenges,” *Algorithms*, vol. 13, no. 3, 2020, doi: 10.3390/a13030062.

[59] X. Feng *et al.*, “Characterization of penetration induced thermal runaway propagation process within a large format lithium ion battery module,” *J Power Sources*, vol. 275, Nov. 2014, doi: 10.1016/j.jpowsour.2014.11.017.

[60] A. Kriston *et al.*, “External short circuit performance of Graphite-LiNi1/3Co1/3Mn1/3O2 and Graphite-LiNi0. 8Co0. 15Al0. 05O2 cells at different external resistances,” *J Power Sources*, vol. 361, pp. 170–181, 2017.

[61] A. Rheinfeld, J. Sturm, A. Frank, S. Kosch, S. v Erhard, and A. Jossen, “Impact of cell size and format on external short circuit behavior of lithium-ion cells at varying cooling conditions: modeling and simulation,” *J Electrochem Soc*, vol. 167, no. 1, p. 013511, 2019.

[62] M. Murnane and A. Ghazel, “A Closer Look at State of Charge (SOC) and State of Health (SOH) Estimation Techniques for Batteries,” 2017.

[63] J. P. Rivera-Barrera, N. Muñoz-Galeano, and H. O. Sarmiento-Maldonado, “SoC Estimation for Lithium-ion Batteries: Review and Future Challenges,” *Electronics (Basel)*, vol. 6, p. 102, 2017.

[64] M. Coleman, C. K. Lee, C. Zhu, and W. G. Hurley, “State-of-Charge Determination From EMF Voltage Estimation: Using Impedance, Terminal Voltage, and Current for Lead-Acid and Lithium-Ion Batteries,” *IEEE Transactions on Industrial Electronics*, vol. 54, pp. 2550–2557, 2007.

[65] C. Huang, Z. Wang, Z. Zhao, L. Wang, C. S. Lai, and D. Wang, “Robustness Evaluation of Extended and Unscented Kalman Filter for Battery State of Charge Estimation,” *IEEE Access*, vol. 6, pp. 27617–27628, 2018, doi: 10.1109/ACCESS.2018.2833858.

[66] M. R. M. Kassim, W. A. W. Jamil, and R. M. Sabri, “State-of-Charge (SOC) and State-of-Health (SOH) Estimation Methods in Battery Management Systems for Electric Vehicles,” in *2021 IEEE International Conference on Computing (ICOCO)*, 2021, pp. 91–96. doi: 10.1109/ICOCO53166.2021.9673580.

[67] R. Zhou, S. Fu, and W. Peng, *A Review of State-of-health Estimation of Lithiumion Batteries: Experiments and Data*. 2020. doi: 10.1109/APARM49247.2020.9209548.

[68] D. D. Agwu, F. Opara, N. Chukwuchekwa, D. Dike, and L. Uzoechi, “Review Of Comparative Battery Energy Storage Systems (Bess) For Energy Storage Applications In Tropical Enviroments,” Sep. 2018.

[69] D. Ranawat and M. P. R. Prasad, “A Review on Electric Vehicles with perspective of Battery Management System,” in *2018 International Conference on Electrical, Electronics, Communication, Computer, and Optimization Techniques (ICEECCOT)*, 2018, pp. 1539–1544. doi: 10.1109/ICEECCOT43722.2018.9001321.

[70] S. Tie and C. W. Tan, “A review of energy sources and energy management system in electric vehicles,” *Renewable and Sustainable Energy Reviews*, vol. 20, pp. 82–102, Apr. 2013, doi: 10.1016/j.rser.2012.11.077.

[71] C. Mahmoudi, A. Flah, and L. Sbita, “An overview of electric Vehicle concept and power management strategies,” in *2014 International Conference on Electrical Sciences and Technologies in Maghreb (CISTEM)*, 2014, pp. 1–8. doi: 10.1109/CISTEM.2014.7077026.

[72] M. K. Yoong *et al.*, “Studies of regenerative braking in electric vehicle,” in *2010 IEEE Conference on Sustainable Utilization and Development in Engineering and Technology*, 2010, pp. 40–45. doi: 10.1109/STUDENT.2010.5686984.

[73] V. Totev, V. Gueorgiev, and P. Rizov, “Regenerative braking of electric vehicles,” in *2019 11th Electrical Engineering Faculty Conference (BulEF)*, 2019, pp. 1–5. doi: 10.1109/BulEF48056.2019.9030768.

[74] S. S. Bhurse and A. A. Bhole, “A Review of Regenerative Braking in Electric Vehicles,” in *2018 International Conference on Computation of Power, Energy, Information and Communication (ICCPEIC)*, 2018, pp. 363–367. doi: 10.1109/ICCPEIC.2018.8525157.

[75] L. Joseph and K. S. Sreerag, “A Novel Energy Regeneration Technique in Brushless DC Motor for Electric Vehicles”.

[76] M. Yang, H. Jhou, B. Ma, and K. Shyu, “A Cost-Effective Method of Electric Brake With Energy Regeneration for Electric Vehicles,” *IEEE Transactions on Industrial Electronics*, vol. 56, no. 6, pp. 2203–2212, 2009, doi: 10.1109/TIE.2009.2015356.

[77] M. Gupta, “Evaluation of Regenerative Braking and its Functionality in Electric Vehicles,” in *2020 International Conference for Emerging Technology (INCET)*, 2020, pp. 1–6. doi: 10.1109/INCET49848.2020.9154047.

[78] J. Dixon, “Energy storage for electric vehicles,” in *2010 IEEE International Conference on Industrial Technology*, 2010, pp. 20–26. doi: 10.1109/ICIT.2010.5472647.

[79] K. Wagh and P. Dhatrak, “A review on powertrain subsystems and charging technology in battery electric vehicles: Current and future trends,” *Proceedings of the Institution of Mechanical Engineers, Part D: Journal of Automobile Engineering*, p. 09544070211025906, Jul. 2021, doi: 10.1177/09544070211025906.

[80] E. Wang and M. O. E.-T. Donateo, “A Hybrid Energy Storage System for a Coaxial Power-Split Hybrid Powertrain,” in *Hybrid Electric Vehicles*, F. Yang, Ed., Rijeka: IntechOpen, 2017, p. Ch. 4. doi: 10.5772/67756.

[81] A. Berrueta, A. Ursua, I. San Martin, A. Eftekhari, and P. Sanchis, “Supercapacitors: Electrical Characteristics, Modeling, Applications, and Future Trends,” *IEEE Access*, vol. 7, pp. 50869–50896, Jan. 2019, doi: 10.1109/ACCESS.2019.2908558.

[82] S. Shiraishi, “Chapter 27 - Electric Double Layer Capacitors,” in *Carbon Alloys*, E. YASUDA, M. INAGAKI, K. KANEKO, M. ENDO, A. OYA, and Y. TANABE, Eds., Oxford: Elsevier Science, 2003, pp. 447–457. doi: https://doi.org/10.1016/B978-008044163-4/50027-9.

[83] L. Zhou, C. Li, X. Liu, Y. Zhu, Y. Wu, and T. van Ree, “7 - Metal oxides in supercapacitors,” in *Metal Oxides in Energy Technologies*, Y. Wu, Ed., Elsevier, 2018, pp. 169–203. doi: https://doi.org/10.1016/B978-0-12-811167-3.00007-9.

[84] K. Machida, S. Suematsu, S. Ishimoto, and K. Tamamitsu, “High-Voltage Asymmetric Electrochemical Capacitor Based on Polyfluorene Nanocomposite and Activated Carbon,” *J Electrochem Soc*, vol. 155, no. 12, p. A970, 2008, doi: 10.1149/1.2994627.

[85] A. Muzaffar, M. B. Ahamed, K. Deshmukh, and J. Thirumalai, “A review on recent advances in hybrid supercapacitors: Design, fabrication and applications,” *Renewable and Sustainable Energy Reviews*, vol. 101, pp. 123–145, 2019, doi: https://doi.org/10.1016/j.rser.2018.10.026.

[86] R. S. Sankarkumar and R. Natarajan, “Energy management techniques and topologies suitable for hybrid energy storage system powered electric vehicles: An overview,” *INTERNATIONAL TRANSACTIONS ON ELECTRICAL ENERGY SYSTEMS*, vol. 31, no. 4, 2021, doi: 10.1002/2050-7038.12819.

[87] M. O. Badawy and Y. Sozer, “A partial power processing of battery/ultra-Capacitor hybrid energy storage system for electric vehicles,” in *2015 IEEE Applied Power Electronics Conference and Exposition (APEC)*, 2015, pp. 3162–3168. doi: 10.1109/APEC.2015.7104804.

[88] Z. Song *et al.*, “Multi-objective optimization of a semi-active battery/supercapacitor energy storage system for electric vehicles,” *Appl Energy*, vol. 135, pp. 212–224, 2014, doi: https://doi.org/10.1016/j.apenergy.2014.06.087.

[89] P. Aruna and P. v Vasan, “Review on Energy Management System of Electric Vehicles,” in *2019 2nd International Conference on Power and Embedded Drive Control (ICPEDC)*, 2019, pp. 371–374. doi: 10.1109/ICPEDC47771.2019.9036689.

[90] Tahir, T. Zarma, A. Galadima, and A. Maruf, *A Review of Motors for Electric Vehicles*. 2019.

[91] K. V. Singh, H. O. Bansal, and D. Singh, “A comprehensive review on hybrid electric vehicles: architectures and components,” *Journal of Modern Transportation*, vol. 27, no. 2, pp. 77–107, 2019, doi: 10.1007/s40534-019-0184-3.

[92] W. Cao, S. Bukhari, and L. Aarniovuori, “Review of Electrical Motor Drives for Electric Vehicle Applications,” *Mehran University Research Journal of Engineering and Technology*, vol. 38, pp. 525–540, Jul. 2019, doi: 10.22581/muet1982.1903.01.

[93] C. C. Chan, “The state of the art of electric and hybrid vehicles,” *Proceedings of the IEEE*, vol. 90, no. 2, pp. 247–275, 2002.

[94] C. C. Chan, K. T. Chau, and K. T. Chau, *Modern electric vehicle technology*, vol. 47. Oxford University Press on Demand, 2001.

[95] T. A. Zarma, A. A. Galadima, and M. A. Aminu, “Review of motors for electric vehicles,” *J Sci Res Rep*, vol. 24, no. 6, pp. 1–6, 2019.

[96] S. J. Rind, Y. Ren, Y. Hu, J. Wang, and L. Jiang, “Configurations and control of traction motors for electric vehicles: A review,” *Chinese Journal of Electrical Engineering*, vol. 3, no. 3, pp. 1–17, 2017.

[97] P. Yedamale, “Brushless DC (BLDC) motor fundamentals,” *Microchip Technology Inc*, vol. 20, no. 1, pp. 3–15, 2003.

[98] W. R. Oney, “High power density brushless dc motor,” Feb. 05, 1980, *Google Patents*.

[99] P. C. Sen, “Electric motor drives and control-past, present, and future,” *IEEE Transactions on Industrial Electronics*, vol. 37, no. 6, pp. 562–575, 1990.

[100] H. A. Toliyat and G. B. Kliman, *Handbook of electric motors*, vol. 120. CRC press, 2018.

[101] E. Levi, R. Bojoi, F. Profumo, H. A. Toliyat, and S. Williamson, “Multiphase induction motor drives-a technology status review,” *IET Electr Power Appl*, vol. 1, no. 4, pp. 489–516, 2007.

[102] M. Zeraoulia, M. E. H. Benbouzid, and D. Diallo, “Electric motor drive selection issues for HEV propulsion systems: A comparative study,” *IEEE Trans Veh Technol*, vol. 55, no. 6, pp. 1756–1764, 2006.

[103] D. W. Novotny and T. A. Lipo, *Vector control and dynamics of AC drives*, vol. 41. Oxford university press, 1996.

[104] M. R. Ab Ghani, N. Farah, and M. R. Tamjis, “Field oriented control of 6/4 SRM for torque ripple minimiaztion,” in *2016 International Conference on Electrical, Electronics, and Optimization Techniques (ICEEOT)*, IEEE, 2016, pp. 4418–4424.

[105] L. Kumar and S. Jain, “Electric propulsion system for electric vehicular technology: A review,” *Renewable and Sustainable Energy Reviews*, vol. 29, pp. 924–940, 2014.

[106] L. Chang, “Comparison of AC drives for electric vehicles-a report on experts’ opinion survey,” *IEEE Aerospace and Electronic Systems Magazine*, vol. 9, no. 8, pp. 7–11, 1994.

[107] M. Zeraoulia, M. E. H. Benbouzid, and D. Diallo, “Electric motor drive selection issues for HEV propulsion systems: A comparative study,” *IEEE Trans Veh Technol*, vol. 55, no. 6, pp. 1756–1764, 2006.

[108] M. S. Kumar and S. T. Revankar, “Development scheme and key technology of an electric vehicle: An overview,” *Renewable and Sustainable Energy Reviews*, vol. 70, pp. 1266–1285, 2017.

[109] Satyam Panchal, “Experimental Investigation and Modeling of Lithium-ion Battery Cells and Packs for Electric Vehicles,” PhD Thesis , University of Ontario Institute of Technology, 2016. Accessed: May 28, 2022. [Online]. Available: https://ir.library.dc-uoit.ca/bitstream/10155/747/1/Panchal_Satyam.pdf

[110] A. Oubelaid, N. Taib, and T. Rekioua, “Performance Assessment of a Direct Torque Controlled Electric Vehicle considering Driving Cycles and Real Load Conditions,” in *2019 International Conference on Advanced Electrical Engineering (ICAEE)*, IEEE, 2019, pp. 1–6.

[111] T. J. Barlow, S. Latham, I. S. McCrae, and P. G. Boulter, “A reference book of driving cycles for use in the measurement of road vehicle emissions,” *TRL Published Project Report*, 2009.

[112] Manoj Embrandiri, “Implementation and In-depth Analyses of a Battery-supercapacitor Powered Electric Vehicle (E-Kancil),” PhD Thesis , University of Nottingham, Nottingham, 2013. Accessed: Jun. 02, 2022. [Online]. Available: http://eprints.nottingham.ac.uk/14269/1/PhD_thesis_full_%28Manoj_Embrandiri_June_2014%29.pdf

[113] M. Farrag, C. S. Lai, M. Darwish, and G. Taylor, “Improving the Efficiency of Electric Vehicles: Advancements in Hybrid Energy Storage Systems,” *Vehicles*, vol. 6, no. 3, pp. 1089–1113, 2024, doi: 10.3390/vehicles6030052.

[114] H. F. Gharibeh, L. M. Khiavi, M. Farrokhifar, A. Alahyari, and D. Pozo, “Power Management of Electric Vehicle Equipped with Battery and Supercapacitor Considering Irregular Terrain,” in *2019 International Youth Conference on Radio Electronics, Electrical and Power Engineering (REEPE)*, 2019, pp. 1–5. doi: 10.1109/REEPE.2019.8708770.

[115] T. Sadeq, K. Chew, and M. Ezra, “Current Control of Battery-Supercapacitors System for Electric Vehicles based on Rule-Base Linear Quadratic Regulator,” *Advances in Science, Technology and Engineering Systems Journal*, vol. 6, pp. 57–65, Jan. 2021, doi: 10.25046/aj060107.

[116] I. Baboselac, Ž. Hederić, and T. Bensic, “MatLab simulation model for dynamic mode of the Lithium-Ion batteries to power the EV,” *Technical Journal*, vol. 11, pp. 7–13, Jan. 2017.

[117] M. Farrag, C. S. Lai, and M. Darwish, *A Comparison of PI and RBF Brushless DC Motor Speed Control Methods*. 2023. doi: 10.1109/UPEC57427.2023.10294765.

[118] M. E. E. A. Farrag, *Investigation of advanced control for the unified power flow controller (UPFC)*. University of Northumbria at Newcastle (United Kingdom), 2002.

[119] R. Katuri and S. Gorantla, “Design and Simulation of a Controller for a Hybrid Energy Storage System Based Electric Vehicle.,” *Mathematical Modelling of Engineering Problems*, vol. 6, no. 2, 2019.

[120] K. Mobariz, E. Mobarez, and M. Ashry, *Fuel Cell Propulsion Control System Based On PID Approaches*. 2021. doi: 10.1109/ICENCO49852.2021.9698973.

[121] M. Kumar, S. Sen, A. K. Prajapati, and S. Diwania, “A Comprehensive Power Management Approach for Hydrogen Fuel-cell-Based Hybrid EVs Using PID Controller,” in *2023 IEEE IAS*

Global Conference on Renewable Energy and Hydrogen Technologies (GlobConHT), IEEE, 2023, pp. 1–6.

[122] W. Huang, Z. Lu, X. Cao, and Y. Hou, "Hierarchical Coordinated Energy Management Strategy for Hybrid Energy Storage System in Electric Vehicles Considering the Battery's SOC," *Systems*, vol. 11, no. 10, p. 498, 2023.

[123] W. Xin, E. Xu, W. Zheng, H. Feng, and J. Qin, "Optimal energy management of fuel cell hybrid electric vehicle based on model predictive control and on-line mass estimation," *Energy Reports*, vol. 8, pp. 4964–4974, 2022.

[124] J. Hao, S. Ruan, and W. Wang, "Model Predictive Control Based Energy Management Strategy of Series Hybrid Electric Vehicles Considering Driving Pattern Recognition," *Electronics (Basel)*, vol. 12, no. 6, p. 1418, 2023.

[125] L. Li, F. Tao, and Z. Fu, "Robust mode transition control of four-wheel-drive hybrid electric vehicles based on radial basis function neural network estimation-a simulation study," *COMPEL-The international journal for computation and mathematics in electrical and electronic engineering*, vol. 40, no. 4, pp. 870–887, 2021.

[126] T. Harris, *Implementation of radial basis function artificial neural network into an adaptive equivalent consumption minimization strategy for optimized control of a hybrid electric vehicle*. West Virginia University, 2020.

[127] K. S. K. Veni, N. S. Kumar, and J. Gnanavadivel, "Low cost fuzzy logic based speed control of BLDC motor drives," in *2017 International Conference on Advances in Electrical Technology for Green Energy (ICAETGT)*, IEEE, 2017, pp. 7–12.

[128] B. Bairwa, M. Murari, M. Shahapur, M. R. Kavya, and M. F. Khan, "Speed Control of BLDC Motor Using PI Controller," in *2023 International Conference for Advancement in Technology (ICONAT)*, IEEE, 2023, pp. 1–6.

[129] A. Ouarda, B. El Badsi, and A. Masmoudi, "DTC of B4 inverter fed two-phase IM drives," in *2016 IEEE Vehicle Power and Propulsion Conference (VPPC)*, IEEE, 2016, pp. 1–6.

[130] A. L. Saleh and A. A. Obed, "Speed control of brushless DC motor based on fractional order PID controller," *Int J Comput Appl*, vol. 95, no. 4, 2014.

[131] D. E. Beladjine, D. Boudana, A. Moualdia, M. Hallouz, and P. Wira, "A comparative study of BLDC motor speed control using PI and ANN regulator," in *2021 18th International Multi-Conference on Systems, Signals & Devices (SSD)*, IEEE, 2021, pp. 1291–1295.

[132] M. Farrag, C. S. Lai, and M. Darwish, "Optimising EV Efficiency with Hybrid Energy Storage and Advanced Control Strategies," in *Proceedings of the 2024 for the 59th International Universities Power Engineering Conference (UPEC)*, Cardiff.

[133] Q. Zhang, F. Ju, S. Zhang, W. Deng, J. Wu, and C. Gao, "Power Management for Hybrid Energy Storage System of Electric Vehicles Considering Inaccurate Terrain Information," *IEEE Transactions on Automation Science and Engineering*, vol. PP, pp. 1–11, Jan. 2017, doi: 10.1109/TASE.2016.2645780.

[134] Argonne National Laboratory, "Electric Vehicle TestingPublic." Accessed: May 02, 2024. [Online]. Available: https://www.anl.gov/taps/electric-vehicle-testing

[135] T. Barlow, S. Latham, I. S. McCrae, and P. Boulter, “A reference book of driving cycles for use in the measurement of road vehicle emissions,” *TRL Published Project Report*, 2009, [Online]. Available: https://api.semanticscholar.org/CorpusID:106562433

Appendices

Appendix A: Appendix A: MATLAB Simulation Code and Setup Details for Battery and Supercapacitor Discharge Characteristics

```
% MATLAB Simulation: Battery and Supercapacitor Discharge Characteristics
clc;
clear;
close all;

% Simulation parameters
dt = 0.01; % Time step (s)
time = 0:dt:10; % Simulation time (s)
R_load = 1; % Load resistance (Ohm) to increase current and emphasize SC discharge

% Battery parameters
V_battery = 12; % Battery initial voltage (V)
capacity_battery = 1000 * 3600; % Battery capacity in Coulombs (Ah to C)

% Supercapacitor parameters
V_SC = 12; % Supercapacitor initial voltage (V)
C_SC = 10; % Reduced supercapacitor capacitance (F) for faster voltage drop

% Initialize variables for simulation
V_battery_arr = V_battery * ones(size(time)); % Battery voltage array
V_SC_arr = zeros(size(time)); % SC voltage array
P_battery_arr = zeros(size(time)); % Battery power array
P_SC_arr = zeros(size(time)); % SC power array

% Discharge simulation
for t_idx = 1:length(time)
    t = time(t_idx);

    % Supercapacitor voltage and current
    if V_SC > 0
        I_SC = V_SC / R_load; % Current through SC (Ohm's law)
        V_SC = V_SC - (I_SC * dt / C_SC); % Voltage drop (I = C*dV/dt)
    end

    % Battery discharge (current calculated to maintain voltage)
    I_battery = V_battery / R_load;
    P_battery = I_battery * V_battery; % Power delivered by battery
    P_SC = I_SC * V_SC; % Power delivered by SC

    % Store results for plotting
    V_SC_arr(t_idx) = V_SC;
    P_battery_arr(t_idx) = P_battery;
    P_SC_arr(t_idx) = P_SC;
end

% Plot results in 2x2 grid
figure;

% 1. Battery Voltage
subplot(2, 2, 1);
plot(time, V_battery_arr, 'b', 'LineWidth', 1.5);
title('Battery Voltage');
xlabel('Time (s)');
ylabel('Voltage (V)');
```

```
ylim([11.9, 12.1]); % Battery remains stable
grid on;

% 2. Supercapacitor Voltage
subplot(2, 2, 2);
plot(time, V_SC_arr, 'r', 'LineWidth', 1.5);
title('Supercapacitor Voltage');
xlabel('Time (s)');
ylabel('Voltage (V)');
ylim([0, 12]); % SC drops to 0
grid on;

% 3. Battery Power
subplot(2, 2, 3);
plot(time, P_battery_arr, 'b', 'LineWidth', 1.5);
title('Battery Power');
xlabel('Time (s)');
ylabel('Power (W)');
ylim([0, 150]); % Power remains stable
grid on;

% 4. Supercapacitor Power
subplot(2, 2, 4);
plot(time, P_SC_arr, 'r', 'LineWidth', 1.5);
title('Supercapacitor Power');
xlabel('Time (s)');
ylabel('Power (W)');
ylim([0, 150]); % Power drops rapidly to 0
grid on;
```

List of Publications

Journals

- Farrag, Mostafa, Chun Sing Lai, Mohamed Darwish, and Gareth Taylor. 2024. "Improving the Efficiency of Electric Vehicles: Advancements in Hybrid Energy Storage Systems" Vehicles 6, no. 3: 1089-1113. https://doi.org/10.3390/vehicles6030052

Conferences

- M. Farrag, C. S. Lai, and M. Darwish, "Optimising EV Efficiency with Hybrid Energy Storage and Advanced Control Strategies," 2024 59th International Universities Power Engineering Conference (UPEC), Cardiff, UK, forthcoming.
- M. Farrag, C. S. Lai and M. Darwish, "A Comparison of PI and RBF Brushless DC Motor Speed Control Methods," 2023 58th International Universities Power Engineering Conference (UPEC), Dublin, Ireland, 2023, pp. 1-5, doi: 10.1109/UPEC57427.2023.10294765.
- M. Farrag, C. S. Lai and M. Darwish, "Overview of Electric Vehicle Interconnected Subsystems," 2022 57th International Universities Power Engineering Conference (UPEC), Istanbul, Turkey, 2022, pp. 1-6, doi: 10.1109/UPEC55022.2022.9917616.